KOVINE ZLITINE TEHNOLOGIJE

METALS ALLOYS TECHNOLOGIES

LETO 26 št. 4. 1992

IZDAJAJO ŽELEZARNA JESENICE, RAVNE, ŠTORE IN INŠTITUT ZA KOVINSKE MATERIALE IN TEHNOLOGIJE LJUBLJANA
REVIJA JE PREJ IZHAJALA POD NASLOVOM ŽELEZARSKI ZBORNIK

ISSN 1318-0010

Navodila avtorjem za pripravo člankov za objavo v reviji *Kovine, zlitine, tehnologije*

V letu 1992 uvajamo nov način tehničnega urejanja in priprave za tisk revije *Kovine, zlitine, tehnologije*. Da bi pocenili tiskarske stroške, skrajšali čas od prejema članka do njegove objave in prepustili avtorju končno odgovornost za morebitne neodkrite tipografske napake, smo se v uredništvu odločili, da izkoristimo možnosti, ki jih danes nudi *namizno založništvo*.

Za oblikovanje in pisanje člankov smo izbrali TEX oziroma LATEX sistem, ki je za pisanje tehničnih člankov in knjig v svetu najbolj razširjen. TEX oziroma LATEX oblikovalnik besedil je izdelan za skoraj vse vrste računalnikov, od IBM PC kompatibilnih računalnikov, Apple Macintosh računalnikov, Atarijev, pa do velikih računalnikov. Besedila, oblikovana v LATEX-u, so enostavno prenosljiva, saj imajo obliko ASCII zapisa. Kodiranje naših šumnikov je enotno rešeno, tako da lahko pošljete članek, napisan v LATEX-u, kamorkoli po svetu, pa z njimi ne bo težav. Zato naprošamo avtorje, če je le mogoče, da napišejo svoje članke z LATEX oblikovalnikom besedil, sicer pa naj nam poleg besedila na papirju pošljejo vsaj disketo z običajnim ASCII zapisom besedila brez kakršnih koli drugih ukazov za formatiranje.

Vsebina članka

Kako naj članek izgleda vsebinsko, naj si avtorji ogledajo v starih izdajah Železarskega zbornika. Vsak članek pa mora vsebovati:

- slovenski in angleški naslov članka,
- imena ter naslove avtorjev,
- povzetka v angleščini in slovenščini,
- reference, ki naj bodo v besedilu članka označene z zaporednimi številkami, primer[1-5]. Način citiranja članka: avtor, inicialkam naj sledi priimek, naslov članka, ime revije, letnik, strani, leto. Način citiranja knjige: avtor, naslov, založnik in kraj izdaje, leto, po potrebi poglavje ali strani.

Besedilo članka naj bo razdeljeno na razdelke (označene z zaporednimi številkami) in po potrebi še na podrazdelke (označene z decimalno številko, kjer celi del označuje razdelek.

Slike

Vse slike naj bodo na posebnih listih papirja, z jasno označeno številko slike. Slike naj bodo označene z zaporednimi številkami povsod v članku. Originali za vse vrste slik naj bodo ostri in brez šuma. *Risbe* naj bodo narisane s črnim na belem ozadju. Vse oznake in besedila na risbah naj bodo v istem jeziku kot besedilo članka in dovolj velike, da omogočajo pomanjšanje slike na 8 cm. Le izjemoma lahko slika sega čez obe koloni besedila (16.5 cm). *Fotografije* so lahko katerekoli običajne dimenzije, na svetlečem papirju in z dobrim kontrastom. Mikroskopska in makroskopska povečevanja označite v podpisu na sliki, še bolje pa z vrisanjem ustrezne skale na fotografiji.

Za vsako sliko naj avtor predvidi, kam naj se slika v besedilu članka uvrsti, kjer naj se nahaja ustrezen podnapis z zaporedno številko slike (na primer: "Slika 3 prikazuje...", nikakor pa ne: "Na spodnji sliki vidimo...").

Tabele

Avtor naj se izogiba zapletenih tabel z mnogo podatki, ki bralca ne zanimajo, posebej še, če so isti podatki tudi grafično ponazorjeni. Nad vsako tabelo naj se nahaja zaporedna števila tabele s pojasnilom. Tabele naj bodo povsod v članku označene z zaporednimi številkami.

Pisanje besedil na računalniku

Avtorje naprošamo, da pri pisanju besedil na računalniku upoštevajo naslednja navodila, saj le-ta precej olajšajo naše nadaljnje delo pri pripravi za tisk:

- ne puščajte praznega prostora pred ločili (pikami, vejicami, dvopičji) in za predklepaji oziroma pred zaklepaji,
- puščajte prazen prostor za vsemi ločili (pikami, vejicami, dvopičji)—razen decimalno piko,
- pišite vse naslove in besede z majhnimi črkami (razen velikih začetnic in kratic),
- besedilo naj ne vsebuje deljenih besed na koncu vrstice.

Če avtor pripravlja ilustracije na računalniku, ga naprošamo, da priloži datoteke s slikami na disketo z besedilom članka, s pojasnilom, s katerim programom so narejene.

Pisanje v LATEX-u

Uporabljajte *article style*, sicer pa se držite vseh LATEX konvencij. Vse matematične izraze, imena spremenljivk in podobno (razen SI enot) pišite v matematičnem okolju. Uporabljajte že vgrajene fonte, med pripravo za tisk jih bomo zamenjali z ustreznimi PostScript fonti.

Krtačni odtis

Krtačni odtis—končna podoba članka—bo poslan avtorju v končno revizijo. Avtorja naprošamo, da čim hitreje opravi korekture in ga pošlje nazaj na uredništvo. Hkrati naprošamo avtorje, da popravljajo samo napake, ki so nastale med stavljenjem članka. Če avtor popravljenega članka ne vrne pravočasno, bo objavljen nepopravljen, kar bo tudi označeno.

Uredništvo

KOVINE ZLITINE TEHNOLOGIJE

METALS ALLOYS TECHNOLOGIES

KOVINE ZLITINE TEHNOLOGIJE
Izdajajo (Published by): Železarna Jesenice, Železarna Ravne, Železarna Štore in Inštitut za kovinske materiale in tehnologije Ljubljana

Izdajanje KOVINE ZLITINE TEHNOLOGIJE delno sofinancira:
Ministrstvo za znanost in tehnologijo

NASLOV UREDNIŠTVA (EDITORIAL ADRESS): KOVINE ZLITINE TEHNOLOGIJE,
Železarna Jesenice d.o.o., 64270 Jesenice, Slovenija
Telefon: (064) 81 441
Telex: 37 219
Telefax: (064) 83 397
Žiro račun: 51530-601-25734

Stavek in prelom: Igor Erjavc, **Tisk:** Gorenjski tisk, Kranj, **Oblikovanje ovitka:** Ignac Kofol
Fotografija na ovitku: Franci Sluga

Po mnenju Ministrstva za znanost in tehnologijo Republike Slovenije št. 23-335-92 z dne 09. 06. 1992 šteje KOVINE ZLITINE TEHNOLOGIJE med proizvode, za katere se plačuje 5-odstotni davek od prometa proizvodov.

Contents
Vsebina

Kovine, zlitine, tehnologije / letnik 26 / številka 4 / strani 313 do 317 / 1992

Computer Simulation and Optimization of VOD Treatment

Računalniška simulacija in optimiranje VOD obdelave

N. Smajić, *Inštitut za kovinske materiale in tehnologije, Lepi pot 11, 61001 Ljubljana*

Mathematical model and the software CAPSS (Computer Aided Produc tion of Stainless Steel) developed as a part of URP-C2-2566 research program were used for computer simulation of EAF-VOD-CC stainless steelmaking technology line. Basic aim of model testing was to optimise VOD treatment with emphasis on obtaining the maximum productivity at the lowest possible thermal load of VOD ladle and EAF tap temperature. It was concluded that only computer controlled oxygen blowing can secure maximum productivity at the acceptable thermal load of VOD ladle and lowest EA furnace tap temperature.

V okviru petletnega raziskovalnega programa URP-C2-2566 izdelani model in računalniški program CAPSS (Computer Aided Production of Stainless Steel) je bil uporabljen za računalniško simulacijo EOP-VOD-KL tehnologije za izdelavo nerjavnih jekel. Osnovni namen modelnih poskusov je bil optimiranje VOD obdelave s posebnim poudarkom na zagotavljanju maksimalne produktivnosti VOD naprave ob najmanjši možni toplotni obremenitvi VOD ponovce in minimalni temperaturi preboda. Ugotovili smo, da le računalniško programirano pihanje zagotavlja maksimalno produktivnost ob še sprejemljivi toplotni obremenitvi VOD ponovce in minimalni temperaturi preboda.

1 Introduction

The production in metallurgical industries was for a very long time based dominantly on experience. However, the development of theory of metallurgical processes and metallurgical thermodynamics coupled with small-size and yet powerful computers has made it possible to combine the experience with theoretical knowledge, which can result in a significant improvement of operation performance and raising techno-economic production parameters to an essentially higher level.

The application of computers in steelmaking has become indispensable due to high competition and ever increasing demands for lower price, better quality and narrower tolerances of steel properties such as strength, ductility, hot and cold deformability, chemical composition, corrosion resistance, etc. The concept of TQC (Total Quality Control) which excludes any refuse is based on absolutely reliable control of quality. At present TQC is obligatory for all high priced products. Consequently, it is imperative also in the manufacture of stainless steel since the value of a heat of high quality stainless steel can amount up to 300,000 US$. Naturally, there is no room for any allowable refuse despite the fact that technological regulations at present recognize allowable waste. Conventional technologial regulations deal with imaginary "average" heat and "normal" conditions. For that reason and because of great value, each heat of stainless steel must be regarded as unique i.e., it must be processed in a specific way taking into account actual initial state and conditions (chemical composition, temperature, VOD ladle state, pumping system state, etc.). There is no such thing as standard process parameter. Every deviation of initial conditions from some imaginary standard can and must be compensated for by adequate adaptation of process parameters. Such a complex assignment can successfully be carried out only by computer aid.

The work was carried out as a part of the project Stainless Steel which is aimed at the reduction of production costs, improvement of the quality of stainless steel, development of new high quality and extra clean e.g. superferritic stainless steels and the optimization of EAF-VOD-CC tehnological line operation.

The research was concentrated to vacuum oxygen decarburization rate, which should be increased as much as possible since VOD treatment is serious bottleneck of the technological line particularly when producing ELI (Extra Low Interstitials) steel. In addition better control of melt temperature and lower carbon, nitrogen and phosphorus content especially in case of extra clean steel must also be considered in any optimization of VOD treatment.

2 Computer simulation and model tests

Main part of the research was carried out in the form of computer simulation of VOD treatment which is a key part of the technological line.

The model tests performed by use of CAPSS (Computer Aided Production of Stainless Steel) were undertaken

- to increase productivity by shortening of VOD treatment,
- to improve techno-economic production parameters and
- to determine most rational and expedient measures to be taken in order to improve the present technology

2.1 CAPSS

The PC oriented software CAPSS has been developed in Mathematical Modelling and Computer Simulation Department of IMT (Institute of Metals and Technologies) Ljubljana on the basis of a sophisticated mathematical

model elaborated through extensive theoretical studies and investigations[1–10]. The model has been devised primarily for thermodynamical analysis of the Fe-Cr-C-Si-Mn-Al-Ti-O-N system in molten state which is essential in the production of stainless steel.

CAPSS integrates thermodynamic principles, industrial experience, theory of metallurgical processes and expert knowledge required for the economic and massive production of high quality austenitic, ferritic and superferritic conventional, ELC and ELI (Extra Low Carbon, Interstitials) stainless steel.

Thermodynamical data and published informations on VOD operation results were obtained from reference[11–33]. CAPSS was calibrated by a posteriori analysis of a number of heats which had been produced in steelworks Jesenice to determine some empirical unmeasurable constants typical for the steelworks. CAPSS was developed for:

- Off-line control of VOD (Vacuum Oxygen Decarburization) unit of EAF-VOD-CC technological line for the production of stainless steel
  - to reduce the operating costs
  - to increase the productivity and
  - to secure the high quality of produced steel
- Research and development purposes
  - to perform model tests by simulation of VOD operation in order to determine the effect of a change in process variables (oxygen blowing rate, oxygen and argon comsumption, lime addition, etc.) or initial conditions (e. g. melt composition, temperature, etc.) on operation results (productivity, production costs, quality of steel produced, etc.)
  - to optimize production technology and
  - to develop new grades of stainless steel
- Education and training purposes
  - for training of technical personnel in newly installed VOD units or steelworks and
  - for education of University students

2.2 *Computer control of VOD treatment*

Advantages of the computer control of VOD treatment are numerous and evident. Firstly, immediate and continuous inspection of the process of vacuum oxidation and development of melt temperature. It offers the possibility to stop oxygen blowing at exactly right time i.e., at desired final carbon content. The progress and rate of oxidation are continuously monitored and controlled in order

- to prevent melt temperature from exceeding allowable upper limit,
- to assure the lowest heat loading of ladle lining and
- to attain the maximum productivity and the lowest possible loss of chromium.

Computer control is beneficial also for reduction stage of VOD treatment since it

- offers monitoring of the reduction of chromium from slag and temperature changes,
- assures exact calculation of proper addition of lime and reducing means and
- helps to synchronize the operation of whole technological line EAF-VOD-CC and especially of VOD unit and consequent continuous casting machine.

For research and development purposes simulation of imaginary or real but future heats known also as model test is particularly useful. Similar model tests performed in the form of simulation of real past heats i.e., a posteriory analysis is very instructive in education and training of technical personnel. It can reveal errors and wrong decisions made in the past during VOD treatment of a given heat. Simulation and analysis of previous heats can be extensive and include all heats manufactured e.g. in the last month or year. Such an analysis is valuable for evaluation of the existent technology. It can help to find out and determine oscillations of techno-economic parameters (productivity, specific consumption of energy and raw materials, etc.) due to instable technology, unsuitable technical regulations, poor performance of technical personnel or inadequate maintenance. Particularly valuable is analysis of extreme heats i.e., exceedingly good and bad operation results. It can result in significant technological improvements and more suitable regulations. By all means it is first and obligatory step toward the introduction of computer control of steelmaking.

3 Optimisation of VOD treatment by computer simulation

3.1 *ELI stainless steel*

When producing ELI e.g., superferritic stainless steel denitrogenization of melt proceeds under deep vacuum (approx. 100 Pa) at a high carbon content. Of course, such a vacuum can be made only in especial and additional stage of vacuum treatment without oxygen blowing. There can be one, two or even more denitrogenization steps which depends on initial melt temperature and amount of heat losses. The extent and kinetics of this intermediary denitrogenization treatment can also be determined by model tests. Therefore, the efficiency of one stage and the necessity for multistage denitrogenization treatment to obtain required total (C+N) content can be established. As regards the oxygen blowing technique there are two methods namely, uniform and "smart" oxygen blowing. In final stage of oxidation decarburization rate is very small since the most part of oxygen is uitilized for harmful oxidation of chromium. Therefore, it should be smart and useful to decrease oxygen blowing rate gradually toward the end of decarburization.

Uniform oxygen blowing is another blowing technique which applies steady blowing rate e.g., 900 m^3/h and does not take into account rapid and continuous increase in the chromium/carbon activity ratio occuring in the final stage of decarburization. This change of thermodynamic conditions results in a drastically reduced decarburization rate and increased chromium oxidation rate which is accompanied with steep rise in melt temperature. Consequently, the final stage of decarburization is most delicate since VOD ladle lining must be prevented from thermal overloading. On the other side computer simulation in the form of model tests aimed at the optimization of VOD treatment should also optimize the productivity. The most appropriate compromise between high productivity and temperature limitation can be find out only by the use of computer simulation and model tests.

Model tests carried out by the use of CAPSS were planned to compare "smart" and uniform blowing (900 m^3/h) to find out the advantages and deficiencies of each.

The attention has ben focused at the productivity, extent of chromium oxidation to slag, maximum temperature at the end of oxidation and volume and kinetics of denitrogenization. Initial melt composition and temperature was 17.0% Cr, 1.20% C, 0.1% Si, 0.5% Mn, and 1550°C, respectively. Final carbon content should be lower or equal to 0.02 wt.% C. VOD treatment should be as short as possible to obtain high productivity of VOD unit however, melt temperature should not exceed 1700° degrees. The results of model tests are presented in figs. 1–4.

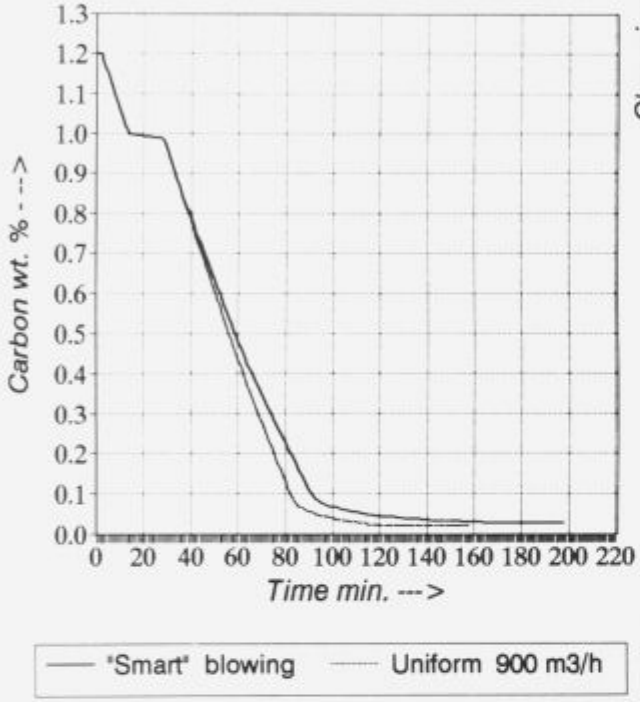

Figure 1. Influence of blowing technique on VOD productivity.
Slika 1. Vpliv načina pihanja na produktivnost VOD naprave.

As can be seen from **fig. 1** "smart" blowing characterized by continuously diminishing blowing rate toward the end of decarburization, as compared to uniform 900 m^3/h rate, results in a serious drop of productivity i.e., prolongation by 40 mins. of the time required for decarburization from 1.2% C to 0.02% C.

Quite unexpectedly, **fig. 2** shows that adaptation of blowing rate to the continuous change in thermodynamic conditions as applied by "smart" blowing does not reduce the extent of chromium oxidation to slag. There is no change in final chromium content which clearly does not depend on oxygen blowing method.

Uniform and intense oxidation with 900 m^3/h blowing rate results in the reduction of time required for VOD treatment by 40 mins. as can be seen from **fig. 3.** However, this increase in productivity could be too expensive since maximum melt temperature would exceed prescribed 1700°C limit.

Fig. 4 shows that blowing technique exerts practically no influence on the volume and kinetics of denitrogenization. Because of a higher melt temperature at uniform blowing favorable influence of temperature on denitrogenization of stainless steel can be seen.

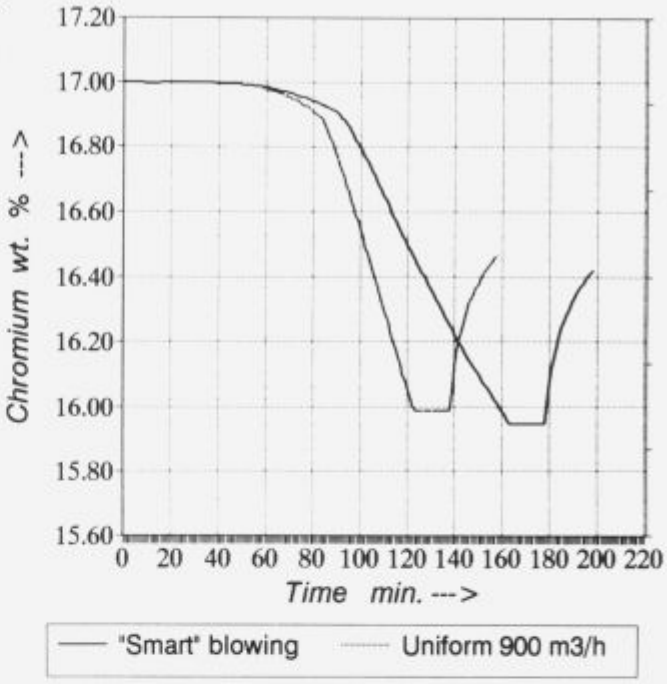

Figure 2. Effect of blowing method on the oxidation of chromium.
Slika 2. Vpliv načina pihanja na obseg in potek oksidacije kroma.

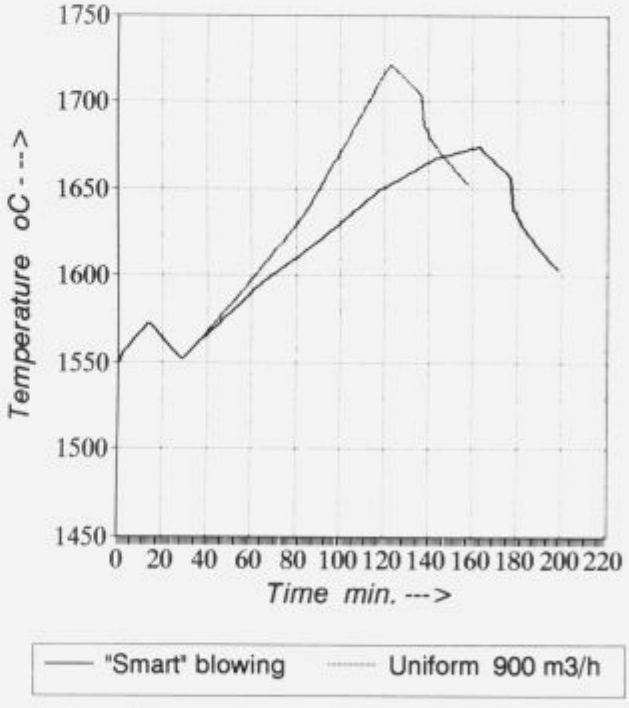

Figure 3. Effect of blowing method on melt temperature.
Slika 3. Vpliv načina pihanja na potek temperature taline.

3.2 Conventional stainless steel

The manufacture of ELI stainless steel e.g., superferritic steel differs from production technology for conventional stainless steel by intermediate stop of oxygen blowing followed by special usually 15 mins. long denitrogenization step at a high carbon content (approx. 1.0% C). Initial carbon content of melt planned for the manufacture of com-

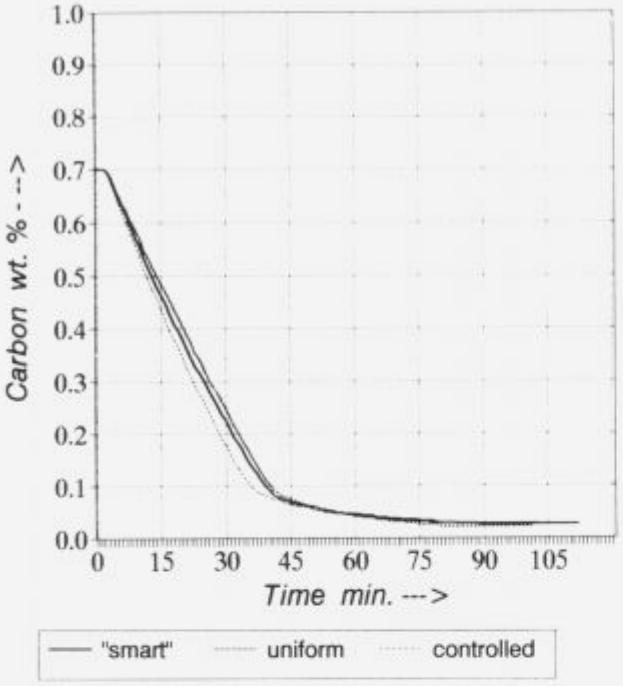

Figure 4. Influence of blowing technique on denitrogenization.
Slika 4. Vpliv načina pihanja na potek in hitrost razdušičenja.

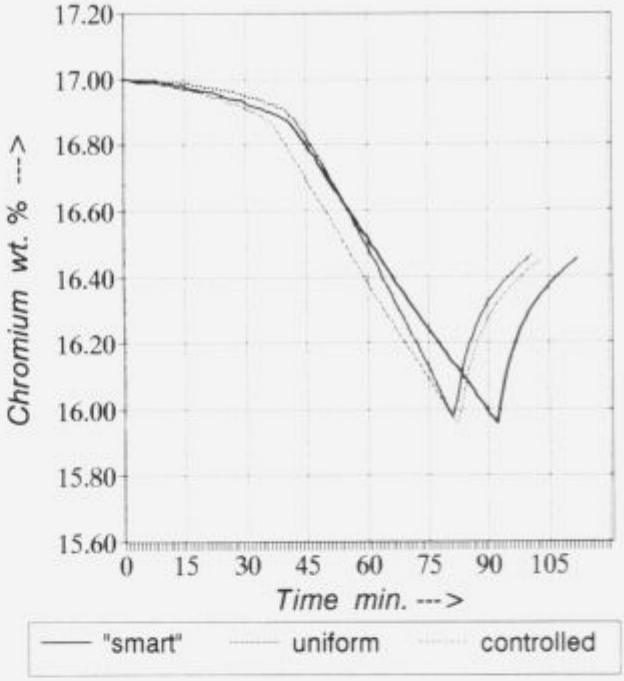

Figure 5. Optimization of VOD productivity by selection of proper blowing technique for common stainless steel.
Slika 5. Optimiranje produktivnosti z izbiro načina pihanja pri izdelavi klasičnega nerjavnega jekla.

mon stainless steel is therefore significantly lower in order to shorten VOD treatment. Final carbon conten of common steel is higher which also helps to reduce the time required for vacuum oxygen decarburization. Special denitrogenization stage is not necessary since low nitrogen content is not prescribed for common stainless steel. Except for ELC grades technological process for commnon stainles steel does not include final vacuum degassing stage followed by reduction. Therefore vacuum decarburization treatment can be performed also by controlled blowing rate in addition to "smart" and uniform blowing. The need for additional i.e., controlled oxygen blowing appears as a consequence of wider range wherefrom process parameters can be selected. The first aim of controlled blowing technique is to maximize the productivity of EAF-VOD-CC production line by shortening duration of VOD treatment which is the slowest stage and therefore VOD unit acts as a bottleneck. The problem is serious particularly in case of UHP electric furnace coupled with VOD unit. However, maximization of productivity by optimization of VOD must take into account following requirements:

- EAF tap temperature should be as low as possible,
- highest allowable temperature at the end of oxidation is 1700°C and
- melt temperature at the end of VOD treatment should correspond to the requirements of continuous casting (CC).

Exact solving of the problem is not possible. A compromise is needed between the contradictory requirements mentioned. Computer simulation i.e., a series of model tests carried out during tapping, ladle transport and preparation for VOD treatment is only possible. **Figs. 5, 6** and **7** present results of model test planned to determine most appropriate controlled blowing technique in order to optimize VOD treatment.

As seen from **fig. 5** "smart" blowing requires longest time for decarburization. There is no essential difference in decarburization time at uniform and controlled blowing technique (101 mins. and 102 mins., respectively).

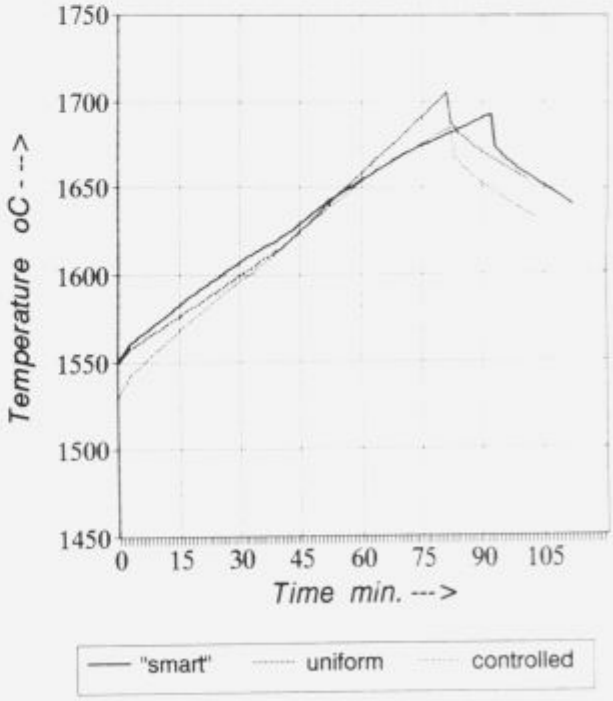

Figure 6. Influence of blowing method on chromium oxidation.
Slika 6. Vpliv načina pihanja na oksidacijo kroma v žlindro.

In all three cases chromium content at the end of treatment is the same as seen in **fig. 6.** This holds for both oxidation and reduction stage. However, it can be seen that during processing chromium content of melt is on the average lowest at controlled blowing because of lower initial temperature.

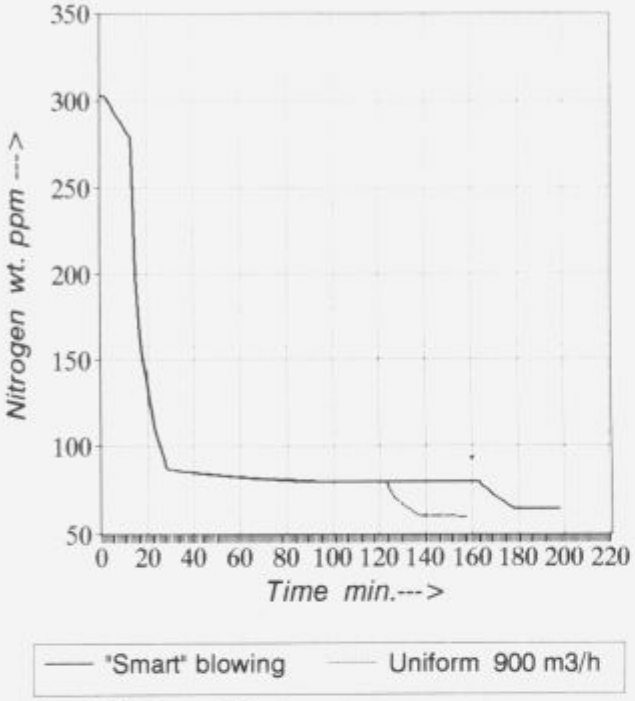

Figure 7. Influence of blowing method on thermal load of VOD ladle.
Slika 7. Vpliv načina pihanja na toplotno obremenitev VOD ponovce.

At uniform 900 m^3/h oxygen blowing rate (**fig. 7**) melt temperature at the end of oxidation just exceeded the allowable limit (1700°C). Heat load of VOD ladle is lowest at controlled blowing which is optimized to obtain practically the same productivity (102 vs. 101 mins.) at EAF tap temperature reduced by 20°C.

4 Conclusion

By the use of PC oriented software CAPSS which had been developed as a part of the research programme URP-C2-2566 computer simulation of stainless steelmaking EAF-VOD technology was carried out.

A series of model tests was performed to investigate the influence of three different oxygen blowing methods on the productivity of 90 ton VOD unit, chromium losses with slag, volume and kinetics of denitrogenization, and thermal load of VOD ladle.

Based on the results obtained following conclusions can be drawn.

- Common oxygen blowing technique known as "smart" blowing does not make it possible to reduce chromium losses. However, it has very negative influence on the productivity of VOD unit and consequently whole steelmaking EAF-VOD-CC technological line.
- Uniform oxygen blowing with constant blowing rate does not increase chromium losses to slag. By proper selection of blowing rate this blowing method can result in a higher productivity however, VOD ladle lining can be thermally overloaded.
- Best results can be achieved by computer controlled blowing rate which ensures highest possible productivity at lowest tap temperature and thermal load of VOD ladle.

5 References

[1] N. Smajić: Mathematical Model for EAF-VOD Stainless Steelmaking, Proceedings of 6. CENIM, Madrid, October 1985.

[2] N. Smajić: Modelle Thermodinamique de l'Elaboration de l'Accier inoxydable suivant le Procede VOD, Proceedings of 25. JAS, St. Etienne,1986.

[3] N. Smajić: Verifikacija matematičnega modela za računalniško vodenje EOP-VOD tehnologije izdelave nerjavnih jekel, Žel. Zbornik, 1986, 3.

[4] N. Smajić: Študij kinetike vakuumskega razdušičenja superferitnih talin, Poročilo Metalurškega inštituta v Ljubljani, N 89-007, 1989.

[5] N. Smajić: Superferitna nerjavna jekla, Žel. zbornik, 1988,2.

[6] N. Smajić: Vakuumsko razdušičenje nerjavnih jekel, Žel. zbornik, 1990, 1.

[7] N. Smajić: Production D'Acier Ferritique Inox Avec Carbone et Azote Tres Bas Par La Technologie EAF-VOD, Bulletin du Cercle de Metaux, 29ems Journees 'Etudes de Metaux, Avril 1990, Saint Etienne.

[8] N. Smajić: Vakuumsko razdušičenje nerjavnih jekel, Žel. zbornik, 24, 1990, št. 1.

[9] N. Smajić: CAPSS, Demonstration on Technova 92 International, Graz 1992.

[10] N. Smajić: Integralni matematični model EP-VOD tehnologije, Poročilo IMT N. 92-09, Ljubljana, 1992.

[11] Mc Coy et al., Electr. Furn. Conf. Proc. 21, 1963, 17–26.

[12] Hilty, D.C. cit. v Handbook of Stainless Steel, 1977, 3–32.

[13] Peckner, D.: Handbook of Stainless Steel, Mc Graw Hill Book Inc., N.Y. 1977, 3–26.

[14] Otto J. et al., Stahl und Eisen 96, 1976, 1939–45.

[15] Otto J., Disertation, Aachen 1975.

[16] M. Schmidt et al., Stahl und Eisen, 88, 1968, 153.

[17] H. Bauer et al, ibid. 90, 1970, 725.

[18] C. Wagner: Thermodynamics of Alloys, Addison-Wesley, Cambridge, 1952.

[19] J.F. Elliot et al., Thermochemistry for Steelmaking, vol. 2, Addison-Wesley, London 1963.

[20] Ban-ya et al., Tetsu-to-Hagane, 60, 1974, 1443.

[21] F. Tsukamoto, Transactions of ISIJ, 26, 1986, 273-81.

[22] B.I. Leonovič et al., Metalli, 1980, 4.

[23] Fujio Ishii et al., Tetsu-to-Hagane 68, 1982, 946-55.

[24] K. Mori, Transactions of ISIJ, 28, 1988, 246–261.

[25] N.P. Vladimirov et al., Metalli, 5, 1973, 89–95.

[26] M. Murakami et al., Transactions ISIJ, 27, 1987.

[27] K. Ishihara et al., Proceedings of 100th ISIJ Meeting, October, 1980, 836.

[28] K. Mori et al., Tetsu-to-Hagane, 52, 1966, 1443-45.

[29] V.P. Luzgin et al., Izvestija VUZ, Čern. Metal. 9, 1963, 50–54.

[30] J.V. Javojskij, Izvestija VUZ, Černaja Met. 1977, 7.

[31] E.T. Turkdogan et al., Trans. Metall. Soc. AIME, 1963, 227.

ŽELEZARNA JESENICE

64270 JESENICE, Cesta Železarjev 8 · telefon: (064) 81-341, 81-441, 84-262
teletax: (064) 83-395 · telex: 37-219, 37-212 zeljsn · telegram: Železarna Jesenice

IZDELUJE

ELEKTRO PLOČEVINE IN TRAKOVI

NERJAVNA JEKLA

MIKROLEGIRANA JEKLA

VISOKO OGLJIČNA JEKLA za poboljšanje

- ☐ debelo, srednje in tanko pločevino
- ☐ hladno valjane trakove in pločevino
- ☐ dinamo trakove in pločevino
- ☐ nerjavne trakove in pločevino
- ☐ vlečeno, brušeno in luščeno jeklo
- ☐ valjano in vlečeno žico
- ☐ patentirano žico
- ☐ pleteno patentirano žico za prednapeti beton
- ☐ hladno oblikovane profile
- ☐ kovinske podboje za vrata
- ☐ dodajni material za varjenje
- ☐ žičnike
- ☐ tehnične pline

NUDIMO TUDI STORITVE

- ☐ prevaljanja, vlečenja, iztiskanja in toplotne obdelave pločevine in žice
- ☐ tehnične dejavnosti: elektro, strojne, konstrukcijske, obrtne in tehnične

Kovine, zlitine, tehnologije / letnik 26 / številka 4 / strani 319 do 328 / 1992

Microalloying of Steel

Mikrolegiranje jekla

F. **Vodopivec**, *Inštitut za kovinske materiale in tehnologije, Lepi pot 11, 61001 Ljubljana*

Mechanisms of the effect of microalloying on strength and toughness of steels. Influence on grain size, precipitation hardening, processes of hot deformation, and economy of microalloying with Al, Nb, V, and Ti.

Mehanizmi vpliva mikrolegiranja na trdnostne lastnosti in žilavost jekla. Vpliv na velikost zrn, izločilno utrditev, procesi vroče deformacije in gospodarnost mikrolegiranja z Al, Nb, V in Ti.

1 Introduction

The microalloying of steel is a technology which has been intensively developed for about 25 years, and it exploits the theoretical knowledge on mechanisms of precipitation hardening, grain size control, and deformation of steel. The term "microalloying" is used because steels are alloyed with up to 0.05% of various elements, and an important influence on the following characteristics and properties is achieved:

- austenite and ferrite grain size are diminished, and because of it yield stress, strength, and toughness are increased while the ductile/brittle fracture transition temperature is diminished;
- precipitation hardening is achieved, this increases the yield stress and strength of steel, diminishes the toughness and increases the ductile/brittle fracture transition temperature;
- the hardenability is improved and austenite/ferrite transition temperature is lowered;
- the susceptibility of steel to strain ageing is eliminated;
- the content of dissolved oxygen and sulphur in steel are diminished and the purity of steel is improved;
- the shape and composition of non-metallic inclusions are changed and the isotropy of properties and the machinability of steel are improved;
- the texture in non oriented electrical sheets is improved and the energy losses diminished.

Microalloying elements are: aluminium, base element for steel deoxidation and for the decrease of oxygen is solution, niobium, titanium, vanadium, zirconium, boron, calcium, tellurium, antimony, tin, nitrogen, and in some cases also sulphur and lead. In this paper only microalloying elements in the narrower sense will be discussed, i.e. those which influence the microstructure, strength and toughness of steel: aluminium, niobium, titanium, vanadium, and nitrogen which are in various combinations the basic constituents of high-strength structural steels and modern machine-building steels. In order to understand better the influence of microalloying elements on the mechanical properties and the hot working process it is necessary to know the processes and reactions in steel involving these elements, and their compounds with nitrogen and carbon which form precipitates called in the following as dispersoide phases. The influenced processes are austenite grain growth, precipitation hardening in ferrite, and recrystallization of austenite during hot rolling.

2 Size and stability of austenite grains

The first condition for the formation of small ferrite grains during the cooling of steel are small austenite grains and are obtained either by recrystallization of austenite after hot rolling at a relatively low temperature if a suitable delay of austenite grain growth is achieved during the hot working, or during the cooling after normalization. Austenite grains grow through migration of boundaries, which can be hindered or stopped if the boundary is pinned to precipitates of dispersoide phases. When migration progresses, at first a concavity is formed at the precipitate, then the grain boundary envelopes it and finally bypasses it. This process requires an additional energy. The driving force for the growth is the tendency of material to reach a minimal total energy (E_s) through the change of the shape and the size of grains, and is obtained by the minimal specific surface energy of grains. The total energy consists of the volume (E_v) and the surface component (E_p). E_v is proportional to the grain volume, thus to D^3, if D is linear dimension of grain, while the surface component is proportional to D^2. Schematically it can be written $E_s = K D^2 + K_1 D^3$. The specific energy is thus:

$$\frac{E_s}{D^2} = \frac{1}{D+1}$$

E.g.: for $D = 1$, $E_s/D = 2$; for $D = 2$, $E_s/D = 1.5$; for $D = 3$, $E_s/D = 1.33$, etc. Thus total energy is the lower the coarses is the grain size.

The prevention of the migration of a grain boundary is achieved when the distance among the precipitates is below a critical value. Instead of the distance between the precipitates, which is difficult to be measured, the more easily measurable precipitation size (d) and volume part of dispersoide phase (f) are used in the analytical treatment of grain growth. The relationship between the grain size—D, the volume part of precipitates—f, and their size—d is according to Zener[1] given by the equation:

$$\frac{D}{2} = \frac{4d}{3f}$$

The above equation was further developed for the growth of austenite grains in structural steel by Gladmann and Pickering[2]. They have assumed that in grain growth the energy

$$E = \frac{2Sy}{D}\left(\frac{2}{Z} - \frac{3}{2}\right)$$

is released. In the equation S—represents the boundary migration, y—the surface energy of austenite, and Z—the ratio between the size of a growing grain and the average grain size in the matrix.

It is evident that the grain growth is possible only if $Z > 4/3$, otherwise the growth energy change is positive and a spontaneous process is not possible. An exception represents the cases of very great growth driving force, e.g. a grain shapes which greatly deviates from the equilibrium. The equation was further transformed into the expression connecting the critical size of precipitates, d_k, with other easily measurable parameters:

$$d_k = \frac{6Df}{2\pi}\left(\frac{3}{2} - \frac{2}{Z}\right)^{-1}$$

The grain growth occurs if the size of precipitates is $d > d_k$. The equation shows that grains grow with the growth of the critical size and the decrease of the content of precipitates, as well as with the increasing non-uniformity of grain size. A spontaneous growth is initiated the easier the greater is the initial non-uniformity of austenite grain size. For better understanding it can be mentioned that after one-hour of heating of a Cr-Ni carburizing steel at 920°C, i.e. before anormal grain growth, the ratio of maximal and minimal grain size is $Z = 3.18$.

By the same quantity of the dispersoide phase the precipitates are the more efficient the smaller is their size, i.e. the greater is their volume density and thus the smaller is their mutual distance. Precipitates are not completely stable at the grain growth temperature and grow at prolonged annealing time and especially at higher temperatures loosing the pinning efficiency. In structural steel the precipitates of sizes below 10 nm represent a low hindrance for grain growth because of their instability caused by the high ratio of surface to the total energy.

Efficient precipitates are formed by dispersoide phases which are dissolved in austenite at the heating of steel before the hot rolling or forging. As steels are becoming cool, the solubility of dispersoide phase is diminished, and precipitates are formed with size depending on the temperature and the length of isothermal annealing.

During the transformation and the recrystallization the growth rate of all grains is not uniform, single grains grow faster, reach a lower total energy, become more stable, and at sufficient temperature grow at the expense of their neighbours. This is the explanation why a microstructure of grains of different size is found in normalized steel with a too low quantity of the precipitates for complete pinning of the migration of austenite grain boundaries. The grains can grow also by coalescence if their space orientation is similar and are parted by low-angle boundaries. This occurs in textured materials.

The boundary migrating at the extent of a neighbour grain is concave. A simplified explanation is that the atoms on the concave side are on average more time bound in the crystal lattice. The migration of crystal boundary is produced by the difference in the number of atoms which are deplaced over the grain boundary because of thermal oscillation. The number of jumps from the convex to the concave side of the boundary is equal to the number of jumps in the reverse direction, but on the concave side more of oscillating atoms are retained. This produces a flow of atoms from the convex to the concave side, i.e. the shift of crystal boundary in the opposite direction.

The theoretical explanation for the migration process of a crystal boundary towards the centre of curvature is found in ref.[3], where it is suggested that the driving force for the boundary migration is the decrease of surface energy. The rate of migration is described by a parabola of the form

$$D = D_0 + K^{1/n}$$

with D_0—an initial grain size, D—the grain size after an annealing time t, and n—the growth exponent. Theoretically n is 2 while empirically the values between 2 and 4 were measured.

The connection between the grain size (D) and the yield stress (R_E) is given by the Hall-Petch equation

$$R_E = R_{E_0} + KD^{-1/2}$$

with R_{E_0} as a constant depending on the composition and the microstructure of steel[4]. The constant K is a measure for the hindering effect of crystal boundaries on the mobility of dislocations.

In **Fig. 1** taken from the ref.[5] the relation between the grain size, expressed by $D^{1/2}$ and the ASTM number, and the yield stress of steel with 0.17% C and 0.8% Mn is shown. The decrease of the grain size from ASTM number 5 to ASTM number 10, obtained through the microalloying produces an increases in yield stress of steel for about 50%. This increase takes place at an increased toughness and a decreased ductile/brittle fracture transition temperature (T_p) at notch toughness test. The proposed relation is

$$\frac{1}{T_p} = T_0 + KD^{-1/2}$$

with T_0 and K constants depending on the composition and the microstructure of the steel[4].

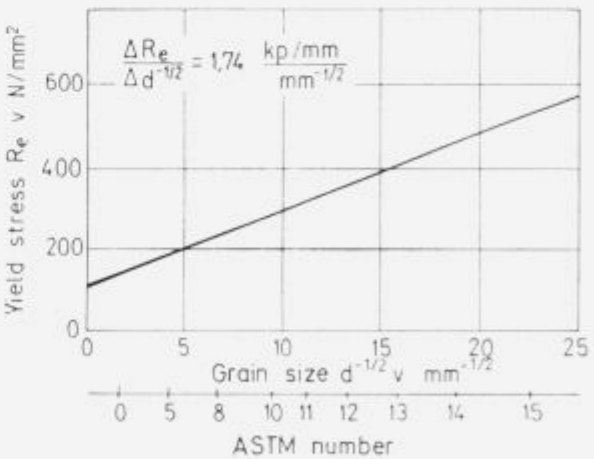

Figure 1. Relation between the grain size expressed as $D^{-1/2}$, the ASTM number, and the yield stress of steel with 0.17% C and 0.8% Mn (Ref.[5]).

Slika 1. Odvisnost med velikostjo zrn izraženo kot $D^{-1/2}$ in ASTM razredom ter mejo plastičnosti jekla z 0.17% C in 0.8% Mn. Po viru[5].

The movement of dislocations in the lattice is hindered by the Peierls-Nabarro force (τ_{pn}), and each crystal boundary produces an additional obstacle for the movement. The

total force (T_s) essential for the movement of dislocations in polycrystalline material is:

$$T_s = \tau_{pn} + KD^{-1/2}$$

A piling-up of dislocations at the grain boundary is required in order to accumulate a sufficient driving force for the penetration of dislocation into the neighbour grain with a different space orientation[6].

3 Dispersoide phases

Dispersoide phases are carbides and nitrides, very frequently also carbonitrides since carbides and nitrides of microalloying elements are mutually completely soluble. The composition of dispersoides depends on the amounts of microalloying elements, nitrogen, and carbon in steel. If the content of microalloying elements, nitrogen or carbon is too high, dispersoide phases can form already in the melt or during the solidification of steel. The size of precipitates in this case is 100 nm or more, accordingly small is their volume density, and low the hindering effect at standard size of austenite grains. In microalloyed steel in which the content of microalloying elements for the most part does not exceed 0.05%, the sufficient volume density of precipitates is not achieved if they are formed in the melt or during the solidification. In this case they are enriched on the solidification interfaces or in eutectic clusters, which decreases the ductility of the steel. Such example represent AlN and Nb(CN) formed during the solidification of steel manufactured in electric arc furnace[7], with a high content of nitrogen, aluminium, and niobium.

The mechanism of growth of precipitates involves the solution of small particles with a greater specific surface energy and the diffusion of microalloying components on coarse, more stable particles.

The growth of precipitates, often named as Ostwald ripening, is described by the Wagner[8] equation

$$d_t^3 - d_0^3 = \frac{16\sigma DCV}{9RT}t$$

with

d_t	precipitate diameter after the annealing time t
d_0	precipitate diameter in time 0
σ	surface tension between the matrix and precipitate
D	diffusivity of constitutive atoms
C	concentration of constitutive atoms
V	molar volume of precipitate
R	gas constant
T	absolute temperature

The equation shows that the rate of precipitate growth will be at constant other conditions the faster, the faster is the diffusivity, the greater is the concentration of constitutive atoms in solution, and the higher is temperature. Thus the ideal dispersoide is that with the lowest solubility of constituents, and with the lowest diffusivity of microalloying element, since the diffusivity of nitrogen and carbon in interstitial solution is very fast.

Let us assume that the steel contains 0.03% AlN which ensures the austenite grains size after normalization of 6–7 ASTM number[9]. **Fig. 2** presents the calculated AlN precipitate size for such a steel after one hour holding at various temperatures, the content of aluminium nitride, the volume density of precipitates, and the relative austenite grain size. The solubility product used for the calculation is in good agreement with the AlN solubility determined for Cr-Ni carburizing steel[9]. If the heating temperature of steel is increased from 900 to 950°C, the same hindering effect can be obtained with an about 40% higher content of nitride, while above 1000°C the pinning effect of aluminium nitride is very rapidly diminished.

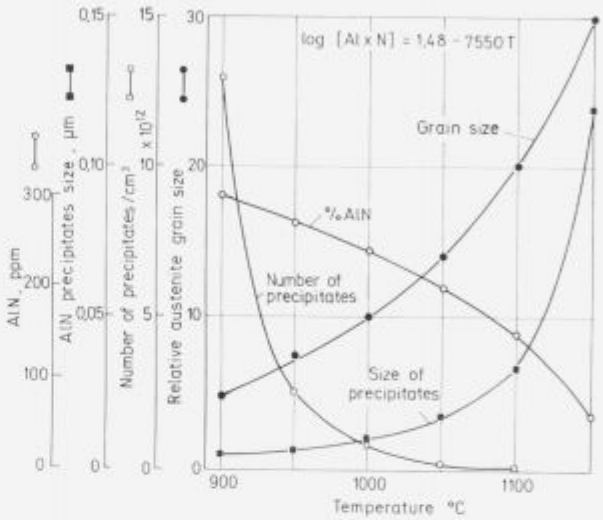

Figure 2. Relation between the annealing temperature and the precipitate size, the number of precipitates per unity of volume, the content of AlN in solution, and the austenite grain size. The theoretical AlN content is 0.03%. The calculation is based on the AlN solubility product given in ref.[2].

Slika 2. Odvisnost med temperaturo žarjenja in velikostjo izločkov, številom izločkov na enoto prostornine, količino AlN v raztopini in velikostjo zrn austenita. Teoretična vsebnost AlN 0.03%. Izračun je izvršen na osnovi topnostnega produkta za AlN v viru[2].

In microalloyed steel usually there are 2 or 3 grain growth inhibitors; AlN, Nb(CN), TiC and VN. The presence of precipitates formed by the addition of 0.03% niobium to the steel with 0.10–0.20% C ensures grain sizes of ASTM number 10–11 after normalization.

The most frequent dispersoide is aluminium nitride (AlN) which is found in all steels deoxidized, and thus microalloyed with aluminium. The solubility of AlN and of other dispersoide phases in austenite in structural steels is given by the solubility product. Ref.[10] gives the following solubility product for aluminium nitride

$$\log(\mathrm{Al} \times \mathrm{N}) = -6770/T + 1.48$$

In the above equation N and Al represent the weight content of both elements in solution in the steel, and T is the temperature in K. According to ref. [10], [11], and [12] the solubility products for other dispersoide phases are

$$\log(\mathrm{Ti} \times C) = -10475/T + 5.33 \quad [11]$$
$$\log(\mathrm{Ti} \times N) = -8000/T + 0.32 \quad [12]$$
$$\log(\mathrm{V} \times C) = -9500/T + 6.72 \quad [11]$$
$$\log(\mathrm{V} \times N) = -8330/T + 3.46 \quad [10]$$
$$\log(\mathrm{Nb} \times C + N) = -6770/T + 2.26 \quad [10]$$

In some references also other equation for the solubility of dispersoides is found but they do not differ significantly from the above given.

The solubility of all the dispersoides, but of vanadium carbide, in austenite with up to 0.2% C and 0.01% N is small and at the normalizing temperature less than 10% of the quantity at the temperature of about 1200°C. On the contrary, the solubility of vanadium carbide in austenite is very high, and this dispersoide is completely dissolved already at about 900°C in steel with 0.2% C. Other dispersoides are very stable because of the low solubility at the normalizing temperatures and the inhibition of grain growth is diminished only at higher temperatures.

During the cooling from the solubility temperature and at isothermal holding during such cooling the formation of precipitates is very slow (**Fig. 3**) due to slow formation of nuclea though the solid solution is highly oversaturated[13]. The explanation for the slow formation of nuclea is the great dilution since the content seldom exceeds 0.03% which e.g. represents 3 atoms of titanium per 10000 atoms of iron. The number of atoms of microalloying elements is thus very low and consequently the rate of formation of sufficient statistic aggregations of atoms from which precipitation nuclea are formed is very slow. The kinetics of the precipitation during the holding after direct cooling from the solubility temperature is a slow parabola highly different from that describing the formation of precipitates in austenite quenched from the solubility temperature and then reheated (**Fig. 3**). The kinetics of AlN formation is in this case a step parabola indicating that the rate of growth of precipitates is determined by the diffusion rate of aluminium on the nuclea formed during the reheating of steel, due to the high oversaturation because of the cooling to ambient temperature or to the double transition of the austenite/ferrite phase boundary on which the solubility of AlN is changed strongly.

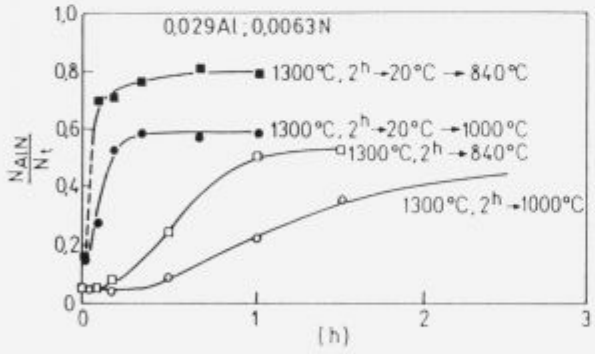

Figure 3. Kinetics of AlN precipitation after various thermal history of steel with 0.11% C, 0.49% Mn, 0.029% Al, and 0.0063% N.
Slika 3. Kinetika precitipacije AlN po različni termični zgodovini jekla z 0.11% C, 0.49% Mn, 0.029% Al in 0.0063% N.

It must be mentioned that niobium if its concentration exceeds about 0.035% and at high nitrogen contents—the limit is at about 0.012%, is bound during the solidification process into a carbonitride very rich in nitrogen and practically unsoluble during heating the steel before the rolling[7]. Niobium bound in this phase is lost as active microalloying element, thus the microalloying with niobium in steel molten in electric arc furnace is economical only up to about 0.03%. In CrMn case hardening steel by already 0.02% Nb the same stability and size of austenite grains is achieved as with the same amount of aluminium or with 0.1% vanadium (**Fig. 4**). The specific weight of niobium carbide is higher than that of aluminium nitride, the weight solubility of both in austenite is similar, thus the same weight content of niobium in austenite gives less precipitates. Consequently, if seems probable that niobium hinders the migration of boundaries also by some other mechanism, e.g. by a segregations on grain boundaries which produces a greater number of precipitates on these boundaries as it could be expected from the average niobium content in steel. Ref.[14] presents micrographies showing that the boundaries or subboundaries of austenite grains are marked with strings of precipitates which confirm the possibility of an intercrystalline segregation of niobium. The size of austenite grains is thus related to the thermal deformation history of steel. Ref.[15] describes a bimodal size distribution of precipitate after the rolling of niobium steel from 1050°C which can also be explained supposing an intercrystalline segregation of niobium.

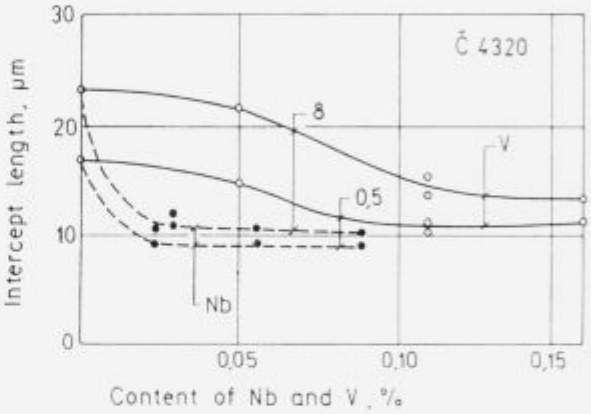

Figure 4. Relation between the amounts of niobium and vanadium in steel and the size of austenite grain after half-hour and 8-hour austenitizing at 920°C. Basic steel composition: 0.18% C, 0.95% Mn, 0.28% Si, 1.0% Cr and, below 0.002% Al (Ref.[16]).
Slika 4. Odvisnost med količino niobija in vanadija v jeklu in velikostjo zrn austenita po polumi in 8 umi austenitizaciji pri 920°C. Osnovna sestava jekel: 0.18% C, 0.05% Mn, 0.28% Si, 1.0% Cr, pod 0.002% Al_t. Po viru[16].

4 Microalloying and precipitation hardening

The precipitation hardening is one form of dispersion hardening, i.e. hardening caused by a new phase which is found in small quantities in the metallic matrix. The general expression describing the relations between the quantity of precipitates (f), their size (d), the shear modulus (G), the Burgers vector of dislocations (b), and increase of strength (ΔR_T) was proposed by Hornbogen[17] in the following form

$$\Delta R_T = K \frac{Gbf^{1/3}}{d}$$

K is a constant with a value $K = 1$ for a polycrystalline material and uniformly distributed spheroidal particles of the new phase. The hardening is proportional to the third root of the quantity of precipitated phase and inversely proportional to the particle size of that phase. It is thus more strongly dependant on the size than on the quantity of precipitates. The precipitation hardening is stable only till the shear moduls is not diminished because of the temperature change or the precipitates do not hinder the moving of dislocations. In microalloyed steel the precipitates formed at

the normalizing temperature, which are a very efficient hindrance for grain growth, do not cause precipitation hardening. This would be obtained only by a much greater number of precipitates, at least for one order of magnitude greater than it is usually found in microalloyed steel. In such a case the ductility and the toughness of steel would be diminished.

The highest precipitation hardening of microalloyed steel is obtained if precipitates are formed below about 620°C when the shear modulus of ferrite is high enough, and the internal stresses due to the formation of coherent precipitates are not relaxed. Coherent precipitation occurs by carbonitrides, carbides, and nitrides of niobium, vanadium, and titanium which have a cubic crystal lattice, but not by the hexagonal aluminium nitride which produces thus virtually no precipitation hardening of ferrite. The lattice parameter of cubic precipitate is different than that of ferrite. Both lattices can accommodate by elastic deformation and the internal stresses on the contact surfaces are proportional to the hardening, generally called as coherent hardening. The stress field around the precipitates hinders the movement of dislocations in a greater volume of matrix than the precipitate alone. At increasing size of precipitates the coherence is lost and the boundary between the precipitates and the matrix becomes an actual phase boundary without elastic accommodating stresses. The hardening is achieved only by hindering of dislocations moving at plastic deformation. This hardening is called a dispersion hardening and it can be calculated according to the Hornbogen equation. In this type of hardening all carbide and nitride phases, including aluminium nitride and cementite, behave in equal way, and the effect depends on the amount and the size of precipitates.

The moving dislocation can cut small precipitates without stress field[18]. The critical size of precipitate depends mainly on their shear modulus, e.g. for copper precipitates in ferrite the critical size is about 10 nm and, for TiN precipitates only 3 nm. Precipitation hardening of microalloyed steel is relatively strong. For the evaluation of the hardening effect of niobium carbonitride the following semiempirical expression was developed by Yeo and coworkers[19]

$$\Delta Re = \frac{1575}{d}(\%\mathrm{Nb}^{1/3} - 0.12)$$

with Nb as niobium content in weight %, d—the size of niobium carbonitride precipitates, and ΔRe—the increase of yield stress.

The exponent at the niobium content proves that the expression was derived through simplification of the Hornbogen equation. A disadvantage of the expression is the lack of parameters considering the temperature of formation of precipitates and the shear modulus, thus it can be used only for heat treatment by quenching and ageing at a selected temperature.

Fig. 5 presents the influence of precipitates size at constant niobium content, and the content of niobium at constant size of 50 nm precipitates on the hardening effect. Already a small amount of niobium is efficient if present in steel in small precipitates. The increase of the content of niobium does not improve the hardening effect to an economically justified extent. Fig. 5 further proves that precipitates of an average size of 25 nm, which can be found in microalloyed steel after normalizing, cause hardly a hardening effect.

Practically only a part of precipitation hardening effect can be industrially exploited however it is not negligible

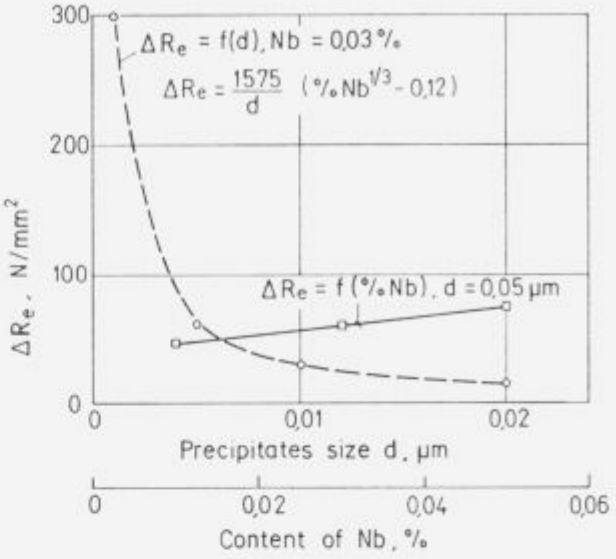

Figure 5. Relation between the size of precipitates in steel with 0.03% Nb or NbC concentration in 5 nm precipitates, and the increase of yield stress.

Slika 5. Odvisnost med velikostjo izločkov v jeklu z 0.03% Nb oz. količino NbC v izločkih z velikostjo 5 nm in povečanjem meje plastičnosti.

from the viewpoint of the material strength. E.g. a small change in basic composition of the steel with a yield stress above 350 N/mm^2, and microalloying with niobium and vanadium can give a yield stress above 470 N/mm^2, where precipitation hardening due to formation of vanadium carbide during the cooling of steel after normalizing contributes for about 50 N/mm^2 [20]. As already mentioned, the precipitates formed in the approximate temperature range 570 to 620°C are efficient. At lower temperatures the formation of precipitates is too slow due to the slow diffusion of vanadium, and it could be exploited only by a longer annealing or in a very slow cooling which is economic only in coils. The effects of the diminution of grain size and of the precipitation hardening on the yield stress are additive, their influence on the other two very important properties, the notch toughness and the ductile/brittle fracture transition temperature, is opposite. Diminished grain size increases the toughness and decreases the transition temperature while the precipitation hardening has an opposite effect. **Fig. 6** presents, according to data in ref.[4], some relations which confirm the above conclusions for a standard as normalized Nb-V microalloyed steel. By thermal treatment, e.g. by normalizing and through the rate of cooling, a rather different relation between the yield stress and the toughness transition temperature can be achieved, even an unacceptable transition temperature can be obtained which nullifies all the advantages of microalloying.

5 Microalloying and hot deformation

Most steel products are manufactured by hot rolling when the steel cross section is reduced from pass to pass at dropping temperature till a final thickness of plate, strip or bar is obtained. A similar sequence of events is found by forging only the sequence of partial deformations is less uniform. During the rolling process the steel is cooled partially by radiation and the convection into the surroundings, and partially by contact with the cooling water, rolls, hammers or

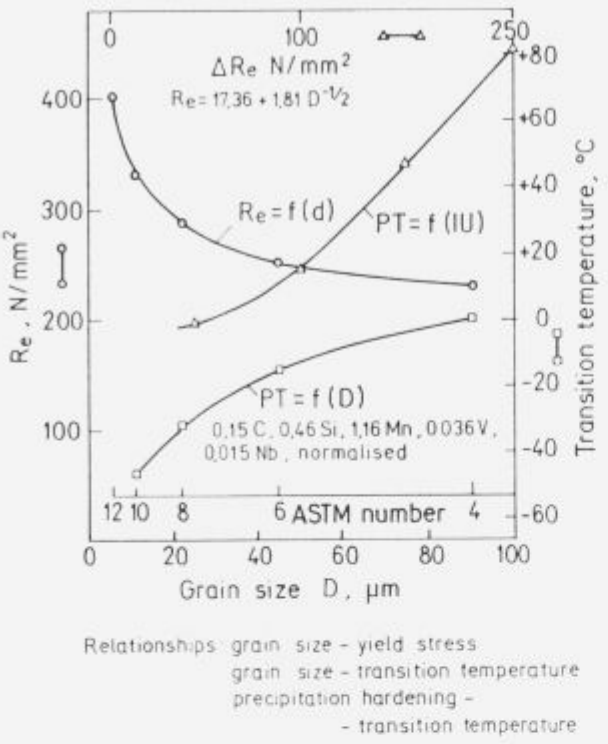

Figure 6. Relation between the grain size in as normalized steel, the precipitation hardening, and the yield stress increase due to the precipitation hardening (ΔRe), and the notch toughness transition temperature (PT).

Slika 6. Odvisnost med velikostjo kristalnih zrn v normaliziranem jeklu, oz. izločilno utrditvijo in mejo plastičnosti povečano zaradi izločilne utrditve (ΔRe) ter prehodno temperaturo žilavosti (PT).

other cooler parts of equipment. Because of the successive deformations the steel is in deformed state for some time and it contains a great number of point and line defects. The rate of diffusion processes in the deformed matrix is very fast. Jonas and coworkers[21,22] found that the nucleation rate of precipitates was for an order of magnitude faster during the deformation, and that the rate of precipitates growth in deformed austenite was for two orders and during the deformation even for three orders of magnitude greater than in not deformed or in recrystallized austenite. The static recrystallization which eliminates from austenite the deformation energy delayed for a few seconds corresponds thus to a 100 or even 1000 sec. long annealing. Any component which delays the recrystallization thus highly accelerates the process of precipitaton but only as long as austenite remains unrecrystallized. As soon as the recrystallization is finished the rate of precipitation is diminished again. E.g. in laboratory rolling of 12 mm plates from 60 mm billets the steel remained between the rolls for 0.47 seconds, and total time of rolling was 70 seconds. Let us assume a great rate and an uniform precipitation in the period when steel is deformed between the rolls. The rate of precipitates growths is described by approximate cubic parabola which can be simplified for a rough evaluation into the expression $d^{1/3} \approx Kt$, t being the time. The calculation shows that the ratio of precipitates size in unrecrystallized austenite (d_{an}) and in recrystallized austenite (d_{ar}) is $d_{an}/d_{ar} = 4.5$. If steel is rolled by uncompleted interpass recrystallization and if it contains a small quantity of microalloying elements the unhomogenity of microstructure represented by the number of anormally grown grains is the greater the lower is the rolling temperature[9,23] because of the unhomogenity of precipitation during the rolling. During the rolling of low and medium alloyed steel with an austenite microstructure static recrystallizaton is the basic process for the elimination of deformation energy. Dynamic softening processes and static recovery are virtually negligible. In absence of interpass recrystallization static recovery rapidly eliminates the deformation hardening, and it does not change the size of austenite grains. Niobium is the microalloying element which has the strongest delaying effect on the rate of static recrystallization of austenite. Two explanations are proposed for the mechanism of the effect of niobium. The first claims that the effect is linked to niobium in solid solution in austenite[24]. The process of static recrystalization is initiated on the grain boundaries, it seems thus that the inhibition of formation of recrystallization nuclea on boundaries is connected to the presence of niobium at these boundaries. **Fig. 7** shows that the temperature of completed interpass static recrystallization of austenite is already by 0.02% niobium increased for about 100°C in the CrMn carburizing steel. The weight content of 0.02% of niobium means that the solution in austenite contains appr. 1.1 niobium atom per 10^4 iron atoms. A logic conclusion is that such a dilution could hardly influence the process linked to shifts of iron atoms and it seems justified to conclude that the austenite grains boundaries are richer in niobium due to a segregation. This explanation is supported also by the fact that small amounts of niobium improve the hardenability of steel through the delaying the nucleation of ferrite below the transformation temperature. Thus niobium can hinder the formation of recrystallization nuclea and ferrite by a similar mechanism.

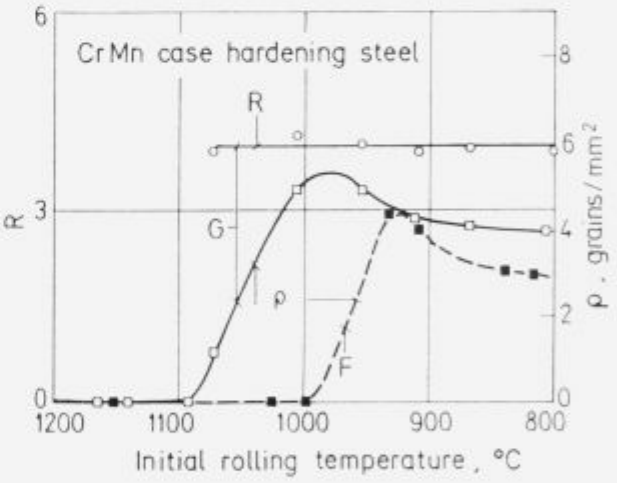

Figure 7. Influence of the initial rolling temperature on the ratio length/width (R) and on the number of unrecrystallized austenite grains (P). Steel G: 0.14% C, 1% Mn, 0.85% Cr, 0.02% Nb, and 0.0078% N; steel F: 0.16% C, 1.1% Mn, 0.98% Cr, 0.025% Al, and 0.0095% N.

Slika 7. Vpliv začetne temperature valjanja na razmerje dolžina/širina (R) in na število nerekristaliziranih zrn austenita (P). Jeklo G: 0.14% C, 1% Mn, 0.85% Cr, 0.02% Nb in 0.0078% N; jeklo F: 0.16% C, 1.1% Mn, 0.98% Cr, 0.025% Al in 0.0095% N.

The second hypothesis links the influence of niobium on the recrystallization on precipitates formed during the deformation. Two questions are not explained by this hy-

pothesis: why the precipitates of other microalloying elements, e.g. TiC, and VN and AlN, which are also formed during the deformation, hinder the static recrystallization of austenite to a much lesser extent (**Fig. 8**), and why the recrystallization process takes place when the content of niobium in solid solution is diminished below a limit of about 0.005% due to the formation of precipitates. Both explanations of the effect of niobium are found in recent papers on microalloying, and it is left to the reader to chose the more probable significance weighting the significance of empirical findings.

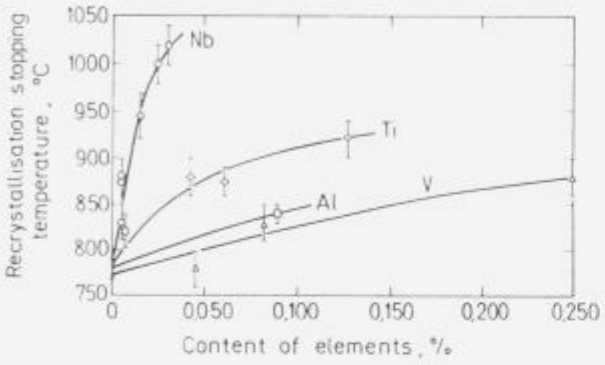

Figure 8. Influence of the content of various microalloying elements on the hindering temperature of static recrystallization of austenite.
Slika 8. Vpliv vsebnosti raznih mikrolegimih elementov na temperaturo zaustavitve statične rekristalizacije austenita.

In **Fig. 9** the effect of rolling temperature on the content of AlN and NbC in various steels, and on the ferrite grain size given as intercept length by rolling 15 mm plates from 60 mm billets in 7 passes is shown. All the steels were heated to 1200°C before the rolling. In steel without niobium where the interpass recrystallization of austenite is fast and complete, only few precipitates are formed during the rolling and the influence of temperature on the amount of precipitates is hardly perceivable because at decreasing rolling temperature the content of AlN formed during the rolling is very slowly increased. The precipitation behaviour in niobium steel is significantly different because austenite remains between passes for longer time unrecrystallized, or the quantity of austenite which does not recrystallize at all between passes is increased, and thus the precipitation is faster. Below a limit temperature austenite remains completely unrecrystallized between passes and the precipitation is accelerated to such extent that practically all AlN and NbC are precipitated in the relatively short rolling time of 1 minute.

On the base of the processes of recrystallization and of precipitation two technologies of rolling of microalloyed steel were developed. In thermomechanical rolling the slabs are rolled to a thickness which is 30–50% greater than the final thickness of plates, the rolling is stopped till steel temperature drops below about 950°C, and then the plates are rolled to the final thickness in several passes, the number depends on the strength of the rolling stand, and cooled in air. Deformed austenite is during the cooling very rapidly transformed into finegrained ferrite and pearlite[25], while AlN and NbC precipitates hinder the growth of ferrite grains after the transformation. A finegrained microstructure with high strength and toughness is obtained, and it supports the precipitation hardening with VC during the air cooling of plates with an acceptable deteriorating effect on notch toughness.

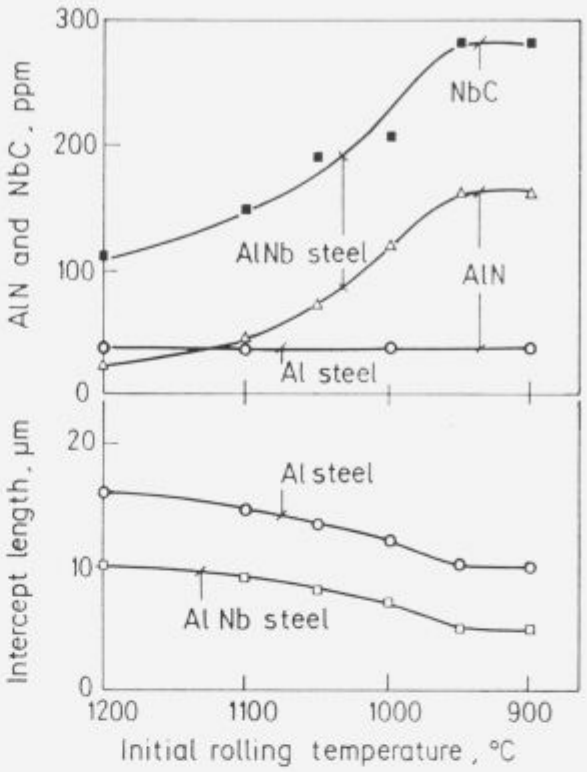

Figure 9. Relation between the initial temperature of two steel with a similar basic composition, one microalloyed with niobium, the amounts of AlN and NbC precipitated during the rolling and the grain size after air cooling.
Slika 9. Odvisnost med začetno temperaturo dveh jekel s podobno osnovno sestavo, eno pa mikrolegirano z niobijem na količino AlN in NbC, ki sta nastala med valjanjem in na velikost zrn po ohladitvi na zraku.

This technology is applied for steel microalloyed with niobium and vanadium which can achieve yield stresses up to 500 N/mm^2 at carbon contents below 0.15%. Similar properties are obtained with the combination of rolling in less controlled temperature range and normalization annealing. **Fig. 10** represents the various hardening mechanisms in normalized steel microalloyed with aluminium, niobium, and vanadium.

The advantages of microalloying can be exploited also through the rolling process with controlled recrystallization. This method demands an exact harmonization of steel composition with the degree of deformation and the pass sequence, since the temperature and the per pass deformation must enable the complete interpass recrystallization, and simultaneously also the formation of precipitates which hinder the growth of recrystallized austenite grains. **Fig. 11** presents mechanical properties of three steel of similar composition which were rolled under conditions of controlled recrystallization. In both microalloyed steels much better properties are achieved than in the comparative steel down to about 800°C when the transformation of austenite during the rolling, the deformation hardening, and the formation of texture during rolling start to occur. By the same rolling conditions the microstructure of vanadium steel is more homogeneous because of less of microstructural unhomogeneity due to the or incompleted interpass recrystallization. At still lower rolling temperatures the deformation hardening,

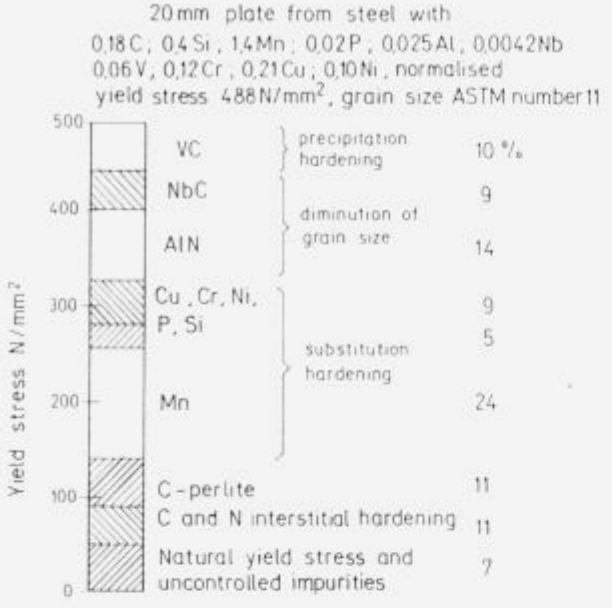

Figure 10. Constitution of yield stress in a 20 mm sheet of normalized microalloyed steel with 0.18% C, 0.4% Si, 1.4% Mn, 0.025% Al, 0.042% Nb, 0.06% V, 0.12% Cr, 0.21% Cu, and 0.10% Ni.

Slika 10. Zgradba meje plastičnosti v 20 mm pločevini iz normaliziranega mikrolegiranega jekla z 0.18% C, 0.4% Si, 1.4% Mn, 0.025% Al, 0.042% Nb, 0.06% V, 0.12% Cr, 0.21% Cu in 0.10% Ni.

microstructural nonhomogeneities, and strain anisotropy increase, therefore a too low finishing temperature has a harmful effect. An even higher strength can be achieved by a proper coiling temperature since slow cooling enables a greater precipitation hardening.

6 Economy of microalloying

Microalloying is the more efficient the more dispersoide is dissolved at heating before hot working. The quantity of dissolved dispersoide is the greater the closer are the concentrations of the constituting elements to the stoichiometric ratio; e.g. the amount of dissolved AlN in austenite will be the greatest if the weight contents of aluminium and nitrogen in steel are 2 : 1. A too great deviation of one or the other element causes that less dispersoide is dissolved in austenite, and less precipitates are formed during the rolling and the cooling. This explains why at high aluminium contents, over 0.04%, austenite grains are coarser and less stable than at a lower content of aluminium and at the same content of nitrogen about 0.01%.

For the stability of austenite grains the nature of precipitates is not important, only their number and stability matter, or more correctly, the number of precipitates per unity of volume of austenite. Theoretically the presence of about 0.03% AlN or of a corresponding quantity of other dispersoides of precipitates of equal size is needed to attain a sufficient stability of austenite grains. The contents of microalloying elements and of dispersoide phases giving equal volume densities of precipitates are given in **Table 1** for the most frequent dispersoides. Aluminium assures a sufficient density of precipitates already at the lowest content, while the highest content is required in the case of vanadium carbide since this carbide is much more soluble

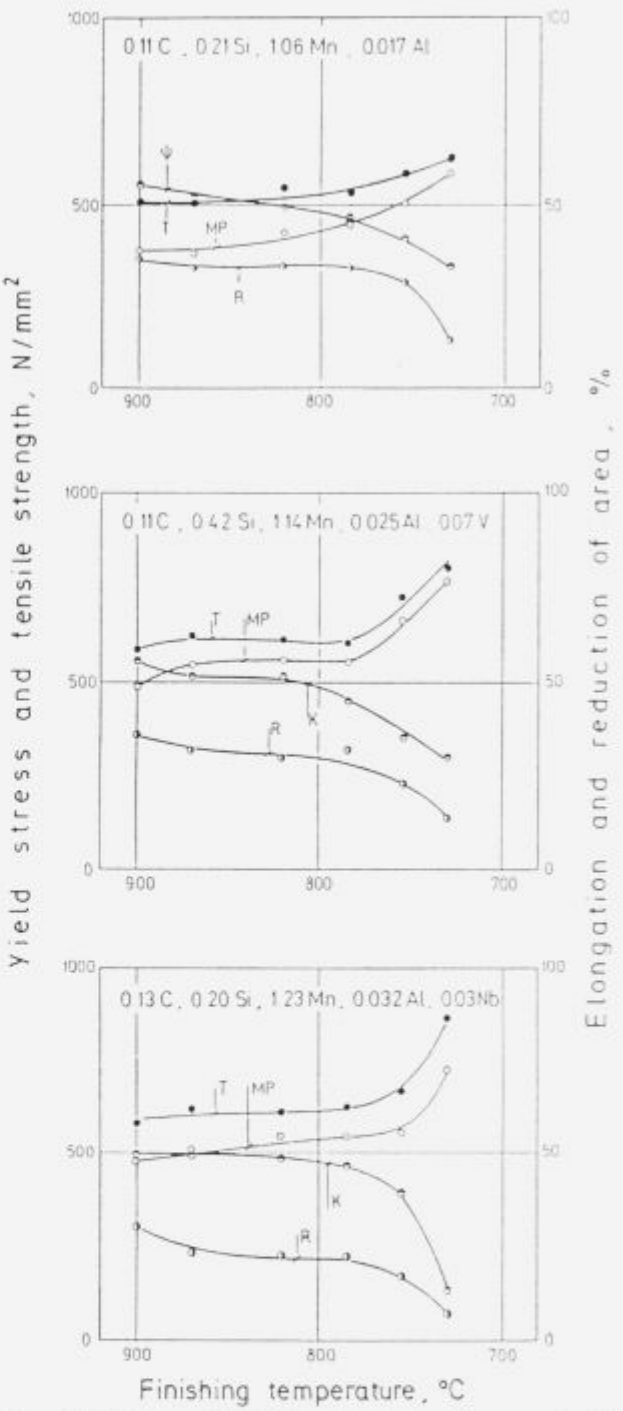

Figure 11. Influence of final rolling temperature on the properties of three steel (Ref.[26]).

Slika 11. Vpliv temperature na koncu valjanja na lastnosti treh jekel. Po viru[26].

in austenite than other phases. **Fig. 4** shows the influence of vanadium and niobium in a case hardening CrMn steel of the same composition, and without aluminium, on the size of austenite grains after annealing at the temperature of 920°C [16]. The equal efficiency in hindering the austenite grain growth is achieved by an about 5 time smaller content of niobium. The reason is the previously mentioned higher solubility of vanadium carbonitride in austenite at the nor-

malizing temperature. The better efficiency of niobium in the control of the austenite grain size indicates that it is a more economic microalloying element. Its deficiency is a lower precipitation hardening during the cooling after the normalizing, thus the properties of steels are improved only because of grain refining. In order to estimate the economy of microalloying it is necessary to know also the interacting effects of dispersoide phases, i.e. the capability of an element to disintegrate the dispersoide phase of other elements, the reactivity of microalloying elements with other elements in steel which do not form efficient dispersoide phases, the diffusivity of microalloying elements, and their minimal efficient contents. Data on the free formation energies of dispersoide and on the diffusivities of microalloying elements in austenite are gathered in **Table 2.** The higher is energy of formation the greater is the stability of the dispersoide phase.

Table 1.

Element		Dispersoide
A, %	B, %	
Al 0.01	Al 0.015 at 0.008 N	AlN
Nb 0.024	Nb 0.036 at 0.18 C	NbC
Ti 0.015	Ti 0.022 at 0.18 N	TiC
V 0.018	V 0.039 at 0.02 N	VN
	V 0.15 at 0.18 C	VC
	V 0.05 at 0.5 C	VC

A—Content of microalloying element which ensures an equal volume of precipitates, and
B—Minimal content of microalloying element which hinders the growth of austenite grains at 920°C.

Table 2. Free energies of formation of dispersoide and the diffusivities of constitutive metals

Free energy of formation				Diffusivity, cm^2/s
kcal/mole		kcal/mole		at 920°C
AlN	46.7			Al 7.0×10^{-9}
TiN	53.5	TiC	40	Ti 7.3×10^{-12}
VN	17.5	VC	18	
NbN	32	NbC		Nb 8.85×10^{-12}

The most stable compound is titanium nitride. At simultaneous presence of several microalloying elements, nitrogen will in equilibrium conditions first of all bind to titanium, probably already in the melt, during the solidification, or soon after the solidification of steel. Titanium consumed, nitrogen can bind to aluminium, then to niobium, and finally to vanadium. This occurs only at annealing which ensures the equilibrium. By shorter annealing, also at normalizing, also the rate of precipitation must be considered. The latter is the higher the higher is diffusivity of cations in austenite (nitrogen and carbon are interstitials and their diffusivity is for several orders of magnitude greater, therefore their diffusion can be neglected when compared with that of aluminium, titanium, etc.). Therefore the highest formation rate would be expected for AlN, than by VN, NbN, and finally TiN. The rate of precipitate formation depends also on the content of microalloying elements in the neighbourhood of precipitation nuclea. The greater is the content expressed in atom.% the higher is its amount in precipitate though its diffusivity is lower than the diffusivity of element with a smaller content in steel.

Among the carbides the most stable is titanium carbide, followed by niobium, and finally vanadium carbide which is completely dissolved in austenite already at the normalizing temperature. Also the solubility of vanadium nitride is relatively high. Thus vanadium is efficient as microalloying element for the control of austenite grain size only at concentrations above 0.1%, while at lower contents it produces a precipitation hardening if such hardening is possible due to the thermal regime.

Microalloying elements react also with other elements and form compounds which do not harden the steel neither influence the mobility of austenite grain boundaries, thus they have no influence on the grain size. E.g. aluminium is first bound to oxygen and only then to nitrogen. Similar is the behaviour of titanium which reacts additionally also to sulphur. Niobium and vanadium react in normally deoxidized steel only to nitrogen and carbon. Therefore the microalloying with aluminium and titanium is efficient only if care is taken that they are not consumed in reactions to oxygen or oxygen and sulphur.

Considering all the influential parameters, the microalloying with aluminium is the least expensive. In steel manufactured by melting in electric arc furnace one finds habitually 0.008 to 0.012% nitrogen and thus with 0.02% aluminium which is not bound to oxygen a sufficient stability of austenite grains is achieved if the annealing temperature does not exceed 920°C. For additional safety a higher content of aluminium 0.025 to 0.030% is recommended. Greater amount does not increase the effect of microalloying since the solubility of AlN in austenite is diminished and a higher temperature of heating of the steel before rolling is required. This is not economical and it is often also harmful for the steel properties after the rolling. A higher aluminium content is also not required for deoxidation since already 0.01% Al reduces the solubility of oxygen in steel melt to about 5 ppm[27]. Aluminium does not bind to carbon and sulphur therefore its efficiency does not depend on the amount of those two elements in steel. Data on the AlN solubility in austenite containing medium and high concentrations of carbon are not disponible, therefore it is not known whether the solubility product in those steels is equal to that in steel with up to 0.2% C. Also if the solubility product would be the same, a different effect of the same quantity of precipitates as in the lower carbon steel is to be expected. The reason is that the mobility of austenite grain boundaries depends also on the surface energy of austenite which further depends on the quantity of alloying elements and impurities in solution.

Titanium diminishes the effect of AlN since it could desintegrate this phase at longer annealing, e.g. during the case hardening annealing. Titanium decreases also the effect of niobium and vanadium. Therefore the combination of titanium and other microalloying elements does not give an effect proportional to the level of alloying. Also the combination of aluminium and vanadium is not especially efficient at a normal nitrogen content, it is successful only by a nitrogen content of above 0.015% and a vanadium contents over 0.1%. This is used in modern steel for thermomechanical (controlled) die forging of parts for car motors. Forgings made of those steel do not require the heat treatment after forging because the controlled cooling ensures a suitable microstructure of steel and the required combination of strength and toughness. This steel contains also 0.01 to 0.02% Ti with the aim that TiN precipitates formed at the

cooling after the solidification (**Fig. 12**), hinder an excessive austenite grain growth during the heating before the die forging. In order to achieve an efficient complex microalloying of such steel with aluminium, nitrogen, vanadium, and titanium it must be continuously cast into billets with a cross sections up to 150 × 150 mm with magnetic stirring.

Therefore it is evident that the most suitable combination of microalloying elements in standard steel with normal nitrogen is aluminium, niobium, and vanadium. The first is bound to nitride, the second into carbonitride with about 90% of carbide, therefore they do not interfere mutually. Both are efficient during the rolling, while vanadium contributes for the precipitation hardening during the cooling from the rolling or normalizing temperature. Niobium also does not react with oxygen and sulphur therefore it is all available for the improvement of steel properties.

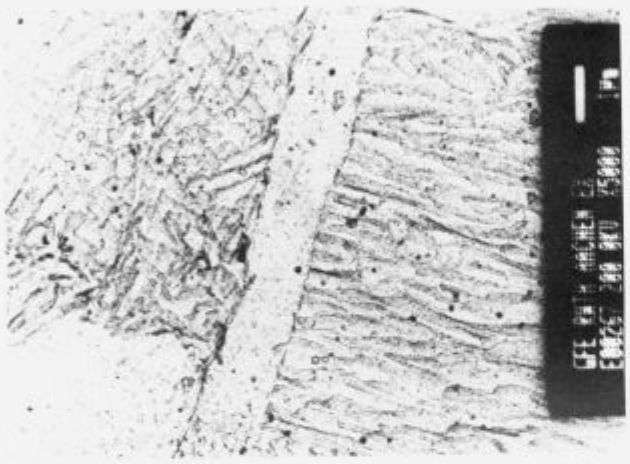

Figure 12. TiN precipitates in steel with 0.32% C, 0.02% Ti, 0.015% N, 0.12% V, 0.025% Al, 0.60% Si, and 1.4% Mn. Carbon extraction replica was prepared from a die forged shaft. TiN precipitates were formed during the cooling below the solidification temperature of steel.

Slika 12. Izločki TiN v jeklu z 0.32% C, 0.02% Ti, 0.015% N, 0.12% V, 0.025% Al, 0.60% Si in 1.4% Mn. Ogljena ekstrakcijska replika je bila pripravljena na utopno skovani ojnici. Izločki TiN so nastali pri ohlajanju kmalu pod temperaturo strjenja jekla.

Titanium also reacts with oxygen and sulphur, therefore an economic microalloying required a good preceding deoxidation and desulphurisation of the steel, i.e. oxygen and sulphur must be bound to aluminium and calcium before titanium is alloyed. The solubility of titanium nitride in molten steel is small, and TiN is formed in the melt already by 0.02% Ti and 0.015% N. Titanium nitride formed in the melt on during the solidification is useless or even harmful. Recent references[28] recommend the titanium contents in steel for controlled forging to be close to 0.01% which ensures that more nitrogen is free for binding into VN precipitates below the solidification temperature which hinder the grain growth at heating before the forging.

In general for structural steels the aluminium/niobium/vanadium combination is the most efficient and the majority of microalloyed steel is based on. The steels for controlled forging and some steels for strips represent an exception. Additional effects are due to the fact that niobium strongly hinders the interpass static recrystallization of austenite already at the level of microalloying. Titanium is used in some hot rolled strips, steels for controlled forging, and case hardening steels with higher grain stability and a narrow-band hardenability microalloyed also with boron. The role of titanium in these steels is not the control of austenite grain size or precipitation hardening but the prevention of the binding of boron to nitrogen which is a precondition for the strong boron effect on steel hardenability.

7 Summary

The paper gives a short review on the influence of aluminium, niobium, titanium, vanadium and nitrogen as microalloying elements on the properties of steel. The size and stability of austenite grains, dispersoide phases formed from microalloying elements, precipitation hardening, influence of microalloying elements on the hot deformation, and the economy use of various elements for microalloying of steel are discussed.

8 References

1 C. Zener: loc. cit. ref. 2.
2 T. Gladman and F.B. Pickering: Journal of ISI 205, 1967, 653.
3 J.E. Bruke and D. Turnbull: Progr. Met. Phzs. 3, 1952, 220. Loc. Cit.: H.V. Atkinskon: Acta Metallurgica 36, 1988, 469.
4 C. Strassburger› Entwicklungen zur Festigkeitsteigerung der Stahle, Verlag Stahl Eisen, Düsseldorf, 1976.
5 W.E. Duckworth: "Metallurgy of structural steels, present and future possibilities" v: Strong and Tough Steels, ISI STP 104, 1967, 61.
6 D. Drobnjak: Fizička Metallurgija, TH Fakultet, Beograd, 1981, p. 173.
7 F. Vodopivec, M.Gabrovšek in B. Ralič: Metals Science 9, 1974, 324.
8 C.Z. Wagner: Z. Elektrochem. 65,1961, 65. Loc. Cit. F.B. Pickering: "Titanium Nitride Technology" in "Microalloyed vanadium Steels": Ed. Akad. Gorn. Hutn. Krakov, 1990, 79.
9 F. Vodopivec, M. Gabrovšek, M. Kmetič in A. Rodič: Metals Technology 11, 1984, 481.
10 T. Gladman, D. Dulieu in I.D. McIvor: "Structure-Properties Relationships in High Strength Microalloyed Steels" in Micro-Alloying 75, UEC, New York, 1977, 32.
11 K. Narita: Trans. ISJ 15, 1975, 145.
12 S. Matsuda in N. Okamoto: Trans. ISJ 18, 1978, 198.
13 F. Vodopivec: Metals Technology 1978, 118.
14 M.J. Grooks, A.J. Garrath-Reed, J.B. Vander Sandi in V.S. Owen: Metallurgical Transactions 12A, 1981, 1999.
15 B. Dutta in A.C. Sellars: Materials Science and Technology 2, 1986, 146.
16 M. Korchinsky; private communication.
17 E. Hornbogen: "Verfestigungsmechanismen in Stahlen" v Die Verfestigung von Stahl: Climax HB, 1969, 1.
18 E. Hornbogen in E. Minuth: Arch. Eisenh. 44, 1973, 621.
19 R.B.G. Jeo, A.G. Melville, P.E. Repas in J.M. Gray: J. Metals 20, 1968, 33.
20 F. Vodopivec in M. Gabrovšek: Železarski zbornik 21, 1987, 19.
21 J.J. Jonas in I. Weiss: Metal Science 3, 1979, 238.
22 I. Weiss in J.J. Jonas: Metallurgical Transactions 11A, 1980, 403.
23 F. Vodopivec, M. Kmetič in A. Rodič: Železarski zbornik 18, 1984, 9.
24 A. le Bon, J. Rofes-Vernis in C. Rossard: Metals Science 9, 1975, 36.
25 D. Kmetič, F. Vodopivec in M. Gabrovšek: Železarski zbornik 14, 1980, 39.
26 F. Vodopivec, M. Gabrovšek, J. Žvokelj in M. Kmetič: Metallurgical Science and Technology 8, 1991, 103.
27 E.T.T. Turkdogan: Arh. Eisenh 54, 1983, 1
28 T. Shiraga, K. Matsumoto, S. Suzuki, M. Ichiguro, H. Kido in T. Abe: NKK Technical Review 53, 1988, 1.

Kovine, zlitine, tehnologije / letnik 26 / številka 4 / strani 329 do 331 / 1992

The Dependence of the Heat Energy Consumption upon the Working Intensity and the Frequency of the Isolation Maintenance of a Pusher-type Furnace

Ovisnost utroška toplinske energije od intenziteta rada i učestalosti održavanja izolacije potisne peći

J. Črnko, *Metalurški fakultet Sisak, Aleja narodnih heroja 3, 44103 Sisak*

The paper covers investigations of the specific heat energy consumption dependence upon the productivity and frequency of the isolation maintenance in a pusher-type furnace of a strip and billet rolling mill.

U okviru ovog rada istraživana je ovisnost specifičnog utroška toplinske energije od produktivnosti i učestalosti održavanja izolacije na primjeru potisne peći u valjaonici traka i gredica.

1 Introduction

Systematic decreasing of the fuel consumption per unit of a product should be one of the most important tendencies in Yugoslav rolling mills. However, the dynamics of the specific fuel consumption decreasing has recently been stopped in some heating furnaces and has assumed, for the various reasons (mostly objective), an inversed trend. Thus, even a decreased working intensity of heating furnaces leads to an increased specific fuel consumption. This often happens to appear in the rolling mills mentioned, especially lately. This is the reason that the paper deals with the investigation of the specific heat energy consumption dependence upon the productivity of heating furnaces and, especially, upon the frequency of isolation maintenance on the example of one of the two pusher-type furnaces of a Sisak Ironwork's strip and billet rolling mill (Sisak, Croatia).

2 Heat energy balance and fuel consumption

Rough values for specific fuel consumption decreasing in the case of increased working intensity of heating furnaces can be obtained by heat energy balance[1,2]. The total heat energy consumption ($\sum E_i$) can be derived into two groups:

1. one depending on the mass of steel being heated in a certain heating furnace:
   - heat energy of steel being heated (E_1),
   - heat energy of scrap developing in the course of steel heating (E_2),
   - heat energy losses (through the walls to the outside, by cooling water etc.) independently to the mass of steel being heated (E_3);
2. one depending on the level of fuel utilization in a certain heating furnace:
   - heat energy losses because of mechanical unburning, incomplete chemical combustion and by fuel gases going out (E_4).

Obviously, it is (per unit share)

$$E_1 + E_2 + E_3 + E_4 = 1 \tag{1}$$

First, let's take that a quantity of conditional fuel X_n is consumed to heat a mass of steel M_n, i.e.

$$E_1 X_n + E_2 X_n + E_3 X_n + E_4 X_n = X_n \tag{2}$$

If the intensity of steel heating increases z times, the consumption of the conditional fuel increases up to the value of X_z, and the equation (2) takes the following form:

$$z(E_1 + E_2)X_n + E_3 X_n + E_4 X_z = X_z \tag{3}$$

From the equation (3) we can now derive a quantity of the conditional fuel X_z, i.e.

$$X_z = X_n \left(\frac{z(E_1 + E_2) + E_3}{1 - E_4} \right) \tag{4}$$

Based on these, it is possible to define a decrease of the specific fuel consumption, as a result of the intensity of steel heating increased z times, as follows:

$$\begin{aligned} \Delta x &= \left(\frac{X_n}{M_n} - \frac{X_z}{M_z} \right) \cdot 100 = \\ &= \left(\frac{X_n}{M_n} - \frac{X_z}{zM_n} \right) \cdot 100 = \\ &= \left(\frac{X_n}{M_n} - \frac{X_n \left(\frac{z(E_1+E_2)+E_3}{1-E_4} \right)}{zM_n} \right) \cdot 100 = \\ &= \frac{X_n}{M_n} \left(1 - \frac{z(E_1 + E_2) + E_3}{z(1 - E_4)} \right) \cdot 100 \end{aligned} \tag{5}$$

Consequently, as a result of the increased working intensity of the heating furnaces, i.e. the process of steel heating being intensified z times, the the specific fuel consumption (in %) will be decreased in a ratio:

$$\left(1 - \frac{z(E_1 + E_2) + E_3}{z(1 - E_4)} \right) \cdot 100. \tag{6}$$

3 Main characteristics of a pusher-type furnace

A three-zonal pusher-type furnace observed, designed by American Rust Furnace Co., was built in the year 1972. Beginning from the charging side the furnace has a preheating zone, a heating zone and a soaking zone. In the preheating and heating zone a charge was heated both from the upper and the lowes side, whereas in the zone of soaking it was heated only from the upper side. Burners were installed laterally on the furnace, above and below the charge in the preheating and heating zone. In the preheating zone five burners were installed above the charge and five burners below the charge. Two burners were installed above the charge on one side and three on the other side of the furnace. The burners were also installed below the charge, but placed inversely to those above the charge. In the heating zone six burners were installed above the charge and six burners below the charge. On each side of the furnace three burners were placed above the charge and three below the charge. In the soaking zone six burners were placed on the frontal side of the furnace. Otherwise, the furnace is not of a conventional profile and is of a conventional temperature regime[3]. By operating measurements it was found that the firing from the lower side and that from the upper side have the equal efficiency. The furnace profile, as well as its main dimensions are presented schematically in **Fig. 1.**

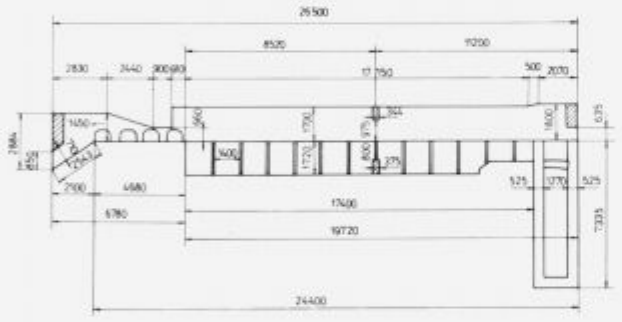

Figure 1. Schematic presentation of a pusher-type furnace profile.
Slika 1. Shematski prikaz profila potisne peći.

During the energetic balancing slabs of St 12 (per DIN) quality, dimensions of 430 × 190 × 3800 mm and mass of 2500 kg singly were heated in the pusher-type furnace. The furnace was fired by natural gas having the heating value of 37300 kJ/m^3. Gas consumption was 2347 m^3/h, and consumption of air necessary for its combustion was 24286 m^3/h. Air temperature at the metal recuperator exit was 300°C. According to the request of the rolling mill train the furnace productivity was kept at 37 t/h, and the slabs were heated up to the final temperature of 1230–1250°C. However, the furnace was designed to achieve the productivity of 67 t/h when heating slabs of stated quality and dimensions. This shows that the coefficient of capacity utilization of the furnace was about 0.55, which indicates that working intensity of the furnace can be increased 1.81 times.

4 Fuel consumption dependence upon the productivity and frequency of a pusher-type furnace maintenance

For a calculation of the specific fuel consumption decrease heat energy consumption in a pusher-type furnace was found.The heat energy consumption (per single items) in the furnace when heating the slabs of the stated quality and dimensions is given in **Table 1.**

Table 1. Heat energy consumption in a pusher-type furnace when heating slabs of St 12 quality and dimensions of 430 × 190 × 3800 mm

Heat energy consumption items	Quantity of heat energy	
	MW	%
E_1	8.998	33.32
E_2	-	-
E_3	6.108	22.61
E_4	11.902	44.07
$\sum E_i$	27.008	100.00

The following step enables to find out how much the specific fuel consumption decreases if the working intensity of the furnace increases 1.81 times.

Applying the equation (6) we get that the specific fuel consumption decreases for 18.09%, providing that, as stated, the working intensity of the pusher-type furnace increases 1.81 times, i.e.

$$\left(1 - \frac{1.81 \cdot 0.3332 + 0.2261}{1.81(1 - 0.4407)}\right) \cdot 100 = 18.09\%$$

The value obtained also anables calculating the specific fuel consumption in the case that the furnace works full capacity. Results of such a calculation show that the specific natural gas consumption in the furnace decreases from 63.43 to 51.96 m^3/t, corresponding to the decrease of the specific heat energy consumption from 2366 to 1938 kJ/kg, i.e. for 428 kJ/kg.

To get a real picture of the dependence of the specific heat energy consumption upon the working intensity of the puscher-type furnace, a three-years period of the furnace work has been analyzed. Only the data referring to the furnace work during the St 12 quality slabs of 430 × 190 × 3800 mm dimensions being heated were delt with. The dependences of the specific heat energy consumption upon the furnace productivity being got that way are presented in a form of a diagram in **Fig. 2.**

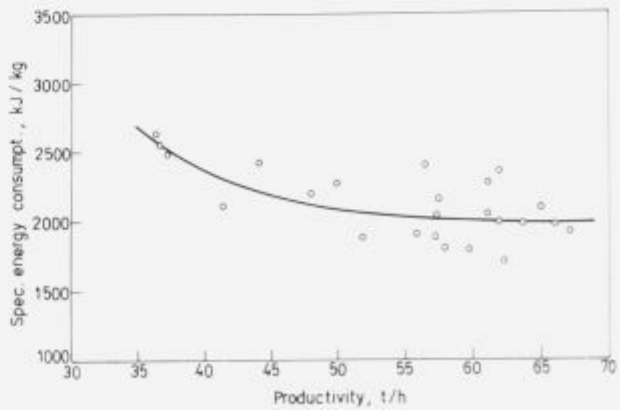

Figure 2. The dependence of the specific heat energy consumption upon the pusher-type furnace productivity.
Slika 2. Ovisnost specifičnog utroška toplinske energije od produktivnosti potisne peći.

Volume in m^3 refers to a normal state.

Comparing the calculated values for the specific heat energy consumption with those obtained by operating measurements for the stated quality and dimensions of the charge, the results of which are presented in a form of a diagram in **Fig. 2,** we can see that the differences are relatively small. Considerable differences are the consequence of including a consumption of natural gas for "blank" firing to the operating data on the natural gas consumption. Also, the changes of energetic losses per items of energetic balance, in the course of the furnace utilization for its isolation reparation between the two stoppings, can bring to some bigger differences between the calculated and operating values for the specific heat energy consumption in a certain furnace productivity.

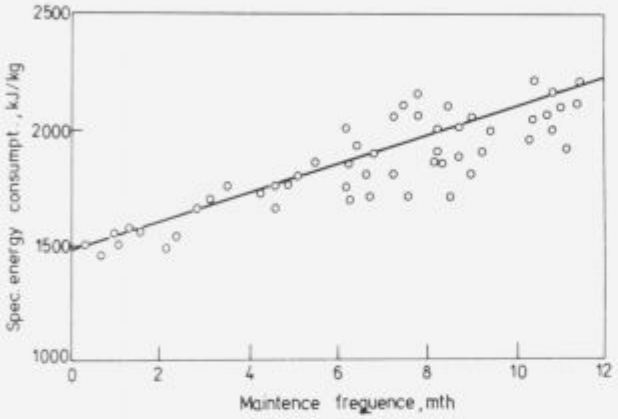

Figure 3. The dependence of the specific heat energy consumption upon the frequency of the isolation maintenance and the pusher-type furnace floor cleaning.

Slika 3. Ovisnost specifičnog utroška toplinske energije od učestalosti održavanja izolacije i čišćenja poda potisne peći.

The analysis carried out for the furnace work between its last two stoppings, because of the beam cleaning and of the isolation reparation, showed that with the productivity of 50 t/h (realized annual productivity) the specific heat energy consumption increases from the initial 1480 to the final 2240 kJ/kg, in other words the average value is 1860 kJ/kg (**Fig. 3**). Beside others, the course of that is almost up to 80% of refractory mass falls off the skid carrier so that energy losses by cooling water are considerable[4]. The increase of isolation maintenance frequency, as well as that of beam cleaning from the layers, to the half of time (6 months) of the previous (12 months) would decrease the average heat energy consumption from 1860 to 1670 kJ/kg (**Fig. 3**), i.e. for 190 kJ/kg.

However, for a rather long period of time in some western countries a quartal frequency of pusher-type furnaces[5] maintenance has been practised, so regarding to this, there are no reasons to make the first step in our strip and billet rolling mills as well.

5 Summary

Results obtained analytically show that the specific heat energy consumption decreases for about 18% if the productivity of the pusher-type furnace observed increases from 37 to 67 t/h. Also, the operating data analysis of the furnace work does not show significant deviations from the results obtained analytically. However, because of the lack of coordination between pusher-type furnaces and rolling mill train capacities, even in normal production conditioris it is impossible to realize. The same way, the increase of the pusher-type furnace isolation maintenance frequency and that of the layers removal from the floor to the period of 6 from so far 12 months, would decrease the specific heat energy consumption for about 10%. This can be realized successfully by better month and week planning of rolling, which would assure heating of the charge having the same quality and dimensions in the course of a few weeks. In such a case it could be possible to stop one of the furnaces if another's passing capacity per hour would satisfy the requests of the rolling mill train. Such periods sometimes occure now, too, as well as those in which plans of rolling change from shift to shift together with plans of heating.

6 References

[1] W. Heiligenstaedt: Wärmetechnische Rechnungen für Industrieofen, Verlag Stahleisen M.B.H., Düsseldorf, 1956, s 6–13

[2] A.N. Nesenčuk et al.: Ognetehničeskie ustanovki i toplivosnabženie, Izdatel'stvo "Vyšejšaja škola", Minsk, 1982, s 35–46

[3] V.A. Krivandin, JU.P. Filimonov: Teorija i konstrukcii metallurgičeskih pečej, Izdatel'stvo "Metallurgija", Moskva, 1986, s 360

[4] Ž. Acs, Lj. Milić, M. Kundak: Zbornik IV. savetovanja "Energetika i zaštita čovjekove sredine u crnoj metalurgiji", UJŽ Beograd, Herceg Novi, 1985, s 119–125

[5] L.J. Grafe: Improving energy utilization in steel reheat furnaces, Iron and Steel Engineer, Vol. 62, No 1, 1985, s 43–47

Kovine, zlitine, tehnologije / letnik 26 / številka 4 / strani 333 do 335 / 1992

Tool-steel Wire Drawing at Elevated Temperatures

Vlečenje žice iz orodnih jekel pri povišanih temperaturah

B. Arzenšek, B. Šuštaršič, G. Velikajne, *Inštitut za kovinske materiale in tehnologije, Ljubljana*
I. Kos, K. Zalesnik, F. Marolt, *Železarna Ravne, Ravne na Koroškem*

Tool steels have in cold state very low workability, therefore they must be frequently recrystallization annealed during the cold drawing process, but some types of steels cannot be cold drawn at all. Their working properties are highly improved at elevated temperatures. This paper analyzes the drawability of wire, made of BRM2 (W.NR-1.3343) steel, and it describes the technology of wire drawing at temperatures up to 700° C.

Orodna jekla imajo v hladnem stanju zelo slabe preoblikovalne sposobnosti, zato jih moramo med hladnim vlečenjem velikokrat rekristalizacijsko žariti, nekatera jekla pa hladnega vlečenja sploh ne prenesejo. Njihove preoblikovalne sposobnosti se precej izboljšajo pri povišanih temperaturah. V delu smo ugotavljali vlečne sposobnosti žice iz jekla BRM2 (W.NR-1.3343) in opisali tehnologijo vlečenja žice pri temperaturah do 700° C.

1 Introduction

High-speed tool steel of BRM2 type is mainly used for tools and spiral drills for machining of steels and alloys, and for manufacturing of high-quality wear-resistant tools. Wear resistance of steel is achieved by a great number of fine secondary carbides which are in the ferritic matrix of steel. Carbides do not give only a high wear resistance of steel but they also contribute to an intensive hardening of steel in cold workability. Thus the wire made of BRM2 steel can sustain in cold drawing almost 20% partial and approximately 45% total reduction degree, therefore it must be more than six times intermediately recrystallization annealed in drawing from 8 to 2 mm diameter. Such a manufacturing of fine wire is rather expensive and long lasting.

Drawability of steel is rather improved at elevated temperatures when wire can be drawn to fine dimensions without intermediate recrystallization annealing. The first drawing tests at elevated temperatures (worm drawing) were made with shorter lengths of wires, and it was found that wire can be drawn at 700°C even to the diameter of 3 mm. Based on results of drawing tests to thin dimension wires, which will be described in details, the technology for worm drawing of wires in coils was prepared.

2 Drawability of the steel at elevated temperatures

Drawing tests of thin wires showed that drawability of BRM2 steel is optimal at 700°C and 15% reduction degree. Drawability of the steel was determined from numbers of draws which wire sustained at various temperatures and from yield stresses calculated by following mathematical expression:

$$q_m = \frac{F_i}{\Delta A_i},$$

where is:

q_m	yield stress in N/mm^2,
F_i	drawing force in N/mm^2 and
ΔA_i	cross-section reduction in single draw in mm^2.

Yield stresses and number of draws, which wire of BRM2 steel sustained at various drawing temperatures, are presented in **Fig. 1.** The plot shows that the wire sustains

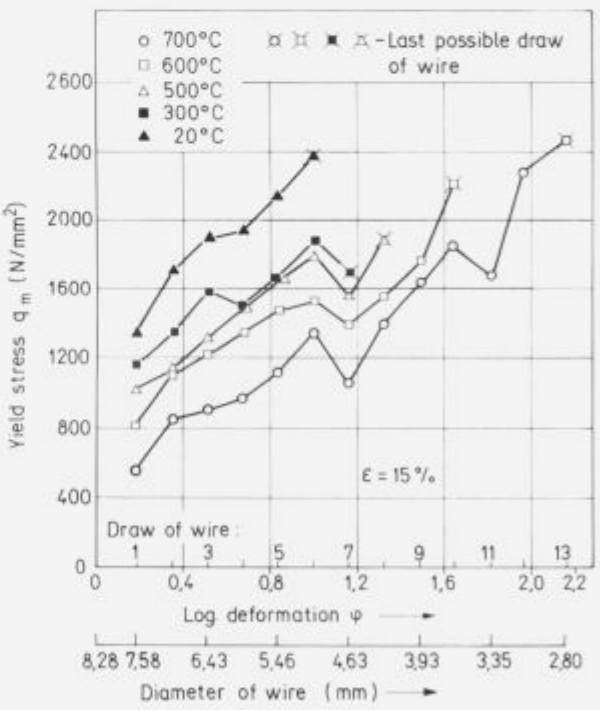

Figure 1. Yield stresses at wire drawing of BRM2 steel at elevated temperatures.
Slika 1. Preoblikovalne napetosti pri vlečenju žice iz jekla BRM2 pri različnih temperaturah.

the cold-drawing reduction without recrystallization annealing from 8 to 5.5 mm. It can sustain some more draws at temperatures up to 550°C, while at 700°C it can be reduced even to 3 mm. Good workability of the steel can be judged

also by yield stresses which values at 700°C are half of the values like in cold drawing. In hot drawing of the wire the recrystallization annealing is not needed since recovery is achieved by heating wire to the drawing temperature and during the drawing process, and at higher temperatures also recrystallization probably occurs. The described tests were made with 2 to 3 m long wire pieces on drawing bench with a drawing velocity of 0.25 m/s. Drawing conditions on a drawing bench are less demanding than in coil drawing. Therefore wire in coil drawing sustains less draws.

3 Technology of wire drawing at elevated temperatures

The aim in preparing the technology of wire drawing at elevated temperatures was to apply the existent equipment for cold drawing to the maximal extent. This on one side reduces the developing costs of the technology, and on the other side it enables cheaper and simpler transmission of the technology into industrial practice. The scheme of thus designed and also tested line is given in **Fig. 2,** while **Fig. 3** shows the picture of it.

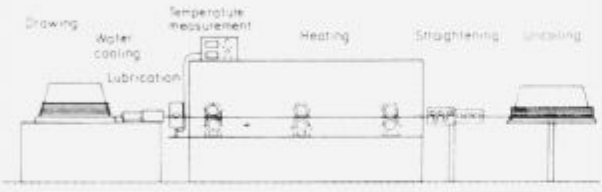

Figure 2. Scheme of wire-drawing line at elevated temperatures.
Slika 2. Shema linije za vlečenje žice pri povišanih temperaturah.

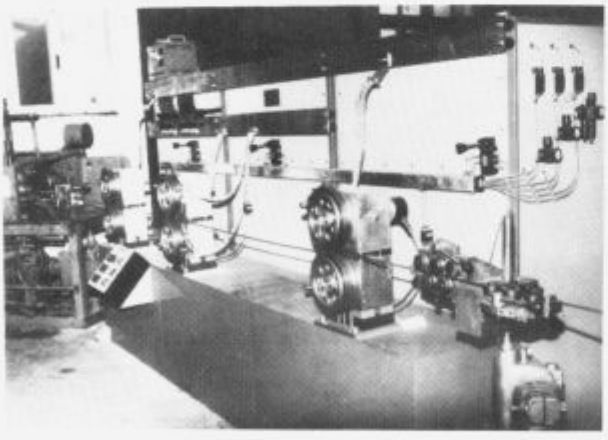

Figure 3. Picture of wire-drawing line at elevated temperatures, built at the Institute of Metals and Technologies in Ljubljana.
Slika 3. Izgled linije za vlečenje žice pri povišanih temperaturah, ki je postavljena na Inštitutu za kovinske materiale in tehnologije v Ljubljani.

The presented line consists of three basic units:

- equipment for conductive heating of wire,
- equipment for temperature measurements on wire during the drawing and
- drawing machine.

In front of the heating equipment also frame for uncoiling and straightening rollers were mounted. In the whole installation only the conductive heating equipment for wire was new. Wire is heated by three pairs of contact rolls. The basic characteristics of the three mentioned units are:

3.1 Heating Equipment

This equipment was purchased at Montanstahl, Switzerland. Its power is 90 kVA, and this was chosen according to the greatest desired diameter 8 mm of heated wire, the highest wire temperature 800°C, and the drawing velocity 0.28 m/s. Heating of wire is a two-stage process. In the interval between the first and second pair of rolls the wire can be heated at most up to 500°C, and between the second and the third pair the temperature is raised further to 800°C. Heating power is adjusted manually while the equipment contains also driwer which prevent overheating of wire in the case of stoppages during the drawing process.

3.2 Equipment for Measuring Wire Temperature

Wire temperature is measured with optical pyrometer. Measuring system is not connected with the heating system, therefore the heating power is regulated manually according to the registrated temperature.

3.3 Drawing machine

Drawing machine is designed for cold drawing of wires thinner than 8 mm. Therefore the drawing drum is constructed in such a way that drawn wire in cold drawing slips uniformly along the drum. Drawing conditions are during the cold drawing rather unchanged. In worm drawing the conditions are changing according to the temperature of worm drawing, wire diameter, and lubrication. In the first worm-drawing tests with the described equipment, slippage of wire on the drawing drum in the upward direction occured, while overlapping of wire windings was experienced with thinner wire. Both phenomena made drawing impossible. The described troubles were solved by mounting special guides for drawn wire which were fixed around the drawing drum. The mentioned guides can be dismounted from the drum after worm drawing so that the same drawing machine can be used also for cold drawing of wire.

Efficiency of worm drawing of wire does not depend only on the sliding of wire along the drawing drum but also on the preparation of wire surface before drawing, on the quality of lubrication, and thus also on the drawing temperature and the wear resistance of dies.

3.4 Preparation of Wire Surface

Efficiency of conductive or contact heating depends a great deal on the quality of contacts between the pair of heating rolls and the heating wire. In bad contacts sparking, incipient melting and quenching of heated wire on contact area can occur. Such an area does not sustain deformation in drawing, and wire breaks. Sparking can occur on badly descaled or rusted areas of wire, therefore the wire surface must be well prepared before drawing. According to the experiences obtained so far, the sandblasted wire surface is the most suitable one especially if it is also copperized. Sandblasted surface is rougher than a pickled one, and thus adhesion of lubricant on the wire surface before drawing is better. Copperizing on the other hand prevents rusting of wire after the drawing.

3.5 Lubrication

In worm drawing lubrication is less effective than in cold drawing, therefore the wire cannot stand higher partial deformations degree than 15%. Graphite was used as lubricant since it was in the regard to persistance and price the only acceptable lubricant which could stand drawing also at temperatures above 500°C. Graphite has good lubrication properties but its adherence to the wire surface is unfortunately weak, therefore it was applied in form of oil paste. Paste has good lubrication power up to 650°C, at higher temperatures its lubrication power is rather reduced due to reduced adherence to the wire surface. Ground and flaky graphite was tested too. A little better lubrication was achieved with flaky graphite but it is rather more expensive. In hot drawing the greatest troubles are caused in lubrication. This problem is not suitably solved, therefore some manufacturerers of fine sections of special steel have substituted hot drawing with rather more expensive microrolling process, where all the problems with lubrication are avoided.

3.6 Wear Resistance of Dies

In drawing hard-metal dies are used so far, but they have good wear resistance only up to 300 or 400°C. At higher temperatures their wear resistance is rather reduced, therefore also ceramic dies, made of silicon carbide, were tested. The mentioned ceramic material has a very good wear resistance even up to 1000°C, but its disadvantages is a low resistance to temperature shocks and its brittleness. In cold and hot drawing tests it was found that ceramic materials stood the drawing process therefore the tests of drawing through ceramic dies will be continued.

In developing the technology of hot drawing of wire a great attention was given also to the yield of drawn wire which is lower than in cold drawing. In hot drawing the beginning and the end of wire coil must be drawn cold. Since BRM2 wire sustains only two coil draws the cold drawn ends should be cut off. Thus the yield of drawn wire is reduced. A trial was made to avoid cutting-off the wire ends by welding another material with good workability on the wire end. The mentioned solution proved as unsuitable due to too long needed times of soft annealing the weld. Therefore the problem was solved by annealing the cold drawn wire ends. For this purpose a special conductive equipment for wire-end annealing was built which enabled annealing of 5 m lengths and thus the yield of BRM2 wire in hot drawing was increased to 100% nearly.

4 Conclusion

Drawing of wire at elevated temperatures rather differs from the cold drawing, therefore many problems appeared in development the drawing technology at elevated temperatures, which were more or less successfully solved to such an extent that already industrial drawing line for wire coils exists. So far over 1500 kg wire of BRM2 steel was drawn from 8 mm to various finer dimensions. The finest diameter of drawn wire was 3,2 mm. The line is improved to such an extent that a large-scale production is negotiated with the Ravne Iron and Steelworks as the tool-steel producer. Double applicability of drawing equipment, i.e. for cold and hot drawing, the developed technology is much cheaper than the competitive microrolling, and it is suitable mainly for smaller manufacturers of various tool steels.

5 References

[1] B. Arzenšek, B. Šuštaršič, I. Kos, K. Zalesnik, F. Marolt, G. Velikajne: Tehnologija vlečenja jekla BRM2 pri povišanih temperaturah, Poročila inštituta za kovinske materiale in tehnologije v Ljubljani, Nal. št. 91-035, Ljubljana, 1992

[2] K.D. Maraite: Ein Beitrag zur Optimierung des Halbwarmziehens, Stahl und Eisen, Umformtechnische Schriften - Band 13, 1988, Verlag Stahleisen, Düsseldorf

[3] H. Tzscheutschler: Untersuchungen der Einsatzmöglichkeiten des Halbwarmziehens, Doktor Dissertation, Aachen, 1982

[4] B. Arzenšek, I. Kos, A. Godec: Vlečenje žice iz orodnega jekla Č.7680 - II. del, Poročila Metalurškega inštituta v Ljubljani, nal. št. 85-063, Ljubljana, 1985

[5] B. Arzenšek, I. Kos, A. Godec: Vlečenje jekla Č.7680 pri povišanih temperaturah, Poročila Metalurškega inštituta v Ljubljani, Nal. št. 86-037, Ljubljana, 1986

[6] I. Kos, B. Šuštaršič, B. Arzenšek, V. Leskovšek: Razvoj tehnologije vlečenja pri povišanih temperaturah - II. del, Poročila Metalurškega inštituta v Ljubljani, nal. št. 80-018, Ljubljana, 1990

TEHNIČNE DEJAVNOSTI

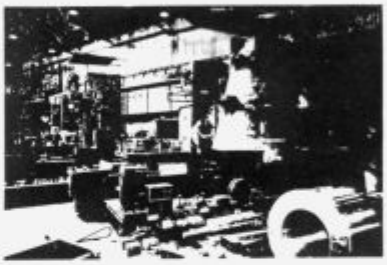

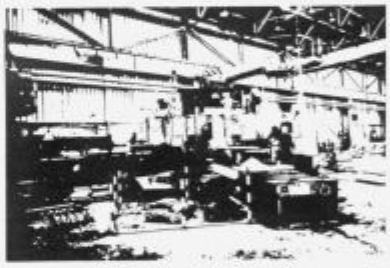

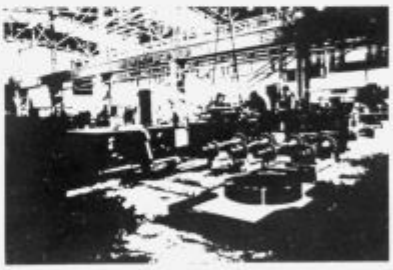

ERZ — elektro delavnice, regulacija in zveze

- elektroinstalacijska dela in popravila elektro motorjev
- popravila in remonti regulacijskih sistemov
- montaža in popravila klimatizacijskih in tehtalnih naprav
- servis ročnih električnih in gospodinjskih strojev
- izdelava in vzdrževanje žičnih, brezžičnih in računalniških zvez

SD — strojne delavnice

- izdelava in popravilo strojnih rezervnih delov
- termična obdelava
- izdelava odkovkov do teže 30 kg
- izdelava in popravilo orodij in hidravlične ter pnevmatske opreme
- izdelava in kompletiranje metalurške in sorodne opreme

KD — konstrukcijske delavnice

- izdelava, popravila in montaža jeklenih konstrukcij
- metalizacija in navarjanje delov z različnimi dodajnimi materiali
- popravila in remonti žerjavov in žerjavnih prog

KOVIN — kovinska industrija

- izdelava opreme in elementov za gradbeništvo
- izdelava hlevske opreme
- izdelava proizvodov galanterije za trg in kooperacijo
- izdelava delov za manjše individualne naročnike

OD — obrtne delavnice

- obrtna kleparska in plastičarska dela
- izvedba sanitarnih, toplotnih, mazalnih in hidravličnih ter ostalih industrijskih instalacij
- izdelava in montaža lesnih izdelkov za manjše serije in individualne naročnik

TIDN — tehnične izboljšave delovnih naprav

- projektiranje delovnih naprav (strojno, elektro, hidravlično in pnevmatsko)
- projektiranje in uvajanje procesno vodenih tehnoloških procesov

ŽELEZARNA JESENICE

64270 JESENICE, Cesta Železarjev 8 - telefon: (064) 81-341, 81-441, 84-262 - telefax: (064) 83-395 - telex: 37-219, 37-212 zeljsn - telegram: Železarna Jesenice

Kovine, zlitine, tehnologije / letnik 26 / številka 4 / strani 337 do 342 / 1992

Resistance of Structural Steel to Crack Formation and Propagation

Odpornost gradbenih jekel proti nastanku in širjenju razpoke

P.D. Odesskij, *Centralnij naučnoisledovatelnij institut strojitelnih konstrukcij, im. V.A: Kučerenko, Moskva*
N. Kudajbergenov, *Kazahskoj Himiko—tehnologičeskij institut, Čimket, Kazahstan*
L. Kosec, *FNT, Odsek za metalurgijo in materiale, Ljubljana*
F. Kržič, *FAGG, Jamova 4, Ljubljana*

Parameters of linear fracture mechanics can be a useful measure for selection of steel with various strength and yield stress (in limits 200 to 1000 MPa). They determine also influence of purity (non-metallic inclusions) and of thermal or thermomechanical treatment.
These parameters are effective only if they are measured in the conditions when the plastic deformation at the initial crack growth is limited to minimal value. This happens in corrosion media by measuring K^c_{IC} and especially in impact loading by measuring K^d_{IC}. These parameters are closely connected with the microstructure and structure of steel. They are suitable for designing structures resistant to brittle fracture if operational (destruction) conditions of those structures are seized, since they occur at high preceeding plastic deformations.

V članku razpravljamo o načinih zboljšanja efektivnih parametrov linearne mehanike loma, ki so merilo kvalitete gradbenih jekel in osnova za izračun konstrukcij odpornih proti krhkemu prelomu. Predmet raziskave je bila skupina maloogljičnih in malolegiranih jekel z napetostjo tečenja 200–1000 MPa. Po kemični sestavi spadajo ta jekla v štiri skupine: maloogljična, mangan silicijeva, manganova mikrolegirana jekla in kompleksno legirana jekla z 0.2–0.6% Mo.
Po trdnosti lahko omenjena jekla razdelimo v tri skupine: v skupino z napetostjo tečenja do 290 MPa (normalna trdnost); v skupino z napetostjo tečenja do 390 MPa (povišana trdnost) in v skupino jekel z napetostjo tečenja več kot 390 MPa (visoka trdnost).
Lomne karakteristike smo raziskovali pri statičnih in dinamičnih obremenitvah ter v korozijskem mediju. Raziskave smo opravili v skladu z GOST in mednarodnimi standardi, pa tudi po originalni metodiki. Največ smo uporabljali epruvete z ekscentrično obremenitvijo (CTS) (sl. 1), dvojno konzolno vpeto klinasto epruveto (sl. 2) in cilindrične preizkušance s koncentrično krožno zarezo z utrujenostno razpoko kot koncentratorjem napetosti (sl. 3). Pri statičnih obremenitvah smo ugotovili pomembne posebnosti v rasti vrednosti K_{IC} s trdnostjo jekla takrat, ko je imelo valjano jeklo "racionalno" mikrostrukturo. Ugotovili smo tudi, da raste vrednost K_{IC} v jeklih s povišano in visoko trdnostjo s čistostjo jekla. Istočasno pa ti parametri niso zelo tesno povezani z mikrostrukturo jekla. Njihova uporaba v inženirskih izračunih pa omogoča oceniti velikost nevarnih napak v konstrukcijah. V članku je tudi pokazano, kako je moč z omejitvijo obsega plastične deformacije (pri dinamičnih preizkusih ali v korozijskih medijih) povečati občutljivost parametrov linearne mehanike loma od mikrostrukture jekla. Te parametre je moč privzeti kot efektivne, kar je na koncu članka prikazano s primerom izračuna primarnega dela plinovoda iz malolegiranega jekla.

1 Introduction

In steel structures good weldable low-carbon and low-alloyed steel with yield stress 200 to 800 MPa are used. In the recent time the resistance of those steels to brittle fracture is more frequently estimated by parameters which caracterize the crack stability[1,2]. Steel resistance to brittle fracture is highly dependant on its microstructure. Thus the mechanical properties of steel, especially the parameters determining the crack stability, are useful in estimating the resistance to brittle fracture. This is especially valid when the value of those parameters is microstructurally a highly sensitive value.

It is very advantageous if those parameters are applicable in designing structures. This condition is fulfilled the more completely the better description of fracture conditions is achieved in this way.

Paper describes the decisive effective parameters of crack stability which are highly dependent on microstructures as a measure of useful properties of structural steel, and they can be also simply applied in engineering design of structures which must be resistant to brittle fracture.

2 Testing of Steel

Plates of all structural steel types being used in former Soviet Union were investigated with a special emphasis on those standardized in GOST 27772-88. Steels differ by their composition, strength, and way of manufacturing.

Steels with yield stresses 230 to 285 MPa are characterized as steel with standard strength, while higher-strength steels had yield stresses 290 to 375 MPa, and high-strength ones above 390 MPa. According to chemical composition the treated steels can be divided in four groups:

- low-carbon steels with up to 0.22% carbon,
- low-alloyed steels, mainly manganese-silicon ones (12G2S, 09G2S, 14G2),
- manganese microalloyed steels (14G2AF, 09G2FB,...),
- complex molybdenum-alloyed steels (12GN2IFAJU).

Classification and composition of those steels is particularly described in ref.[2]. The guaranteed values of yield stresses of the discussed steels after standard working or heat-treatment processes are described in **Table 1.**

Table 1. Guaranteed values of yield stresses of investigated structural steels

Steel	Guaranteed yield stress (MPa)		
	Hot rolled	Normalized	Hardened and tempered
Low-carbon	230–285	230–285	285
Manganese-silicon	335–375	335–375	390
Manganese microalloyed	-	390–440	490
Complex molybdenum alloyed	-	-	590–740

(-) due to low resistance to brittle fracture, the steel is not used in such a state

Steels of the third group (e.g. 09G2FB) are used either as controlled by rolled, or like some others of that group as thermomechanically treated by various processes detailed described elsewhere[2].

3 Investigation Methods

Estimation of the crack stability in ductile structural steel has some specialties. Increase of nominal stress can exceed the yield stress on the crack front in these steels. In all cases it happens before the stress intensity factor reaches its critical value.

At that time plastic deformation takes place at the crack tip in the zone of r_T size (Fig. 4). The size of r_T zone is for the case of plane-stressed state equal to:

$$r_T = \frac{1}{2\pi} \cdot \frac{K_{IC}^2}{\sigma_T}, \qquad (1)$$

and in the case of plane-strain state equal to:

$$r_T = \frac{1}{6\pi} \cdot \frac{K_{IC}^2}{\sigma_T}, \qquad (2)$$

In the conditions of actual stress and strain states during the testing, the size of plastic deformation zone is between the two extremes. The conditions in our testing corresponded to the following size of plastic deformation zone:

$$r_T \approx 0.1 \cdot \frac{K_{IC}^2}{\sigma_T}$$

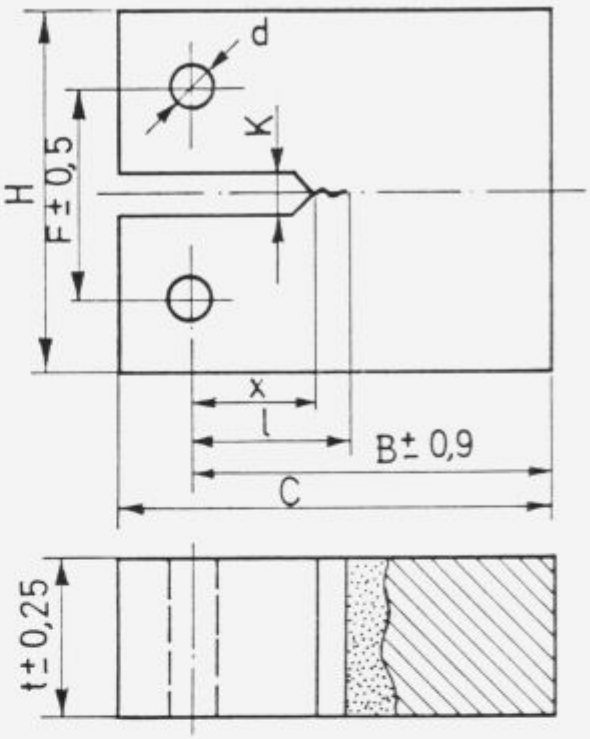

Figure 1. CTS test probe (type 3 according to GOST 25.506-85) for determining crack stability parameters in structural steel. $l = (0.45 \text{ to } 0.55)B$, $t = 0.5B$, $C = 1.25B$, $d = 0.25B$, $K \leq 0.05B$, $F = 0.55B$, $H = 1.2B$

Slika 1. Epruveta CTS (tip 3 po GOST 25.506-85) za merjenje parametrov stabilnosti razpoke v jeklih za gradbene konstrukcije. $l = (0.45 \text{ do } 0.55)B$, $t = 0.5B$, $C = 1.25B$, $d = 0.25B$, $K \leq 0.05B$, $F = 0.55B$, $H = 1.2B$

Correct determination of the fracture toughness value (stress intensity factor) is possible only if the size of r_T plastic deformation zone is essentially smaller than the crack length and effective test probe cross section. In structural steel such a ratio (r_T/l) cannot be easily achieved since they have low yield stresses and high fracture toughnesses K_{IC}. Based on numerous tests detailed described elsewhere[2] some general recommendations for selection of test-probes for static testing depending on plate thickness and steel strength were given. For 40 to 60 mm plates of low-alloyed steel the K_{IC} parameter can be correctly determined at temperatures below $-40°C$ with CTS probes (**Fig. 1**). For 20 to 40 mm plates the contoured double-cantilever doubleaxially notched probe (**Fig. 2**) gives good results since plastic deformation at crack front is highly reduced in it. In many cases, especially in industrial testing, the cylindrical probes with concentric peripheral notch (**Fig. 3**) gave good results.

Measurements were made correspondingly to GOST 25506-85 standard (Determination of characteristics of crack stability in static loading) and to ASTM standards. Rupture conditions were intensified by dynamic loading and using corrosion media. Dynamic tests were made according to ASTM standards5 and to RD50-344-82 instructions for method selection (Determination of characteristics of fracture toughness in dynamic loading). Test were made both with CTS and Charpy probes with fatigue crack according to GOST 9454-78. Influence of corrosive medium on the crack stability was studied with probes according to

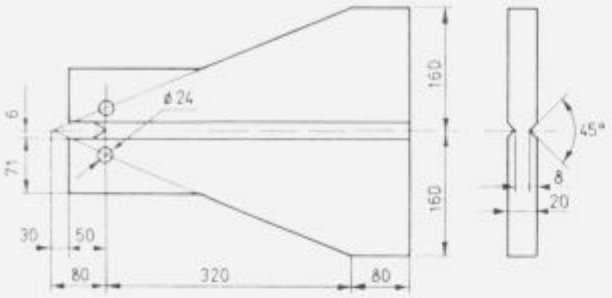

Figure 2. Contoured double-cantilever double axially notched probe.
Slika 2. Dvojno konzolno vpeta klinasta epruveta z dvema osnima zarezama.

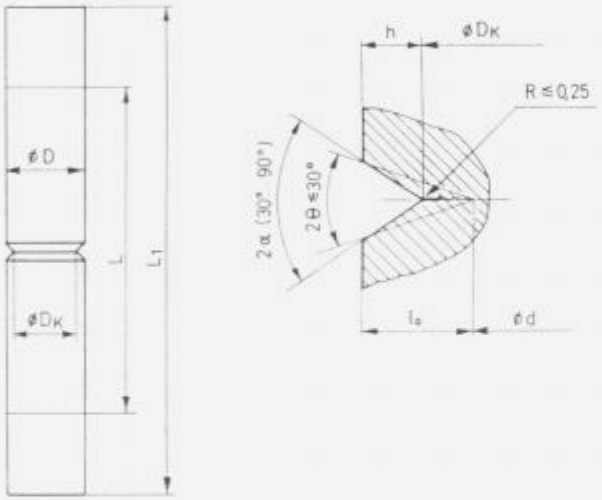

Figure 3. Cylindrical probe with concentric fatigue crack—(type 2 according to GOST 25.506-85). L = length between the clamped parts of probe in the tensile testing machine. $L = 5D$; $d = (0.6 \text{ to } 0.7)D$; $L_1 \geq 7D$; $l_0 = 0.5(D - d) \geq h + 1.5$ mm; $l_0 \geq 3.7 \operatorname{tg} \alpha$; $D_K = D - 2h = (0.65 \text{ to } 0.85)D$.
Slika 3. Cilindrična epruveta s koncentrično utrujenostno razpoko—(tip 2 po GOST 25.506-85). L = razdalja med deloma epruvete, ki se vpneta v trgalni stroj $L = 5D$; $d = (0.6 \text{ do } 0.7)D$; $L_1 \geq 7D$; $l_0 = 0.5(D - d) \geq h + 1.5$ mm; $l_0 \geq 3.7 \operatorname{tg} \alpha$; $D_K = D - 2h = (0.65 \text{ do } 0.85)D$.

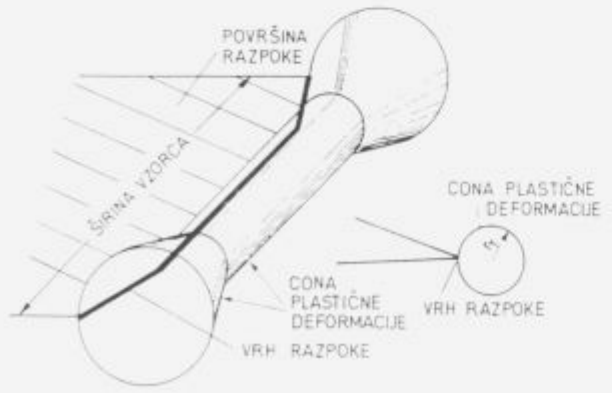

Figure 4. Scheme of crack tip with the zone of plastic deformation.
Slika 4. Shema razpoke s cono plastične deformacije.

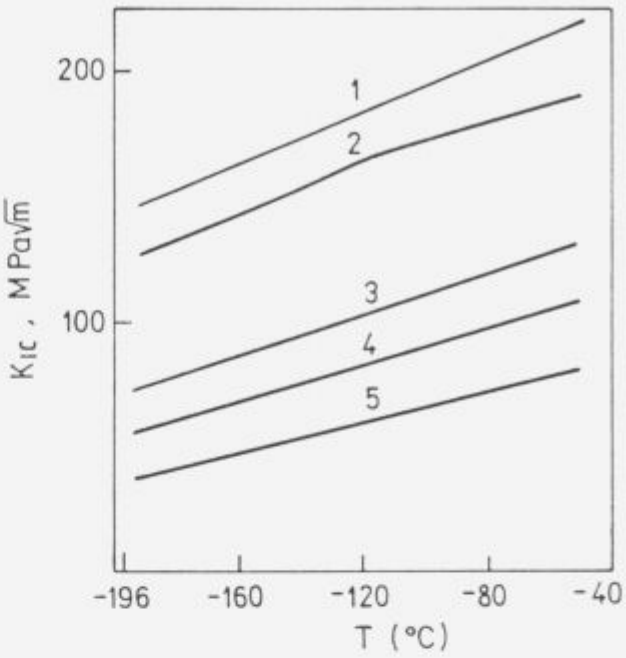

Figure 5. Fracture toughness of structural steel plate. Dependance of K_{IC} on temperature, plate thickness 20 mm. Probe from Fig. 2. 1) Hardened and tempered molybdenum-alloyed steel: 0.12% C, 0.54% Si, 1.05% Mn, 0.5% Cr, 1.47% Ni, 0.12% V, 0.24% Mo, 0.011% Al, 0.022% N, 0.025% S 2) The same steel, plate thickness 40 mm, $R_p = 710$ MPa 3) Hardened and tempered manganese-silicon steel (0.1% C, 1.48% Mn, 0.9% Si, 0.031% S, 0.021% P); $R_p = 435$ MPa 4) Steel above, rolled; $R_p = 350$ MPa 5) Hot rolled low-carbon steel (0.16% C, 0.24% Si, 0.65% Mn, 0.025% S, 0.025% P); $R_p = 265$ MPa.
Slika 5. Lomna žilavost pločevine iz jekla za gradbene konstrukcije. Odvisnost K_{IC} od temperature, debelina pločevine 20 mm. Epruveta slika 2. 1) Poboljšano legirano jeklo z molibdenom: 0.12% C, 0.54% Si, 1.05% Mn, 0.5% Cr, 1.47% Ni, 0.12% V, 0.24% Mo, 0.011% Al, 0.022% N, 0.025% S 2) Isto jeklo, debelina pločevine 40 mm, $R_p = 710$ MPa 3) Poboljšano mangan-silicijevo jeklo (0.1% C, 1.48% Mn, 0.9% Si, 0.031% S, 0.021% P); $R_p = 435$ MPa 4) Jeklo (3) valjano; $R_p = 350$ MPa 5) Vročevaljano malooglično jeklo (0.16% C, 0.24% Si, 0.65% Mn, 0.025% S, 0.025% P); $R_p = 265$ MPa.

GOST 9454-77 in distilled water and in 3% NaCl water solution according to RM SEV method (Corrosion protection in building engineering. Corrosion cracking of high-strength armature steel. Investigation methods, 1986).

Moving rate of the tensile-tester clamping jaws was $2 \cdot 10^{-8}$ mm/min which was sufficient for completing test in one day. Also impact toughness with U and V-notched probes (according to GOST 9454-78) was measured simultaneously with the uniaxially loaded tensile tests according to GOST 1797-84 with flat probes of the same thickness as investigated plate.

4 Results of Tests

Static testing gave a series of relations valid for the crack stability in structural steel (Figs. 5 to 8). It shows that in steel of standard purity and rational microstructure the fracture toughness value increases with the increased strength and with the transition from ferrite-pearlite microstructure

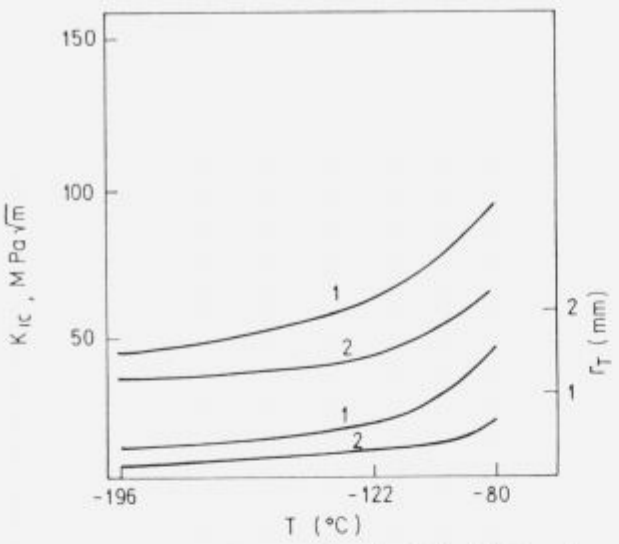

Figure 6. Fracture toughness and the size of plastic deformation zone in normalized steel (0.17% C, 1.56% Mn, 0.4% Si, 0.11% V, 0.015% N, 0.008% S, 0.07% P). Sulphide inclusions are modified by addition of RE, curve (1) vacuum treated steel; $R_p = 460$ MPa.

Slika 6. Lomna žilavost in velikost cone plastične deformacije v normaliziranem jeklu (0.17% C, 1.56% Mn, 0.4% Si, 0.11% V, 0.015% N, 0.008% S, 0.07% P). Sulfidni vključki so modificirani z dodatkom RZ, (1) jeklo vakuumirano; $R_p = 460$ MPa.

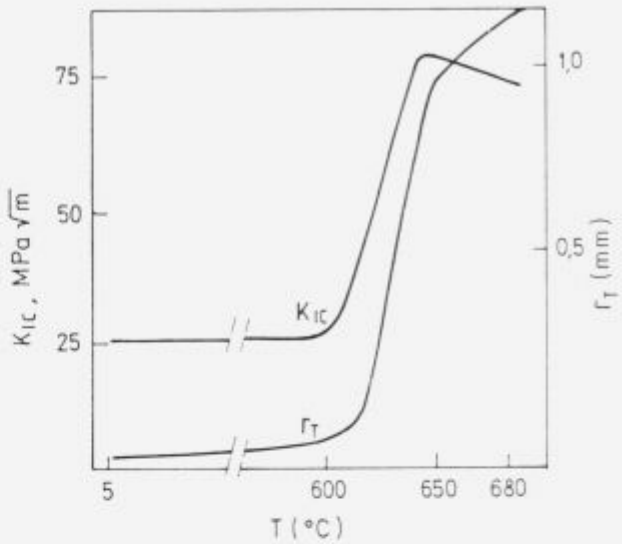

Figure 7. Dependance of fracture toughness and the size of plastic deformation zone on tempering temperature for molybdenum-alloyed steel (0.10% C, 0.37% Si, 1.16% Mn, 3.1% Cr, 1.0% Ni, 0.34% Mo, 0.016% S, and 0.04% P), plate thickness 20 mm, probe type from Fig. 3.

Slika 7. Odvisnost lomne žilavosti in velikosti cone plastične deformacije od temperature popuščanja za jeklo legirano z molibdenom (0.10% C, 0.37% Si, 1.16% Mn, 3.1% Cr, 1.0% Ni, 0.34% Mo, 0.016% S in 0.04% P) debelina pločevine 20 mm, epruveta sl. 3.

to microstructures obtained by hardening and tempering (**Fig. 5**).

Plate thickness reduces the K_{IC} value (Fig. 5) due to the reduced plastic deformation zone (r_T). The investigation results also indicate that fracture toughness of high-strength steel depends on type, amount and distribution of non-metallic inclusions, mainly sulphides (**Fig. 6**). Pure steel (0.008% S) excells the steel with standard amount of sulphur both in the respect of fracture toughness and in size of plastic deformation zone at crack tip (r_T). This confirms the influence of inclusions, on which decohesion takes place (formation of voids), on the conditions of crack initiation[3].

In heat-treated steels the fracture toughness K_{IC} is abruptly reduced if tempering temperature is reduced from 650 to 600°C (Fig. 6). The reason is in changed mechanism which controls the crack initiation. The two-stage process connected to formation of microvoids is substituted by an energy undemanding mechanism of local destruction which is detailed described elsewhere[4].

The reduced tempering temperature reduces the K_{IC} value measured by static loading (**Figs. 6** and **7**) which is in contradiction with the hitherto ideas, especially with the changed size of plastic deformation zone r_T.

This can be explained by applied testing methods which did not allow a suitably high microstructural sensitivity of parameters describing the crack stability in ductile steel with rational microstructure. This is confirmed with two additional cases of unsufficient microstructural sensitivity in estimating K_{IC} value with static tests. **Table 2** presents the relation between the fracture toughness of manganese-silicon steel and the chemical composition and the hardening temperature. Steel samples with various chemical compositions were hardened at optimal temperature of 930°C, and at 1050°C. This temperature was chosen in order to determine the influence of overheating. In all the cases the steel samples were tempered at 650°C.

Investigation results indicated that concentrations of alloying elements had a small influence on mechanical properties. Overheating of steel highly deteriorates the Charpy-test values, transition the impact toughness value which was practically halved. K_{IC} value is not extra highly influenced by overheating; the obtained differencies were below 5% and they are in the region of measuring errors.

The second case is connected to the selection of thermomechanical treatment in manufacturing 50 mm plate with yield stress $R_p \geq 450$ MPa made of microalloyed manganese steel (**Table 3**). Steel was quenched from the rolling temperature and tempered at 650°C. Initial and final rolling temperatures, and the quenching temperature (i.e. interval between finished rolling and quenching in water) were varied. Specifications TMT 1, 2, 3, and 4 in the mentioned table represent various regimes of thermomechanical treatment. K_{IC} values were measured with CTS probes (Fig. 1) having plate thickness. The highest temperature at which the K_{IC} value was correctly measured was −40°C. Table gives the dissipation of results of three tests. Table also suggests the selection of optimal regime of treatment which enables the yield stress above 490 MPa at simultaneously the highest toughness transition temperature, i.e. TMT-1.

Simultaneously it is evident that fracture toughness values ($K_{IC,-40}$ and $K_{IC,-70}$) do not enable to judge which thermomechanical treatment is optimal. These measurements only reliably indicate that TMT-4 treatment (hot rolling) is the most unusitable one. The mentioned cases show that parameters of linear fracture mechanics are microstructurally not enough sensitive to enable the regarding selection of tested steels.

The most probable reason is the high ductility of structural steel; in this case the ductility of high-strength steel which have oversized plasticity zone at crack tip in static

Table 2. Some parameters of brittle-fracture resistance of manganese-silicon steels with yield stress $R_p \geq 390$ MPa, plate thickness 20 mm

Chemical composition of steel %					Quenching temperature	Mechanical properties			
C	Mn	Si	S	P	(°C)	R_p (MPa)	KCV^{-70} (J/cm^2)	T^{50x} (°C)	K_{IC}^{-70xx} (MPa m$^{1/2}$)
0.09	1.42	0.28	0.030	0.022	930	429	64	-20	165
0.09	1.42	0.28	0.030	0.022	1050	432	29	+20	160
0.09	1.30	0.60	0.022	0.019	930	417	84	-40	180
0.09	1.30	0.60	0.022	0.019	1050	414	41	+20	175
0.09	1.42	1.03	0.030	0.023	930	435	69	-20	175
0.09	1.42	1.03	0.030	0.023	1050	445	41	+20	170

x—Toughness transition temperature determination was based on 50% tough fracture
xx—Probe in Fig. 2, −70°C was the highest temperature on which K_{IC} could be estimated

Table 3. Mechanical properties of 50 mm thick plate of microalloyed manganese steel (0.19% C, 1.58% Mn, 0.48% Si, 0.07% V, 0.024% S)

Steel treatment	R_p (MPa)	T_1^{xxx} (°C)	T^{50} (°C)	KCV^{-70} (J/cm^2)	K_{IC}^{-40} (MPa m$^{1/2}$)	K_{IC}^{-70} (MPa m$^{1/2}$)
Hot rolled	420	-70	-20	49	55–76	42–55
Hardened and tempered	500	-60	+20	31	61–82	52–67
TMT 1	520	-100	-40	92	67–103	52–64
TMT 2	570	-60	-20	38	52–91	42–64
TMT 3	620	-40	0	32	64–106	39–67
TMT 4	635	-20	+20	28	45–64	27–48

xxx—Determined by impact toughness criterion 39 J

loaded probes though all the testing conditions described by corresponding standards were fulfilled.

Microstructural dependance of investigated parameters becomes more pronounced in more severe testing conditions which reduce the extent of plastic deformation and the size of plastic deformation zone at the crack tip. This occurs during testing in corrosive media (**Fig. 7**). In these tests the K_{IC} value increases with the increased tempering temperature of steel. The obtained result is the consequence of a high density of disordered dislocation loops. Such a structure is essentially less resistant to stress corrosion[2], especially if hydrogen embrittlement is developed. In steel with such a structure, the KC_{IC} value is essentially lower than the K_{IC} one (Fig. 8).

Behaviour of hardened and tempered steel during loading is characterized by its substructure which is formed in recovery of ferrite and in the beginning of recrystallization. Materials with such a structure are not sensitive to stress corrosion; therefore there it is valid: $K_{IC} = K_{IC}^c$ (**Fig. 8**).

Another way to increase the structural sensitivity of K_{IC} are the impact tests where loading rates are increased for six orders of magnitude. In this case the extent of plastic deformation is reduced to suitable amount, also size of plastic deformation zone at the crack tip is abruptly reduced, and it becomes dependant on steel microstructure. This finding can be confirmed with the investigations of steel of big pipelines which measured K_{IC} values were close to the K_{IC} values determined by static testing (Table 4).

In static loading the CTS probe was applied while for impact tests Charpy test probe with fatigue crack was used.

Steels with equal K_{IC} values exhibit the same sequence

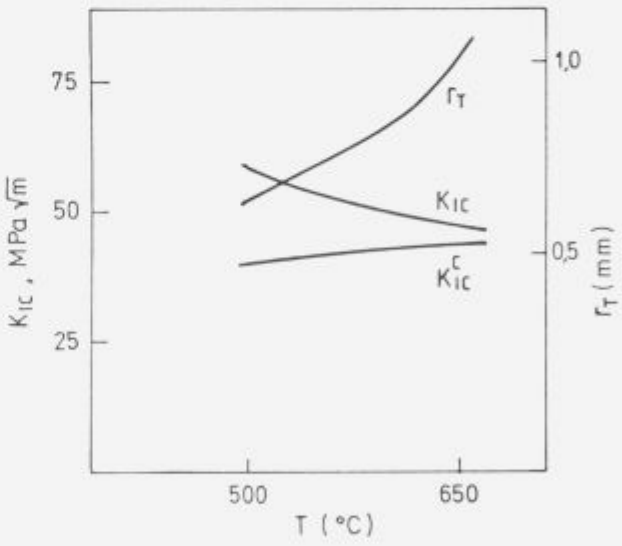

Figure 8. Dependance of fracture toughness and the size of plastic deformation zone on tempering temperature for microalloyed manganese steel (0.14% C, 1.64% Mn, 0.52% Si, 0.07% V, 0.007% N, 0.031% S, 0.013% P). K_{IC}^c—fracture toughness for tests in corrosive medium.

Slika 8. Odvisnost lomne žilavosti in velikosti cone plastične deformacije od temperature popuščanja za mikrolegirano manganovo jeklo. (0.14% C, 1.64% Mn, 0.52% Si, 0.07% V, 0.007% N, 0.031% S, 0.013% P). K_C^c—lomna žilavost pri preizkusih v korozijskem mediju.

Table 4. Fracture toughness and the size of plastic deformation zone on crack tip

Steel treatment	Plate thickness (mm)	Chemical composition (%) C	Chemical composition (%) S	Grain size (μm)	R_p MPa	K_{IC} MPa$^{1/2}$	r_T mm	K_{IC}^d MPa$^{1/2}$	r_T^d mm
Microalloyed Mn steel, hardened with AlN, normalized	12	0.17	0.012	9	418	80	4.2	13.7	0.15
Microalloyed Mn steel, hardened with VN, normalized	12	0.13	0.011	6	425	80	4.1	22.6	0.14
Mn steel alloyed with small amounts of Mo and Nb, controlled rolled	16	0.13	0.011	4	590	84	3.1	37	0.29

after impact testing. Investigations also showed the advantage of controlled rolled plates. Microstructural sensitivity of fracture parameters was also essentially increased, especially the K_{IC}^d and r_T^d values which are in a good correlation with the grain size.

5 Analysis of Results

The described testing results show that the K_{IC} value measured at static loading is not sufficiently microstructurally sensitive property (Figs. 6 and 7, Tables 2 and 3). The needed sensitivity can be achieved by increased test severity or with more demanding tests applying corrosive media or impact loads (Fig. 7, Table 4). Microstructural sensitivity was increased if the extent of plastic deformation was reduced. As a rule, at least three of the following conditions must fulfilled in that case: temperature below 0°C, dynamic tensile load, stress raisers must be present in structure, dimensional factor (great cross section, and the like), and unsuitable steel microstructure. In these cases the parameters of crack stability measured in the conditions of highly limited plastic deformation give good description of fracture conditions.

These parameters were well applied in engineering design of structures. As an example, the crack propagation in the wall of main pipeline will be described. Crack was initiated in the weld on the line of fusion penetration inside the pipeline, and then it propagated towards the external surface. The K_{IC}^d values and the critical crack lengths l_c in the heat affected zones for various steel are reviewed in **Table 5.**

Critical size of defect was calculated by expression[5]:

$$K_{IC} = \frac{pR}{t}\sqrt{\pi l_c}\left(1 + 1.6\frac{l_c^2}{r_T}\right)$$

where p is pressure, R pipe radius, and t wall thickness.

The obtained results show that crack in manganese-silicon steel becomes unstable at low temperatures, and it starts spontaneously to propagate in the axial direction at relatively small penetration into the pipe wall. At those temperatures the use of pipes made of the mentioned steel is not allowed. After controlled rolling the critical size of crack becomes greater than the wall thickness. Thus the stable crack which reaches the pipe surface hinders the spontaneous propagation of crack. At the given temperature the pipe made of the third steel (cited in Table 5) is safe.

Table 5. Fracture characteristics of steel in heat affected zone of pipeline weld

Steel treatment	Plate thickness (mm)	$K_{IC}^{d(-60)}$ (MPa m$^{1/2}$)	$l_c^{(-60)}$ (mm)
Mn-Si steel, normalized	12	24	3
Microalloyed (V) Mn steel, controlled rolled	17	81	24
Mn steel, microalloyed with V and Nb, controlled rolled	14	97	32

Fatigue crack was normal to the plate surface

Determination the fracture toughness at static load at -60°C ($K_{IC} > 100$ MPa m$^{1/2}$) for manganese-silicon steel indicates the safety of that steel, but unfortunately the practical experiences did not confirm it. Thus the parameters of linear fracture mechanics measured in the conditions of very limited plastic deformation did not exhibit only high structural sensitivity but they are also useful in engineering design of brittle-fracture resistance in the cases when they enough accurately describe the mechanism and conditions for brittle fracture of certain steel.

6 References

[1] Werkstoffkunde Eisen und Stahl; Teil 1; Grundlagen der Festigkeit, der Zähigkeit und der Bruchs; Verlag Stahleisen, Düsseldorf, 1983

[2] Tylkin M.A., Bolšakov V.I., Odesskij P.D.: Struktura i svojstva stroitel'noj stali; Moskva, Metallurgija, 1983

[3] Knott J.: Mikromehanizmy razrušenija i treščinostojkost' konstrukcionnyh splavov; Mehanika razrušenija, (prevod iz angl.), Moskva, Mir, 1979, (101–130)

[4] Smith E., et al.: Lokalizacija plastičeskogo tečenija i treščinostojkost vysokopročnyh materialov, Mehanika razrušenija, (prevod iz angl.); Moskva, Mir, 1980, (124–147)

[5] Duffy A.R., et al.: Praktičeskie primery rasčeta na soprotivlenie hrupkomu razrušeniju truboprovodov pod davleniem, Razrušenie, 5; Moskva, Masinostroenie, 1977, (146–209)

Kovine, zlitine, tehnologije / letnik 26 / številka 4 / strani 343 do 349 / 1992

Evaluation of Mn-V Steel Tendency to Hydrogen Embrittlement

Ocjena sklonosti Mn-V čelika prema vodikovoj krtosti

M. Gojić, M. Balenović, *Željezara Sisak "IRI" d.o.o., Sisak*
L. Kosec, *FNT, Odsek za metalurgijo in materiale, Ljubljana*
L. Vehovar, *Inštitut za kovinske materiale in tehnologije, Ljubljana*
L.J. Malina, *Metalurški fakultet Sisak, Sisak*

Recently great attention is given to investigations related to oil - and natural gas exploitation, especially from the aspect of material selection used for production of tubular equipment. In these conditions tubes destructions caused by mechanical damages are less frequent than destructions caused by various corrosion crack forms and especially corrosion cracks in sulphide conditions, with H_2S as a dominant component. Results of mechanical properties and evaluation of tendency of seamless tubes in as rolled and heat treated condition, produced from medium-carbon Mn-V steel to hydrogen embrittlement by method of cathode polarization at the constant current density of 4.0 mA/cm^2 are presented in this paper besides the above stated possible tube destruction forms in the conditions of oil - and natural gas exploitation. The fractographic analysis of fractured samples surfaces after cathode polarization was also performed by scanning electron microscope. It was found that tubes in the as rolled condition (no heat treatment) show great tendency to hydrogen embrittlement with the values of the calculated embrittlement index of 86.4%. By normalization (900° C/30 min. air) of tubes, resistance to hydrogen embrittlement was not improved compared with the as rolled condition. The heat treatment (quenching + tempering) resulted in a great resistance of tubes to hydrogen embrittlement with the calculated embrittlement index of 25.1%. The stated results are proved by the fractographic analysis of morphology of fractures that are explicitly brittle for tubes without heat treatment, but tough for quenched and tempered tubes. Therefore it can be concluded that from the aspect of mechanical properties and corrosion resistance the most suitable tubes for use in the oil - and gas wells are those quenched and tempered at high temperatures (700° C).

Danas se u svijetu velika pažnja poklanja istraživanjima vezanim uz problematiku eksploatacije nafte i zemnog plina, posebno s aspekta izbora materijala koji se koriste za izradu cijevne opreme. Propadanja cijevi u tim uvjetima uslijed mehaničkih oštećenja su manje često nego propadanja uslijed različitih oblika korozijskih raspucavanja, a posebno korozijskog raspucavanja u sulfidnim uvjetima gdje je H_2S dominantna komponenta. U radu su pored navedenih mogućih oblika oštećenja cijevi u uvjetima eksploatacije nafte i zemnog plina prikazani rezultati mehaničkih svojstava kao i ocjena sklonosti valjanih i toplinski obrađenih bešavnih cijevi iz srednjeugljičnog Mn-V čelika prema vodikovoj krtosti metodom katodne polarizacije kod konstantne gustoće struje od 4.0 mA/cm^2. Također je provedena na scanning elektronskom mikroskopu i fraktografska analiza prelomnih površina uzoraka nakon katodne polarizacije. Utvrđeno je da cijevi u valjanom stanju (bez toplinske obrade) pokazuju veliku sklonost prema vodikovoj krtosti s vrijednostima izračunatog indeksa krtosti od 86.4%. Normalizacijom (900° C/30 zrak) cijevi otpornost na vodikovu krtost nije se poboljšala u usporedbi s valjanim stanjem. Međutim toplinskom obradom (kaljenje + popuštanje) postignuta je velika otpornost cijevi prema vodikovoj krtosti s izračunatim indeksom krtosti od 25.1%. Navedene spoznaje dokazuje i fraktografska analiza morfologije preloma koji su za cijevi bez toplinske obrade izrazito krti cijepajući dok su žilavi za zakaljene i popuštene cijevi. Prema tome, ovaj rad dokazuje da su s aspekta mehaničkih svojstava i korozijske otpornosti za primjenu u naftnim i plinskim bušotinama najpogodnije cijevi koje su zakaljene i popuštene na visokim temperaturama (700° C).

1 Introduction

Due to ever increasing demand for energy a great attention is given to investigations related to problems connected to oil and natural gas exploitation, especially to the selection of material for tubular equipment. Thirty five years ago medium quality steels having 400 MPa yield strength were used for tubes and pipes in natural gas and oil exploitation from 1000–3000 meters depths. Nowadays the exploitation proceeds not only in higher depths (10 000 m) but in more severe conditions also because of the presence of highly corrosive acidic gas (H_2S, CO_2), chlorides, high pressure and temperature, etc. Therefore, material for tubular ware have to satisfy high requirements for both mechanical and corrosion properties.

Cracking of tubular equipment in the presence of sulphide is particularly frequent corrosion phenomenon. The

selection of appropriate steel and the heat treatment of final goods to obtain optimal compromise of mechanical and corrosion properties are used as countermeasure[1–6].

Different possible tube damage in oil and natural gas exploitation with special emphasis on SSCC (sulphide stress corrosion cracking) as a form of hydrogen embrittlement is described.

Samples made from hot rolled seamless tube manufactured from medium carbon low alloyed Mn-V steel were investigated. Cathodic polarization following heat treatment carried out under laboratory conditions was used to determine susceptibility to hydrogen embrittlement and evaluate corrosion properties.

2 Forms of oil pipe damage

Tubes and pipes used in natural gas and oil exploitation are known as Oil Country Tubular Goods (OCTG). OCTG is divided into tubing, casing and drill tube used in vertical direction for pumping, external protection and drilling, respectively. In a wider sense OCTG includes also pipe line used for transport purposes mainly in horizontal direction.

Despite complex stresses pure mechanical failure is less frequent as compared to corrosion failure. Economic operation of oil wells is often dependent on proper selection of tube material. The control of corrosion has become one of main factors in the production of energy from geoenergetic sources. Corrosion failure of natural gas and oil exploitation equipment is very serious problem from safety as well as economic viewpoint since the costs in oil industry amount to several hundreds millions of US$ per year. Material failure due to corrosion is also associated with production breaks. Corrosion problems in oil and gas explotation equipment[7–10] can appear in several forms:

- weight loss due to corrosion,
- localized corrosion known as pitting,
- corrosion fatigue,
- galvanic corrosion,
- stress corrosion and
- sulphide stress corrosion cracking (SSCC)

Stress corrosion cracking caused by sulphide is very frequent since typical oil and gas exploitation environment besides chlorides, sulphates, carbonates, CO_2 and moisture contains considerable amount of H_2S also which can reach up to 30%. Hydrogen sulphide attack increases general corrosion, erosion corrosion in turbulent media, stress corrosion cracking, corrosion fatigue of tubes and equipment at bottom of drilled wells etc. Stress corrosion cracking in the presence of sulphide may appear in two forms:

- hydrogen induced cracking (HIC)
- sulphide stress corrosion cracking (SSCC)

Hydrogen induced cracking is characteristic for OCTG equipment made from low alloyed steel with ferrite—perlite microstructure and 700 MPa tensile strength. It can occur even in the absence of external stress. This form of corrosion results from atomic hydrogen absorbed on microstructural defects (hydrogen traps) which recombines into molecular hydrogen.

Sulphide stress corrosion cracking occurs in OCTG equipment made from high strength steel as a form of hydrogen embrittlement. Hydrogen embrittlement has been well known and frequently observed in metals for quite a long time. It is caused mostly by corrosion, galvanisation or leaching associated with the generation of atomic hydrogen which under certain conditions can diffuse into crystalline lattice resulting in the hydrogenization of metal.

In the beginning the effect of hydrogen was attributed to stress corrosion. Recently the similarity between hydrogen embrittlement and certain types of stress corrosion, particularly SSCC[8–10] has been pointed out.

There is no unique theory capable of explaining all phenomena associated with hydrogen attack because it depends on a number of factors e.g. type of steel, its microstructure, electrolyte, etc. At present, the proposed mechanisms of hydrogen attack are based on increase in the inner pressure, surface adsorption, decohesion, increase or decrease in plasticity and the formation of hydride[11]. Acidic enviroment in natural gas and oil exploitation enhances hydrogen embrittlement and SSCC as its particular form because of

- the presence of H_2S at low pH value of media,
- sulphides which increase the amount of hydrogen diffusing into the crystalline lattice of metal and
- tendency for the localization of anodic part of corrosion reaction which promotes initial cracks.

There are two sources of atomic hydrogen; the inner generated by manufacture and heat treatment of steel and the exterior resulting from the effect of definite environment. During application of material hydrogen may be adsorbed from gaseous phase in molecular form with subsequent dissociation into atoms or by electrochemical dissolving of liquid phase i.e. surrounding corrosive media which takes place during the exploitation. In this case hydrogen is formed in molecular or atomic form. The overall reaction of hydrogen formation is

in acidic solutions:

$$2H_3O^+ + 2e^- \rightarrow H_2 + 2H_2O \quad (1)$$

in caustic solutions:

$$2H_2O + 2e^- \rightarrow H_2 + 2OH^- \quad (2)$$

The transport of H_3O^+ ion (from now on H^+) or H_2O molecule to electrode surface and subsequent formation of adsorbed hydrogen atoms can be described by (3) and (4):

$$H^+ + e^- \rightarrow H_{ads} \quad (3)$$

$$H_2O + e^- \rightarrow H_{ads} + OH^- \quad (4)$$

Irrespective on the nature of solution, hydrogen is adsorbed on metal electrode surface. To be continuous the electrochemical process requires permanent presence of H_{ads} on electrode surface from where it can be removed in one among three ways[12,13]:

- by catalytic recombination (Volmer-Tafel's mechanism) where both the adsorption and desorption take place simultaneously:

$$H^+ + e^- \rightarrow H_{ads} \quad (5)$$

$$H_{ads} + H_{ads} \rightarrow H_2 \quad (6)$$

- by Volmer-Heyrowski's mechanism of electrochemical desorption where desorption results from the reduction

Table 1. Chemical composition of the Heat (T) and billet (K)

Steel	Sample	Composition in wt. %								
		C	Mn	P	S	Si	V	Mo	Al	Cr
Mn-V	T	0.33	1.10	0.017	0.004	0.23	0.21	-	0.027	-
	K	0.33	1.14	0.025	0.005	0.29	0.23	0.02	0.04	0.08

of H^+ ion or H_2O molecule according to (7), (8) and (9):

$$H^+ + e^- \rightarrow H_{ads} \quad (7)$$

$$H^+ + H_{ads} + e^- \rightarrow H_2 \quad (8)$$

$$H_2O + H_{ads} + e^- \rightarrow H_2 + OH^- \quad (9)$$

- by emission mechanism where adsorbed hydrogen atoms vaporize from electrode surface:

$$H_{ads} \rightarrow H \quad (10)$$

Consequently, hydrogen atoms adsorbed on the surface (H_{ads}) can recombine into either harmless gaseous hydrogen through (6) which is bubbled out of solution or diffuse into metal and enhance embrittlement:

$$H_{ads} \rightarrow H_{abs}$$

It can be concluded that sulphide stress corrosion cracking is caused by absorbed hydrogen. The dissolving of iron and the presence of H_2S in water solution create conditions for increase in hydrogen content of steel[14]. Usually, only a small part of hydrogen generated on cathode diffuses into metal. Diffusion rate depends on numerous factors, e.g. the type of steel or alloy, its composition and previous thermomechanical treatment, nature of electrode surface, type of electrolyte, its composition, cathode current density, etc.

Hydrogen embrittlement is often used in evaluation of the effect of hydrogen on steel at room temperature which results in a loss of ductility (reduction in elongation and contraction), decrease in tensile strength and enhanced brittleness.

3 Experimental

Mn-V steel billet of $\Phi 135 \cdot 420$ mm dimensions was produced under laboratory conditions on Metallurgical Institute Hasan Brkić, Zenica. The billet was hot rolled into $\phi 60.3 \cdot 4.83$ mm pumping oil tube (tubing) under industrial conditions in Seamless Tube Mill of Željezara (Iron and Steelworks) Sisak. **Table 1** presents Heat (T) and a control (K) analysis of the steel.

Samples cut from rolled tube were subjected to heat treatment (annealing, annealing + tempering, quenching + tempering) in electric resistance chamber furnace. Investigation of mechanical properties were carried out on INSTRON type 1196 machine using samples prepared according to ASTM standard. Brinell or Rockwell C hardness was determined depending on the sample hardness.

Corrosion resistance was measured by the method of cathodic polarization which is known as one among the most appropriate for determination of relative susceptibility to hydrogen embrittlement. After cleansing with acetone the samples for cathodic polarization were put in the electrochemical cell of ZWICK 50 kN tensile machine (**fig. 1**) and subjected to static load of 80% of yield stress.

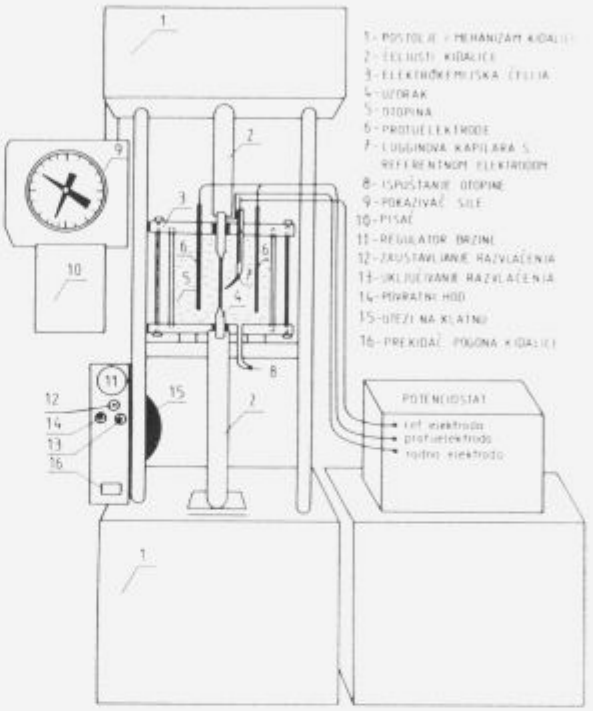

Figure 1. Schematic illustration of equipment for hydrogen embrittlement evaluation by cathodic polarization method.
Slika 1. Shematski prikaz aparature za ocjenu vodikove krtosti metodom katodne polarizacije.

Sample of Mn-V steel was used for working electrode and saturated calomel electrode (SCE) situated in Luggin's capillary tube as a reference. Two graphite Johnson Matthey electrode of 6.5 mm diameter were used as counter electrode.

The solution used was 1N H_2SO_4 with addition of 10 mg/l As_2O_3 used to activate the generation of H_{ads}. The solution was deaerated by nitrogen blowing for 30 min.

For cathodic polarization WENKING potentiostat modell 68 FR 0.5 was used and constant 4 mA/cm^2 current density was applied. After 2 hours of polarization samples were taken out of the cell and immediately tested on INSTRON machine at very low deformation rate of $2.4 \cdot 10^{-4} s^{-1}$. The overall tensile test lasted for 3–4 mins. Afterward the cross section of fractured surface was measured to determine the contraction. Due to the loss of ductility (contraction) embrittlement index F was calculated from:

$$F = \frac{Z_0 - Z_1}{Z_0} \cdot 100$$

where:

Z_0 contraction before polarization
Z_1 contraction after polarization

Table 2. Results of mechanical testing of Mn-V steel tube samples in as rolled and heat treated state.

Sample	Heat treatment	R_e MPa	R_m MPa	A_2" %	Hardness, HB; I	II	III	IV	API grade
2	-	605.5	759.5	25.5	216	216	211	213	L-80
20	900°C/30' air + 670°C/60' air	535.0	657.0	24.6	222	215	229	235	J-55
21	870°C/30' water + 640°C/60' air	794.0	836.0	21.2	276	278	276	278	P-105
23	870°/30' water + 700°/60' air	692.0	723.0	23.4	232	234	255	231	C-90

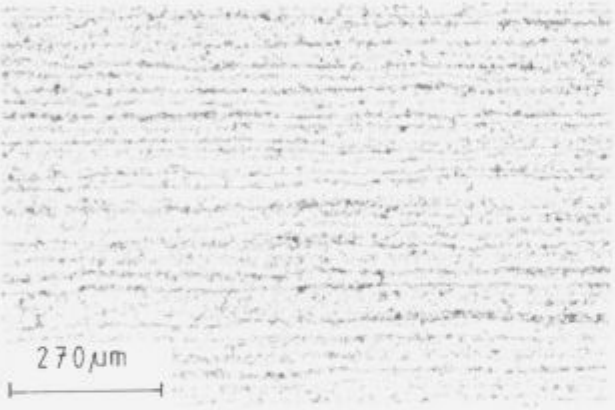

— trakasta feritno-perlitna mikrostruktura —
a) valjano stanje

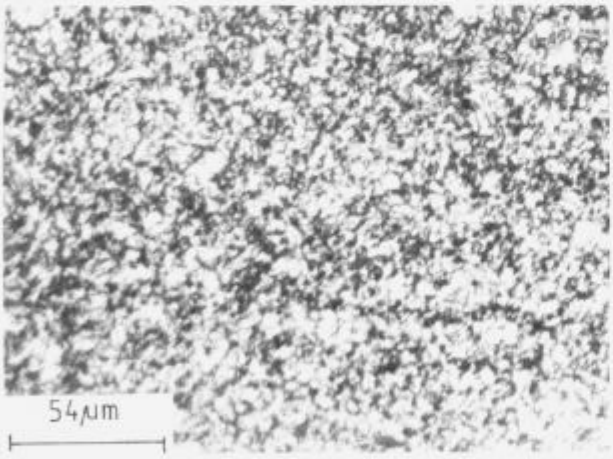

— popušteni martenzit —
b) K: 870°C/30 voda + P: 700°C/60 zrak

Figure 2. Microstructure of tubing Mn-V steel in rolled (a) and heat treated (b) condition.
Slika 2. Mikrostruktura cijevi iz Mn-V čelika u valjanom (a) i toplinsko obrađenom (b) stanju.

4 Results

Results of mechanical and metallographic investigation

Investigation of mechanical properties (tensile strength, yield stress and strain) were carried out on two tube samples in as rolled state and another two in heat treated state. Ring-like $\phi 60.3 \cdot 4.83 \cdot 30$ mm samples were used for Brinell or Rockwell C (for quenched samples) hardness measurement using three impressions per quadrant (in the middle of sample wall). Average values of mechanical properties for as rolled and different heat treated state are seen in **table 2.**

Mechanical properties of Mn-V steel tubes in as rolled state i.e. without heat treatment correspond to L-80 API grade of corrosion resistant OCTG wares. Annealing treatment (900°C/30' in air) followed by tempering at 670°C produces lower quality OCTG wares with mechanical properties correponding to J-55 API grade. Quenching in water coupled with subsequent tempering at 640°C yields OCTG wares of higher mechanical properties (P-105 grade) which are not desired because of poor resistance to SSCC, i.e. a high susceptibility to hydrogen embrittlement. However, tempering at 700°C results in API C-90 grade corresponding to corrosion resistant OCTG wares.

Mechanical properties measured are in accordance with corresponding microstructures as can be seen on **fig. 2.**

Results of cathodic polarization tests

Since the determination of susceptibility to hydrogen embrittlement by catodhic polarization is based on the loss of ductility caused by absorbed hydrogen, samples were subjected to tensile test with $2.4 \cdot 10^{-4} s^{-1}$ deformation rate immediately after the polarization. Embrittlement index F was calculated from equation (11) taking into account contraction measured before (Z_0) and after (Z_1) polarization. The results are given in **table 3.**

Histograms given on **figs. 3** and **4** present the change in contraction and embrittlement index, respectively for as rolled and heat treated Mn-V steel sample caused by cathodic polarization. Samples in as rolled state and that in annealed state show high susceptibility to hydrogen embrittlement i.e. a great decrease in contraction (**fig. 3**) and high index of embrittlement (**fig. 4**). Samples annealed and subsequently tempered at 670°C have significantly lower embrittlement ($F = 28.1\%$ only).

The best resistance to hydrogen embrittlement ($F = 25.1\%$) have samples which were quenched and tempered at 700°C because of highly tempered martensite microstructure as seen in **fig. 2b.** Fracture surface of samples after cathodic polarization was analysed by electron scanning microscope as seen in **fig. 5.** Fracture surface of Mn-V steel samples in as rolled state after cathodic polarization

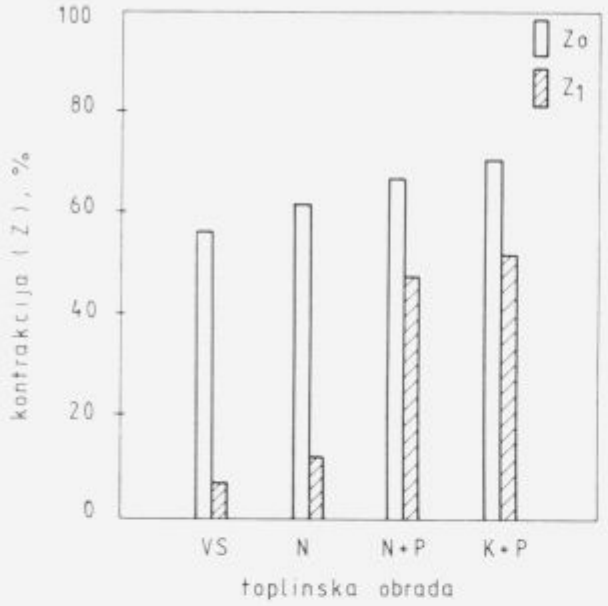

Figure 3. Concentration change resulting from cathodic polarization of Mn-V steel in different heat treatment conditions VS-rolled. Heat treatment

- N: 900°/30' air
- N + P 900°/30' air + 670°/60' air
- K + P: 870°/30' water + 700°/60' air

Slika 3. Promjena kontrakcije uslijed katedne polarizacije za različita stanja toplinske obrade Mn-V čelika. VS—valjano stanje. Toplinska obrada

- N: 900°/30' zrak
- N + P 900°/30' zrak + 670°/60' zrak
- K + P: 870°/30' voda + 700°/60' zrak

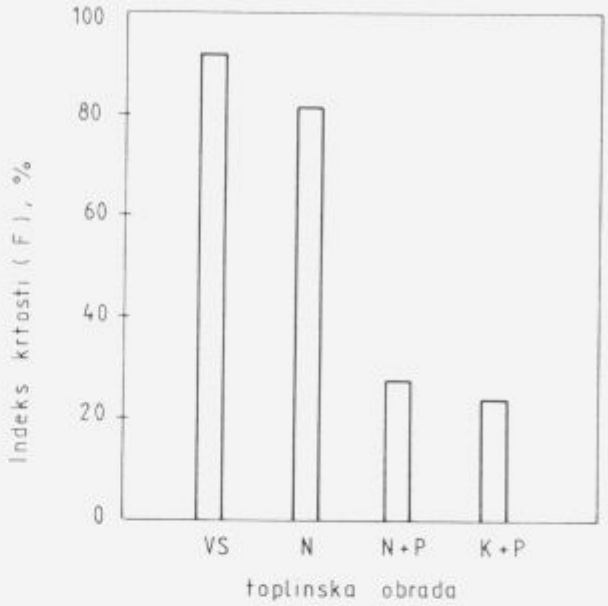

Figure 4. Embrittlement index change resulting from cathodic polarization of Mn-V steel in different heat treatment conditions VS—rolled. Heat treatment

- N: 900°/30' air
- N + P 900°/30' air + 670°/60' air
- K + P: 870°/30' water + 700°/60' air

Slika 4. Promjena indeksa krtosti uslijed katodne polarizacije za različita stanja toplinske obrade Mn-V čelika. VS—valjano stanje. Toplinska obrada

- N: 900°/30' zrak
- N + P 900°/30' zrak + 670°/60' zrak
- K + P: 870°/30' voda + 700°/60' zrak

shows typical brittle fracture (**fig. 5a**) whereas quenched and highly (700°C) tempered samples show ductile fracture (**fig. 5b**) corresponding to a low index of embrittlement (**fig. 4**).

5 Discussion

Despite the fact that mechanical properties of Mn-V steel seamless tube samples in as rolled state correspond to API L-80 grade of corrosion resistant OCTG wares, the cathodic polarization at 4.0 mA/cm^2 current density displayed great susceptibility to hydrogen embrittlement. As a result of cathodic polarization the contraction dropped from initial (as rolled state) 56.9% to 7.7% corresponding to embrittlement index $F = 86.4\%$ (figs. 3 and 4). The susceptibility to hydrogen embrittlement of Mn-V steel tubes in as rolled state is also seen (fig. 5a) from brittle fracture surface. It results from strip like ferrite-perlite microstructure with elongated inclusions (fig. 2a) which is favorable for accumulation of the critical amount of hydrogen required for the initiation of cracking. From the viewpoint of resistance to SSCC viz. hydrogen embrittlement, elongated sulphide inclusions (especially MnS which act as hydrogen trap) and high tendency for segregation of manganese (martensite and bainite islands observed in microstructure) are unfavorable and have a dominant influence on corrosion resistance of Mn-V steel in as rolled state.

The annealing treatment carried out (900°C/30' air) on tested tubes did not improve the resistance to hydrogen embrittlement since strip like ferrite-perlite structure with prevailing influence of MnS inclusions acting as hydrogen traps was preserved. On the contrary, tempering (670°C/60' air) of annealed tubes resulted in considerable increase of the resistance to hydrogen embrittlement since martensite and bainite islands were removed. In respect to mechanical properties the heat treatment combined of quenching and tempering at temperatures within 640–700°C range yielded J-55, P-105 and C-90 (table 2) API grades. Cathodic polarization test of tubes corresponding to API C-90 grade showed high resistance to hydrogen embrittlement with only 25.1% reduction in contraction. The obtained high resistance to hydrogen embrittlement is illustrated also by fig. 5b showing ductile nature of fracture surface.

As compared to samples in as rolled state the microstructure of heat treated sample tubes of Mn-V steel instead of bands of ferrite-perlite was composed of homogeneous highly tempered martensite marked by high ductility and capacity for accumulation of higher amounts of energy generated e.g. by Zappfe's mechanism[11] of hydrogen embrittlement. Since MnS was observed in heat treated samples also, it is evident that highly tempered martensite reduces harmful influence of MnS on corrosion properties of OCTG wares.

Table 3. Loss of ductility of Mn-V steel as determined by the method of cathodic polarization.

Sample	Heat treatment	R_e MPa	Applied stress	Z_0 %	Z_1 %	i mA/cm^2	F %
2-3	-	599.1	0.8 R_e	56.9	7.7	4.0	86.4
20N-4	900°C/30'air	594.5	0.8 R_e	61.1	10.9	4.0	82.0
20-5	900°C/30' air + 670°C/60' air	519.4	0.8 R_e	67.2	48.3	4.0	28.1
23-4	870°C/30' water + 700°C/60' air	681.8	0.8 R_e	70.1	52.5	4.0	25.1

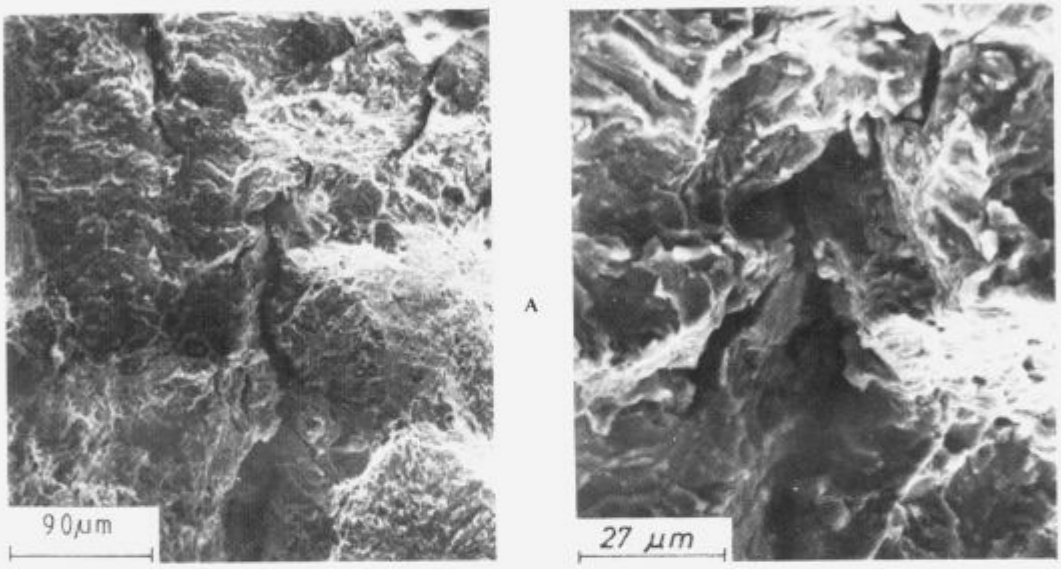

— krti cijepajući prelom —
Uzorak 2—3 (valjano stanje)

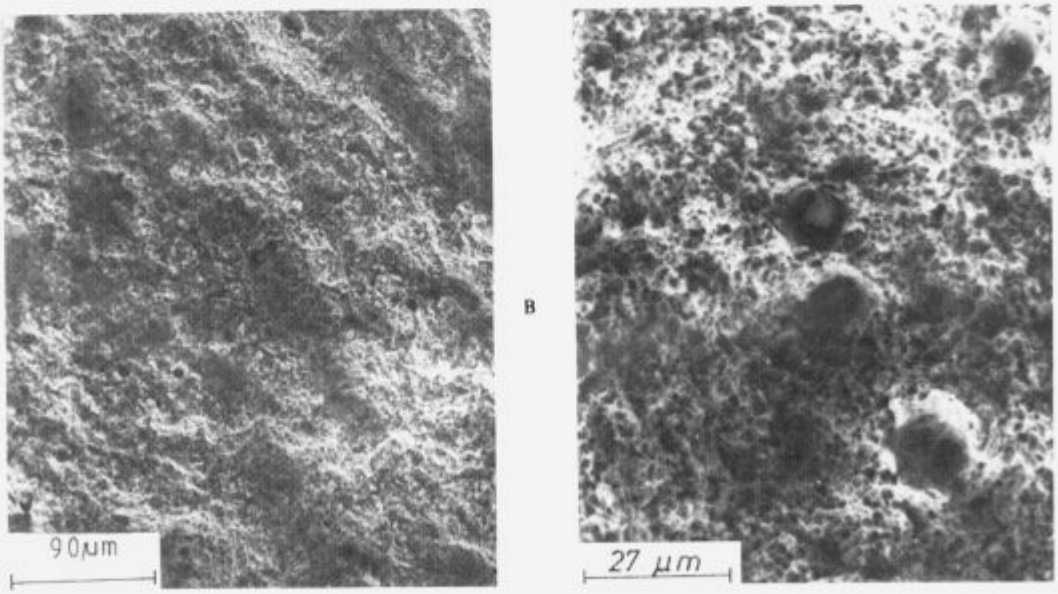

— žilavi prelom —
Uzorak 23—4)K: 870°C/30 voda + P: 700°C/60 zrak)

Figure 5. Fracture morphology of specimens form Mn-V steel in rolled (a) and heat treated (b) condition after cathodic polarization.
Slika 5. Morfologija preloma uzoraka iz Mn-V čelika u valjanom (a) i toplinsko obrađenom (b) stanju nakon katodne polarizacije.

Summary

Based on the investigation of susceptibility to hydrogen embrittlement of seamless Mn-V steel tubes utilized in natural gas and oil industry the following conclusions can be derived.

- Mechanical properties of Mn-V steel tubes in as rolled state with higly oriented ferrite-perlite microstructure correspond to L-80 API grade.
- Beside J-55 and P-105, C-90 API grade conforming to corrosion resistant OCTG wares was also attained by heat treatment (annealing + tempering, quenchung + tempering) of tubes.
- Cathodic polarization of tubes in as rolled state showed small resistance to hydrogen embrittlement since embrittlement index F was 86.4%.
- The resistance to hydrogen embrittlement was not improved by annealing (900°C/30' air) ($F = 82.0\%$) as compared to as rolled state.
- Based on brittle fracture surface revealed by fractographic analysis of samples subjected to cathodic polarization it was established that Mn-V steel tubes in annealed or as rolled state are not suitable for the use in oil industry.
- High resistance to hydrogen embrittlement proven by comparatively small embrittlement index ($F = 25.1\%$) and ductile nature of fracture surface was acquired by quenching and tempering at a high temperature (700°C).
- In respect to both mechanical and corrosion properties Mn-V steel tubes quenched and temepered at a high temperature are suitable for the use in natural gas and oil wells.

Kovine, zlitine, tehnologije / letnik 26 / številka 4 / strani 351 do 355 / 1992

Chromizing of Iron

Difuzijsko kromanje železa

M. Jenko, A. Kveder, *Inštitut za kovinske materiale in tehnologije, Lepi pot 11, 61001 Ljubljana*
S. Spruk, L. Koller, *IEVT, Teslova 30, 61111 Ljubljana*

In the paper, the theoretical aspects of CVD processes of iron chromizing and the comparison with the PVD process, developed by the authors for professional electronic industry are presented.

V sestavku so podani teoretični vidiki CVD postopkov difuzijskega kromanja železa in primerjava s PVD postopkom, ki so ga ovtorji razvili za potrebe profesionalne elektronike.

1 Introduction

Corrosion is one of the most frequent and the most undesired processes on the surface of metals and alloys. Since corrosion is a surface reaction, all types of protective coating must be involved to change the behaviour of metallic component in the surface composition. This change can be achieved by addition of a different material or in the form of outer skin, which provides a barrier between the body and the surrounding corrosive medium. The form of coating is the most common; it includes paints, plastics, metals deposited by electroplating etc. It is also possible to modify the chemical composition of the surface to be protected, by diffusion of a suitable metal or an element into it which will combine with the parent metal or alloy and provide the required resistance to the corrosive medium. Such formed surface alloys are called diffusion coatings. The dimensional change of the protected specimen is smaller than the thickness of the effective surface alloy and it may be neglected.

Chromium diffusion—chromizing is probably one of the most versatile types of diffusion coatings and it is applied to achieve resistance to corrosion, thermal oxidation and abrasion for iron, steel, stainless steel, nickel and its alloys, molybdenum, tungsten and its alloy, etc.

2 Technological development of chromizing

The first attempts to achieve a chromium rich surface on iron by the diffusion process were made by Kelly in 1923[2]. Iron specimens were buried into chromium powder and treated in reducing atmosphere. A chromium rich layer, about 125 μm thick, formed after 4 hours heating at 1300°C, was a protecting layer with good adherence to the underlying metal, resistant to corrosion, as well as to thermal oxidation and, therefore, very interesting for wide commercial use.

Similar investigation was made by H.S. Cooper in 1938[2]. The process of chromizing was applied in a reducting atmosphere at the temperature of 1300°C, lasting 24 hours; the thickness of chromized layer was 250 μm.

A high processing temperature was disadvantage of both procedures.

The chromizing process has undergone considerable development changes over the years and it has been the subject of careful and detailed studies. A major achivement was the introduction of volatile halides. L.H. Marshall developed the first CVD (chemical vapour deposition) procedure of chromizing, using the volatile halides at the processing temperature of 1050°C.

Modern chromizing processes like DAL, BDS, etc. are based on the above mentioned principle[3,4].

Simultaneously, the first experiments of vacuum diffusion chromizing were performed by Hicks as early as 1932. Particles of pure iron were buried in a chromium powder and heated for 96 hours at 1200°C in a vacuum of $4 \cdot 10^{-2}$ mbar. Eight years later, Cornelius and Bollenrath[8] obtained similar results in their experiments; chromium concentration profiles were determined by the X-ray analysis. Further, this process was described by Gorbunov and Dubinin[12].

In Slovenia the vacuum chromizing process (PVD—physical vapour deposition) has been developed at the Institute for Electronics and Vacuum techniques together with the Institute of Metals and Technologies[4,5,17] and has been used for diffusion chromium coating of iron parts of magnetic circuit for miniature relays.

3 Fe-Cr constitution diagram

The iron-chromium constitution diagram is shown in **Figure 1.** At approximatelly 1000°C, it can be seen that the austenite microstructure of the iron remains unchanged until a concentration of approximately 12% chromium is reached when chromium is deposited and it diffuses inwards. At higher chromium concentrations, the microstructure becomes ferritic; continuation of chromizing causes moving of the alpha/gamma boundary into interior. During cooling the ferrite surface layer remains unchanged, while inner austenite is transformed into ferrite. This recrystallization of inner region with less than 12% Cr causes that boundary with 12% Cr is good visible, **Figure 2.** The depth to which extends the 12% Cr boundary is taken as the thickness of chromized layer, **Figure 3.**

Since the rate of diffusion of chromium is greater in ferrite than in austenite, there is a rapid rise in the chromium concentration of the coating towards the surface, and beyond the 12% Cr boundary there is a sharp concentration drop at the ferrite/austenite boundary. Grain boundary diffusion occurs too, but it has a little effect on the coat thickness, **Figure 4.**

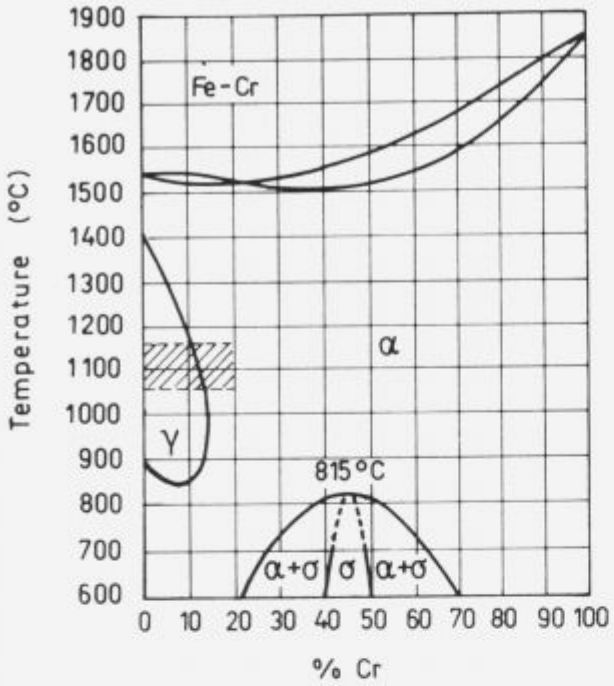

Figure 1. Iron—Chromium diagram[5].
Slika 1. Fazni diagram Fe—C[5].

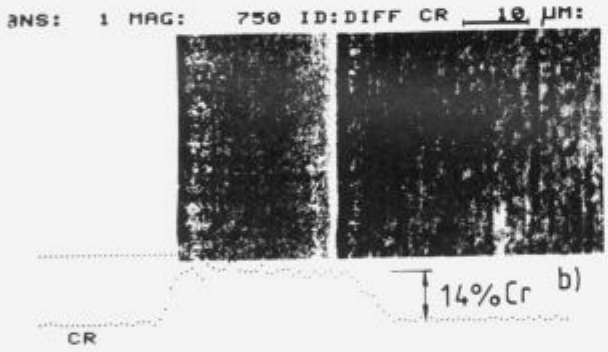

Figure 2. a) Micro-section of vacuum chromized sample. A sharp α/phase boundary is visible (nital etched). b) Cr concentration profile of the same sample.
Slika 2. a) Metalografski posnetek vakuumsko kromanega vzorca železa; vidna je ostra fazna meja alfa/gama (jedkano z nitalom). b) Koncentracijski profil kroma posnet z elektronskim mikroanalizatorjem na istem vzorcu.

The alloyed layer is generally called a coating, but it must be clearly distinguished from the coatings produced by electroplating and spraying processes, since there is no diffusion. The chromized coating represents an inseparable part of the treated specimen, the composition is changing from the surface to the core.

4 Mechanism and kinetics of cromizing the iron

4.1 Chromizing technique with volatile halides

In these processes chromium is brought to the surface of the iron heated to 900–1150°C as a gaseous compound, e.g. chromium chloride, where it is deposited in atomic form by a chemical reaction.

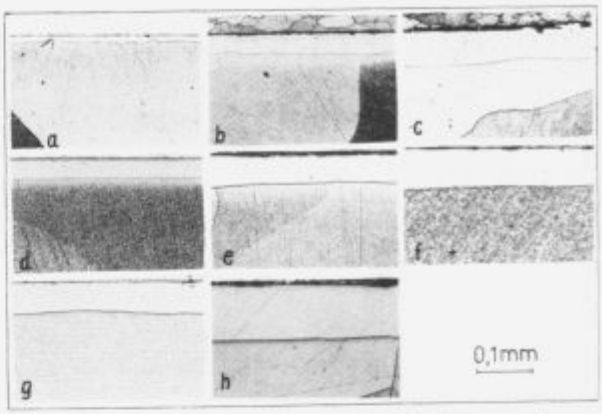

Figure 3. Microsections of vacuum chromized iron samples at: 1050°C (a) 3 hours, (b) 8 hours (c) 12 hours, 1100°C (d) 3 hours, (e) 8 hours, (f) 12 hours, 1150°C (g) 3 hours, (h) 8 hours. Nital etched.
Slika 3. Metalografski posnetki vakuumsko kromanih vzorcev železa pri: 1050°C (a) 3 ure, (b) 8 ur (c) 12 ur, 1100°C (d) 3 ure, (e) 8 ur, (f) 12 ur, 1150°C (g) 3 ure, (h) 8 ur. Jedkano z nitalom.

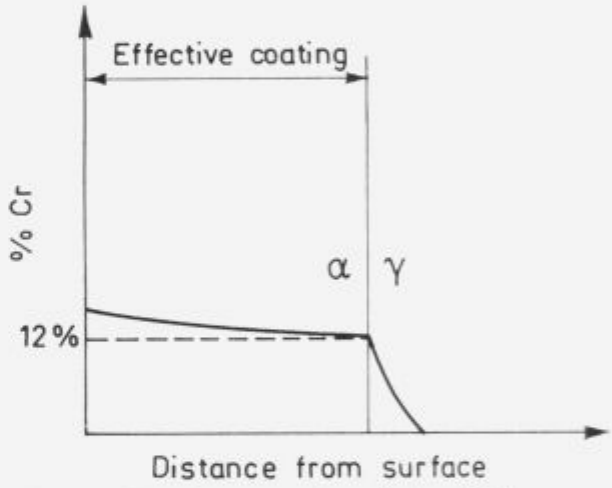

Figure 4. Chromium concentration profile in α-FeCr layer.
Slika 4. Gradient kroma v kromani plasti.

In many chromizing techniques, chromium chloride is applied and an atmosphere containing hydrogen is maintained in the reaction chamber.

The deposition of chromium on iron is described with the following equations:

- Interchange

$$Fe + CrCl_2 = FeCl_2 + Cr \qquad (1)$$

- Reduction

$$CrCl_2 + H_2 = 2HCl + Cr \qquad (2)$$

- Dissociation

$$CrCl_2 = Cl_2 + Cr \qquad (3)$$

In the reaction (1) an atom of iron is removed from the surface for each deposited chromium atom. Since iron and chromium atoms are similar in weight and size, there occur

only slight mass and dimensions changes of iron specimens after the treatment. The reaction is reversible and the equilibrium chromium concentration at the surface depends on the relative vapour pressures of iron and chromium chlorides in gaseous phase.

Reactions (2) and (3) are catalysed by the iron surface. Theoretically the surface chromium concentration may approach 100 per cent, but since it is assumed that the catalytic activity of the iron surface drops with the increasing chromium content, the concentration of chromium is limited. The mass and dimension change are equivalent to the amount of deposited chromium.

Generally, the volatile halides are used for transport of chromium atoms to the surface of iron, where they are adsorbed and diffuse inwards.

In **Figure 5** the layout of BDS (Becker, Daeves, Steinberg) process, a typical CVD process, is shown.

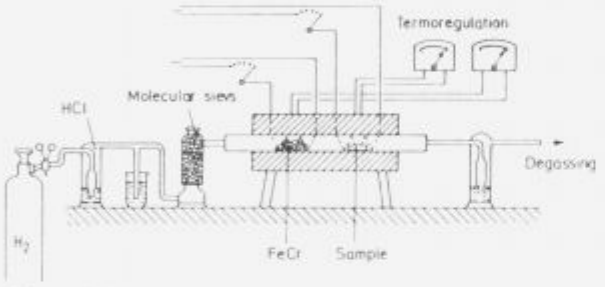

Figure 5. The layout of BDS (Becker, Daeves, Steinberg) process, typical CVD process, is shown.

Slika 5. Shematičen prikaz CVD-BDS postopka.

Vacuum chromizing

There are two possible processes of supplying an iron surface with the chromium atoms:

- transfer due to the close contact of iron surface and chromium granulate enabling the surface diffusion of Cr
- absorption of Cr vapour through the formed gaseous phase

In vacuum chromizing the growth of $\alpha - FeCr$ layer is controlled by two processes:

1. *The arrival and condensation of Cr atoms on the surface of the specimen* given by the condensation rate w:

$$w = \frac{1}{2\pi}\sigma_k p_{Cr}\sqrt{\frac{M}{RT}} \qquad (4)$$

$$w = 0.044\sigma_k p_{Cr}\cdot\sqrt{\frac{M}{T}} \qquad /\mathrm{g\,cm^{-2}s^{-1}}/ \quad (5)$$

where σ_k is the condensation coefficient; p_{Cr} (mbar) is vapour pressure; M is Cr molecular mass and T is absolute temperature (K). The decisive quantity is p_{Cr}, and its temperature dependence is being described by

$$p = 11.743\exp(-394000/RT) \qquad /\mathrm{mbar}/ \quad (6)$$

(R is the gas constant in $\mathrm{JK^{-1}mol^{-1}}$)

2. *Chromium migration from the surface inwards into the specimen* expressed by the interdiffusion coefficient D:

$$D = 2.08\exp(-243000/RT) \qquad (7)$$

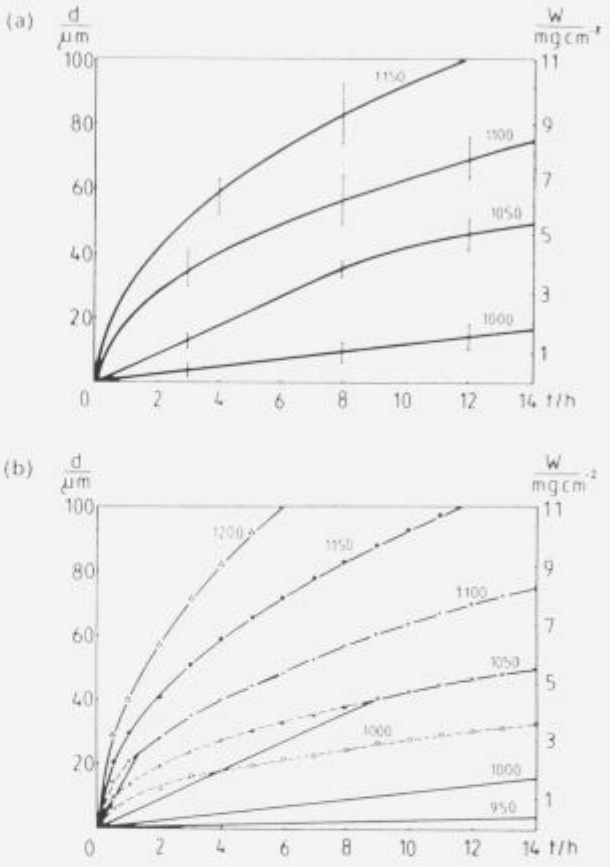

Figure 6. Thickness of the chromized layer, d, and the mass increase, W, as a function of chromizing time t.
a) experimental results b) calculated values.

Slika 6. Debelina vakuumsko kromane plasti d in narastek teže W v odvisnosti od časa t a) eksperimentalni rezultati b) izračunane vrednosti.

By increasing the temperature T, p increases more rapidly than D as the evaporation enthalpy of chromium $\Delta H_{evap} = 394\ \mathrm{kJ\,mol^{-1}}$ is higher than the activation energy for the diffusion $E_{dif} = 243\ \mathrm{kJ\,mol^{-1}}$. This circumstance leads to three different α-FeCr layer growth rates.

(a) At low temperatures $950 \leq \theta \leq 1050°\mathrm{C}$ the slowest process is the Cr condensation. All condensed Cr atoms are transported immediately by diffusion from the surface inwards. Therefore the layer growth rate is linearly proportional to the condensation rate w:

$$w = Dt \quad \text{or} \quad d = Vwt$$

(b) At high temperatures $\theta \geq 1150°\mathrm{C}$, when p is high enough, the slowest process is the diffusion, leading to the parabolic law

$$w = Dt \quad \text{or} \quad d = V\sqrt{2Dt}$$

Table 1. Values applied in the evaluation of the thickness, d, and weight increase, W, of α-FeCr layers given in Figure 6b. D-interdiffusion coefficient, p-equilibrium Cr vapour pressure, w-condensation rate of chromium, t_a, d_a—critical time coresponding α-FeCr layer thickness when the linear growth rate changes into the parabolic one.

°C	900	950	1000	1050	1100	1150	1200	1250
D (cm^2s^{-1})	1.52×10^{-11}	4.20×10^{-11}	1.07×10^{-10}	2.56×10^{-10}	5.72×10^{-10}	1.21×10^{-9}	2.43×10^{-9}	4.65×10^{-9}
p (mbar)	1.0×10^{-7}	8.0×10^{-7}	3.8×10^{-6}	1.5×10^{-5}	5.7×10^{-5}	1.9×10^{-4}	5.9×10^{-4}	1.7×10^{-3}
W ($g cm^{-2}s^{-1}$)	9.23×10^{-10}	7.24×10^{-9}	3.36×10^{-8}	1.35×10^{-7}	4.88×10^{-7}	1.62×10^{-6}	4.88×10^{-6}	1.36×10^{-5}
t_a (s)	4.32×10^{7}	1.94×10^{6}	2.3×10^{5}	3.4×10^{4}	5829	1150	247	59.31
(h)	1200	538.8	63.9	9.52	1.6	0.319	0.069	0.0165
d_a (μm^2)	362.4	127.60	70	41.9	25.8	16.6	10.9	7.3

At these values of T the linear rate appearing in the early stages of growth cannot, be detected.

(c) In the intermediate region $1050 \leq \theta \leq 1150$°C the thickness of α-FeCr layer begins to increase linearly with time. The growth rate changes to a parabolic low at the critical time t, which corresponds to the critical thickness d.

The calculated growth rates of α-FeCr layers are shown in **Figure 6b. Table 1** contains all necessary data; p is obtained from the equation (6), w from the equation (5) assuming $\sigma = 1$, D from the equation (7), t_a and d_a from the relationships given in **Figure 6a.**

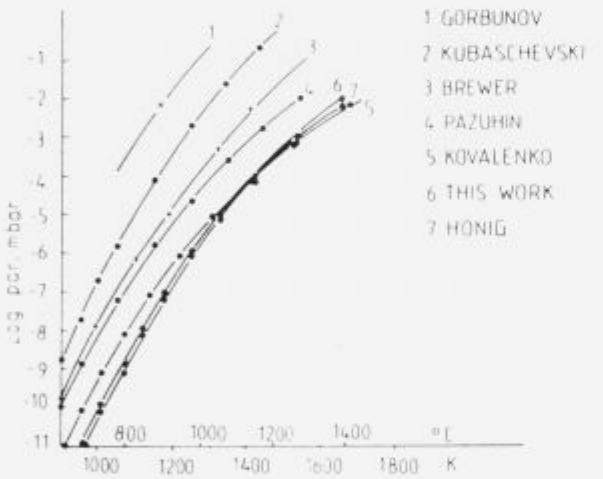

Figure 7. Temperature dependence of equilibrium Cr vapour pressure p according to various references[11–16].

Slika 7. Parni tlak kroma v odvisnosti od temperature po podatkih različnih avtorjev[11–16].

The real Cr vapour pressure p_{real} is equal to the equilibrium pressure p only if the experimental conditions are carefully chosen: $p_{RA} \leq 10^{-4}$ mbar, while the surface of the chromium granulate has to be as clean as possible and the ratio of specimens surface and the granulate amount must be adequate. If these conditions are not correctly chosen then p_{real} can be expressed by p multiplied by three correction coefficients $c_1, c_2, c_3 \leq 1$:

$$p_{real} = c_1 c_2 c_3 p \qquad (8)$$

where:

c_1 takes in account the portion of oxidized surface of granulate;

c_2 takes in account the residual atmosphere;

c_3 takes in account the surface/granulate ratio.

5 Conclusion

The results of this investigation show that none of CVD processes is suitable for the protection of iron parts for magnetic circuit in miniature hermetic relays. For this purpose PVD process of vacuum chromizing was developed. With this procedure the maximal chromium content of 15% Cr at the surface was obtained, enough for corrosion protection in corrosive media which are demanded by MIL-R-39016 and MIL-R-5757. PVD process assures the optimal magnetic properties, a very low coercivity and a good weldability and additionally, it is an environment friendly process.

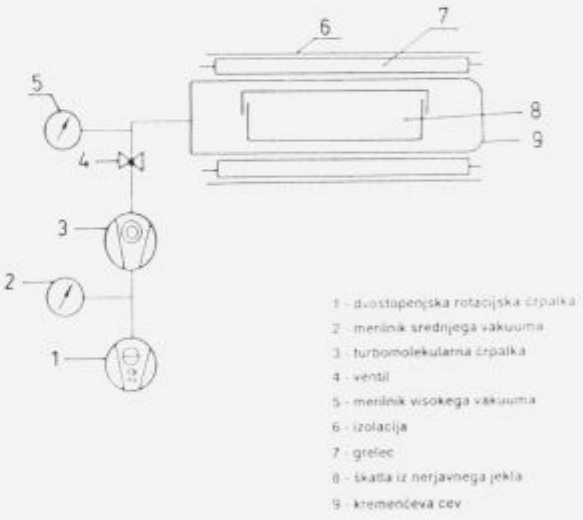

Figure 8. A schematic diagram of PVD—vacuum chromizing procedure[7].

Slika 8. Shematičen prikaz PVD—vakuumskega difuzijskega postopka kromanja.

6 References

[1] N.A. Lockington, in Corrosion, Vol. 2, Principles of Applying Coatings by Diffusion, Butterworths, London 1978.

[2] R.L. Samuel, N.A. Lockington, Met. Treat. 18, 354, 407, 440 (1951).

[3] G. Becker, K. Daeves, F. Steinberg, Stahl und Eisen 61, 289 (1941).

[4] M. Jenko, A. Kveder, R. Tavzes, E. Kansky, J. Vac. Sci. Technol. A3, 6, 2657(1985)

[5] E. Kansky, M. Jenko, Vacuum 37, 1/2, 81 (1987).
[6] M. Jenko, R. Tavzes, E. Kansky, J. Vac. Sci. Technol. A5/IV 2685 (1987).
[7] A.H. Sully, E.A. Brandes, Chromium, Chpt. 7, 258, Butterworth, London (1967).
[8] H. Cornelius, s. F. Bollenrath, Arch. Eisenhuttenwesen, 15, 145 (1941).
[9] L.C. Hicks, Trans. AIME, 113, 13, 163 (1934).
[10] T.P. Hoar, F.A. Croom, J. Iron Steel Inst. 169, 101 (1951).
[11] R.E. Honig, D.A. Kramer, RCA Rev. 30, 285 (1969).
[12] N.S. Gorbunov, Diffusion coatings on iron and steel, Israel program for Sci. translations, Jerusalem 1962.
[13] V.A. Pazuhin, A.J. Fišer, Vakuum v metallurgii, Metallurgizdat, Moskva (1956).
[14] V.F. Kovalenko, Teplofizičeskie Procesy i Elektrovakuumnye Pribory, Sovetskoe radio, Moskva (1957).
[15] J.L. Margrawe, The Characterization of High Temperature Vapours, John Wiley and Sons, New York (1967).
[16] O. Kubaschewski, E.L. Evans, C.B. Alcock, Metallurgical Thermochemistry, Pergamon, Oxford (1967)
[17] M. Jenko, A. Kveder, R. Tavzes, Postopek za protikorozijsko ščitenje majhnih kosov iz čistega železa ob hkratnem doseganju najboljših mehkomagnetnih lastnosti. Številka patenta: P-19470.

KOVINE ZLITINE TEHNOLOGIJE, 26, 1992, 1–4

1. Kronološko kazalo

2. Avtorsko kazalo

Contents

Contents

Chromium diffusion, chromizing of iron, vacuum chro mizing of iron, miniature hermetic relays, Fe-Cr layers resis tive to corrosion media, coercitivity

M. Jenko, A. Kveder, S. Spruk, L. Koller

Chromizing of Iron

KZT, 26 (1992) 4, p 351–355

The theoretical aspects of CVD processes of iron chromizing and the comparison with PVD process are presented. It is shown that none of CVD processes is suitable for the protection of iron parts for magnetic circuit in miniature hermetic relays. For this purpose PVD process of vacuum chromizing was developed. With this procedure the maximal chromium content of 15% Cr at the surface was obtained. Such chromium layer assures the optimal magnetic properties, a very low coercitivity and a good weldability.

Author's Abstract

Vsebina

Vsebina

Difuzija kroma, difuzijsko kromanje, vakuumsko kromanje, miniaturni hermetični releji, Fe-Cr plasti odpome proti koroziji, koercitivnost

M. Jenko, A. Kveder, S. Spruk, L. Koller

Difuzijsko kromanje železa

KZT, 26 (1992) 4, s 351–355

Podani so teoretični vidiki CVD postopkov difuzijskega kromanja železa v primerjavi s PVD postopkom. Raziskava CVD postopkov je pokazala, da za zaščito sestavnih delov železnega magnetnega kroga miniaturnih hermetičnih relejev ni primeren nobeden izmed le-teh. Zato so avtorji razvili PVD postopek - tehnologijo vaku umskega kromanja. S tem postopkom je dosežena maksimalna koncen tracija kroma na površini 15% Cr, kar je dovolj, da so vzorci korozijsko obstojni v medijih, ki jih predpisujejo standardi. S PVD postopkom dosežemo optimalne magnetne lastnosti (nizka koercitivnost) in dobro varivost.

Avtorski izvleček

ŽELEZARNA JESENICE

d.o.o.

64270 JESENICE, Cesta železarjev 8 - telefon: (064) 83-561, 84-261, 81-341
telefax (064) 83-395 - telex: 37219, 37212 zeljsn - telegram: Železarna Jesenice

Slovenija

IZDELUJE

MIKROLEGIRANA JEKLA

NERJAVNA JEKLA

ELEKTRO PLOČEVINE IN TRAKOVI

* debelo, srednjo in tanko pločevino
* hladno valjane trakove in pločevino
* dinamo trakove in pločevino
* nerjavne trakove in pločevino
* vlečeno, brušeno in luščeno jeklo
* valjano in vlečeno žico
* patentirano žico
* pleteno patentirano žico za prednapeti beton
* hladno oblikovane profile
* kovinske podboje za vrata
* dodajni material za varjenje
* žičnike
* tehnične pline

NUDIMO TUDI STORITVE

* prevaljanja, vlečenja, iztiskanja in toplotne obdelave pločevin in žice

* tehnične dejavnosti: elektro, strojne, konstrukcijske, obrtne in tehnične

ŽELEZARNA JESENICE
ACRONI METALURGIJA

IZDELUJE

- MIKROLEGIRANA JEKLA
- NERJAVNA JEKLA
- ELEKTRO PLOČEVINE IN TRAKOVE

MIKROLEGIRANA JEKLA

- vroče valjane trakove in pločevine
- hladno valjane trakove in pločevine
- dinamo trakove in pločevine
- nerjavne trakove in pločevine
- hladno oblikovane profile
- kovinske podboje za vrata

NERJAVNA JEKLA

- NUDIMO TUDI STORITVE

ELEKTRO PLOČEVINE IN TRAKOVI

- prevaljanja, iztiskanja, krojenja in toplotne obdelave pločevin

64270 JESENICE, Cesta železarjev 8 - telefon: (064) 83-561, 84-261, 81-341 - telefax: (064) 83-395
telex: 37219, 37212 zeljsn - telegram: Železarna Jesenice - Slovenija